ENHANCING THE BIOFOULING RESISTANCE OF REVERSE OSMOSIS MEMBRANES BY A NOVEL SURFACE MODIFICATION TECHNIQUE

BY

ASIF MATIN

A Dissertation Presented to the

DEANSHIP OF GRADUATE STUDIES

KING FAHD UNIVERSITY OF PETROLEUM & MINERALS

DHAHRAN, SAUDI ARABIA

In Partial Fulfillment of the
Requirements for the Degree of

DOCTOR OF PHILOSOPHY

In

MECHANICAL ENGINEERING

KING FAHD UNIVERSITY OF PETROLEUM & MINERALS

DHAHRAN 31261, SAUDI ARABIA

DEANSHIP OF GRADUATE STUDIES

This thesis written by Asif Matin under the direction of his thesis advisor and approved by his thesis committee, has been presented to and accepted by the Dean of Graduate Studies, in partial fulfillment of the requirements for the degree of **DOCTOR OF PHILOSOPHY IN MECHANICAL ENGINEERING.**

Thesis Committee

Dr. Zafarullah Khan (Advisor)

Dr. S.M.J. Zaidi (Member)

Dr. Mazen M. Khaled (Member)

Dr. Tahar Laoui (Member)

Dr. Mary C. Boyce (Member)

Dr. Amro M. Al-Qutub

Department Chairman

24/4/12

Dr. Salam A. Zummo

Dean of Graduate Studies

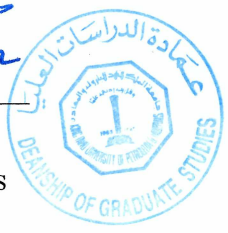

ABSTRACT (ENGLISH)

Name: Asif Matin

Title: Enhancing the Biofouling Resistance of Reverse Osmosis Membranes by a Novel Surface Modification Technique

Major: Mechanical Engineering

Date: January 1, 2012

Water is becoming increasingly scarce as the demand for fresh water continues to increase in a drastic manner. One potential new water resource is desalination of sea and brackish water. Reverse osmosis is one of the many processes used to obtain potable water fit for human consumption from seawater. However, the membranes used in this process are prone to fouling by microorganisms such as bacteria. This study focused on the surface modification of commercial RO membranes by the deposition of random copolymer films.

We copolymerized the hydrophilic hydroxyethylmethacrylate (HEMA) with the hydrophobic perfluorodecylacrylate (PFA) to create randomly amphiphilic thin polymer films using an initiated CVD technique. By adjusting the relative flow rates of the HEMA and PFA comonomers, films over a wide compositional range were synthesized. These films were deposited on commercial membranes and in some cases quartz crystals.

Atomic Force Microscopy results showed the surface of the films to be very smooth with the rms value being only a few nanometers. High-resolution TEM images of the

membrane cross-section show the coatings to possess a high degree of conformality and uniformity. SEM images at high magnifications show a great deal of similarity between the virgin and the coated membranes: the peak-and-valley structure normally associated with polyamide membranes.

QCM studies revealed intermediate film chemistries as having the greatest adsorption resistance to biopolymers known to play a crucial role in membrane Biofouling. Static bacterial adhesion tests demonstrated the superior antifouling properties of the copolymer films to conventional polyamide membranes.

Permeation studies proved the compatibility of the copolymer film to the polyamide surface of the RO membrane in several ways. Firstly, the decline in permeate flux of the commercial membrane due to the presence of the film is negligible. Secondly, XPS analysis confirmed the presence of the film on the membrane surface even after long-term testing at high external pressures. Lastly, long-term tests with feed water of known microbial concentration showed less flux decline for membranes covered with copolymer film.

ABSTRACT (ARABIC)

الاسم: عاصف متين

الموضوع: تحسين مقاومة إلتصاق البكتيريا على أسطح أغشية النتاضح العكسي من خلال إستخدام تقنية واعدة لتحسين الأسطح

القسم: الهندسة الميكانيكية.

التاريخ: 1-01-2012

أصبحت قضية الحصول على الماء قضية ذات إهتمام بالغ خصوصا مع إزدياد الطلب عليها.تمثل تحلية ماء البحار أحد مصادر المياه الواعدة وبالأخص تحليتها عن طريق التناضح العكسي الذي يمكن من جعل هذه المياه صالحة للإستخدام البشري. وعلى الرغم من أنها من أنجع الحلول من أجل الحصول على مياه نقية إلا أن إستخدام هذه التقنية دائما مايرتبط بعوامل تحد من إستخدامه ومن أبرز هذه العوامل هو سماحها للبكتيريا بأن تبني مستعمرات على أسطحها مما يؤدي إلى إنسداد المسامات وتغيير كثير من خصائص النفاذية التي تمتلكها هذه الأغشية. هذه الدراسة تركز بشكل عميق من أجل تحسين أسطح أغشية النتاضح العكسي من خلال ترسيب طبقات من البوليمر.

قامت هذه الدراسة بدمج نوعين من البوليمر إحداها (HEMA) والتي تتميز بعلاقة تجاذبية مع الماء و (PFA) والتي تتميز بعلاقة تنافرية مع الماء ليصبح لدينا في اخر المطاف بوليمر يتميز بوجود هذين الخاصيتين وذلك من خلال إستخدام تقنية (CVD) وعن طريق معايرة معدل التدفق النسبي للمونمرات التالية (HEMA) و (PFA) تم تصنيع طبقات متعددة مختلفة النسب التركيبية بين هذين المادتين. هذه الطبقات تم ترسيبها على أسطح أغشية تناضح عكسي تجارية وأيضا تم ترسيبها على الكوراتز.

نتائج مجهر القوى الذرية تظهر الأسطح المعاد تحسينها وهي ناعمة جدا وبمعدل خشونة لايتجاوز نانمويترات قليلة وكذلك تظهر نتائج المجهر الإلكتروني قائق الدقة صورا لمقاطع عرضية لهذه الأغشية بعد تحسينها وهي تمتلك مستوى عال من التجانس وأيضا يثبت لنا المجهر الإلكتروني التشابه الكبير بين الأغشية الأساسية والأغشية المطلاة وأن الانخفاضات والارتفاعات في السطح ترجع في الأساس إلى أغشية (polyamide).

وتظهر نتائج الدراسات التي تم إجرائها من خلال (QCM) أن الطبقة المتوسطة لديها خاصية الممانعة الشديدة للإلتصاق بكتيريا الوليمر التي تلعب دور مهم جدا في عملية الإنسداد البكتيريا وهذا ماتم إختباره من خلال إجراء

إختبار إلتصاق البكتيريا الساكن ليثبت وبشكل قوي خاصية ممانعة الترسب البكتيريا على هذه الأسطح الأغشية السموزية البوليمرية.

إختبار نفاذية الأغشية المعاد تحسينها تظهر تمازج الطبقة المصنعة وسطح الغشاء الأساسي. أولا، لا يوجد إنخفاض في مستوى النفاذي مع وجود الطبقة المحسنة. ثانيا، من خلال تحليل XPS وتحت إختبار طول المدى وتحت ضغط عال جدا وجود هذه الطبقة المحسنة وثباتها على السطح.

Dedication

To my beloved Father

Table of Contents

Acknowledgements

First of all and most importantly, I would like to glorify and thank Almighty Allah for all his blessings and mercy. Without His will, nothing would have been possible and no difficulty would have been made easy.

Thank you to my advisor, Prof. Zafarullah Khan, for his sincere advice and guidance, during my graduate studies. Also, thanks to him for showing so much patience and consideration throughout the course of my thesis work.

Thanks to the rest of my dissertation committee members for their help and assistance during the different stages: Prof. Zaidi in the permeation tests, Prof. Mazen Khaled during the bacterial adhesion tests, Prof. Tahar Laoui for his input in the defence presentation, Prof. Mary Boyce for being up-to-date with the progress of my work during stay at MIT.

Thank you to Prof Karen Gleason from the Chemical Engineering department at MIT. The facilities of her lab esp. the iCVD reactor proved to be very crucial for my research. Thanks to her group members esp. Dr. Gozde Ozaydin-Ince for thin-film depositions, Ms. Rong Yang for XPS analyses and QCM data interpretation, and Ms. Priya Moni for copolymer film depositions.

The KFUPM-MIT administration deserves special mention here for facilitating my visit to MIT and providing the best possible assistance (moral and financial) required. Profs. Amro Al-Qutub & Nesar Merah, and Mr. Abdul Aleem, all of them were of great help. Likewise, I would like to thank Ms. Angela Mickunas on the MIT side for her welcoming attitude.

Many heart-felt thanks go to my colleagues at MIT, Drs. Farid Fadhillah and Atia E. Khalifa, for their support, advice, and empathetic ears. Without them, graduate school would have been rather mundane.

Special thanks to Dr. Faiz-ur-Rehman and his assistant Owais Badr-uz-Zaman for their help and assistance with the initial setting up and consequent trouble-shooting of the permeation system. My heart-felt thanks to Dr. Amjad Khalil of the Physics dept. and his technician Anand for the preparation and provision of bacterial suspensions for the adhesion tests.

Also, I deeply appreciate Engineer Lateef Hashmi of the Materials Science Laboratory at KFUPM for his cooperation in the SEM analysis of samples exposed to bacterial cells. Khalid Al-Saeed of the Physics department deserves special mention for the XPS analyses of membrane samples coated with copolymer films.

On the MIT side, Libby Shaw and Alan Schwartzmann are deeply appreciated for their assistance in the AFM measurements. Similarly, Patrick Boisvert of the CMSE is thanked

for the SEM analyses of several samples. I would also like to thank Tim McClure for his help and guidance with the QCM analysis.

Last, but not the least, I am extremely grateful to my family members especially my wife for her continuous and relentless support during the entire course of my graduate studies. In addition, my parents deserve special mention for always remembering me in their prayers. I also deeply appreciate my in-laws for their help and sincerity especially during my stay at MIT.

List of Figures

List of Tables

NOMENCLATURE

J_w	Volumetric water flux
J_s	Salt flux
L_p	Membrane permeance to water
B	Membrane salt permeance
Δp	Applied transmembrane pressure difference
$\Delta \pi$	Osmotic pressure
C_f	Salt concentration in feed
C_p	Salt concentration in permeate
D	Diffusion coefficient of water in membrane
D_s	Salt diffusivity in membrane
V	Molar volume of water
R	Ideal gas constant
L	Membrane thickness

Chapter 1. Introduction

1.1 Global Clean Water Crisis

Water is the backbone of the global economy—quality, reliable, and sustainable supplies are vital for agriculture, industry, recreation, energy production, and domestic consumption [1]. In the past few decades, clean water supply has become more and more critical due to excessive use and increasing contamination of natural water sources. Moreover, the demand for drinking water in the world is increasing (Fig.1.1) and regulations on drinking water quality have become a lot more stringent [2]. Improving the effectiveness and efficiency of water purification technology, to produce clean water and protect the environment in a sustainable manner, is considered by many as perhaps the main *challenge* of the 21st century [3].

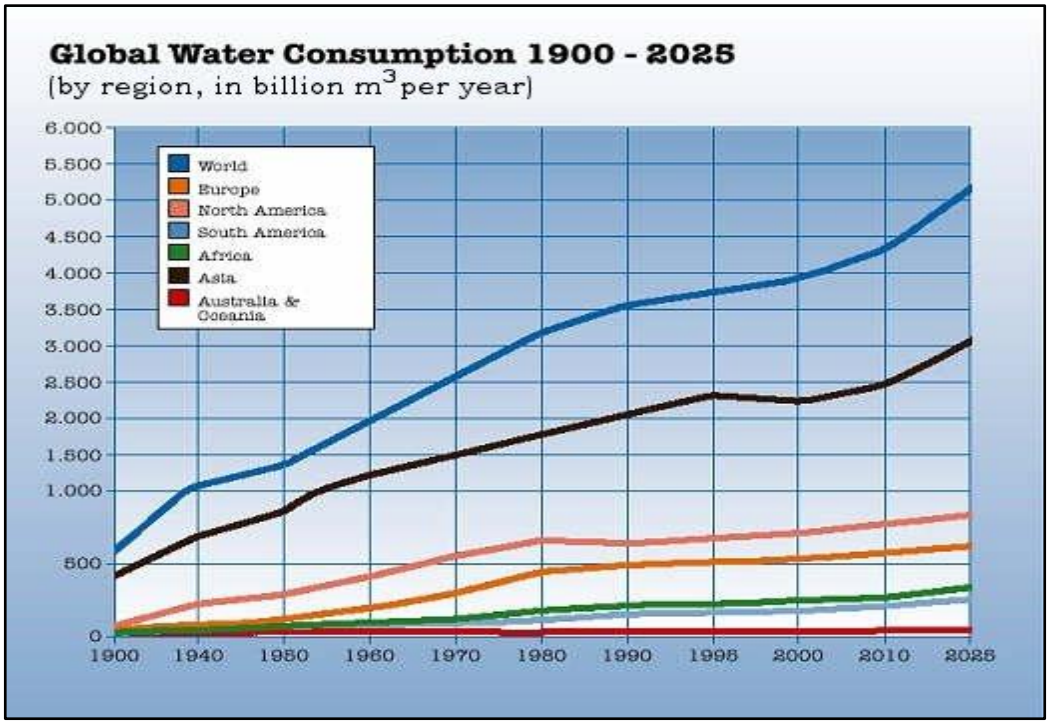

Figure 1.1 Trend of water consumption in different regions and the whole world (*www.umweltbundesamt.de)*

Water scarcity, which occurs not only in arid regions, may be characterized as a mismatch between water supply and water demand: Pollution and exploitation of groundwater aquifers and surface water have led to a decrease of quantity and/or quality of available natural water resources in many regions. The ongoing growth of population, industry and agriculture further increases water demand. In addition, higher living standards, especially in industrial countries, result in higher per capita water consumption and in intensified water scarcity.

There are several principal manifestations of the water crisis.

- Inadequate access to safe drinking water for about 884 million people
- Inadequate access to water for sanitation and waste disposal for 2.5 billion people
- Groundwater over drafting (excessive use) leading to diminished agricultural yields
- Overuse and pollution of water resources harming biodiversity

Over 41% of the world population currently lives in water-stressed regions, and with the global population projected to increase by 80 million people per year, this percentage is expected to rise [4]. Only 2.5% of the world's water is available as fresh water, and most of this water is trapped in glaciers or is far below the earth's surface [5] (Fig. 1.2). Therefore, to meet the growing demand for water, water purification technologies must be improved, and new resources must be tapped.

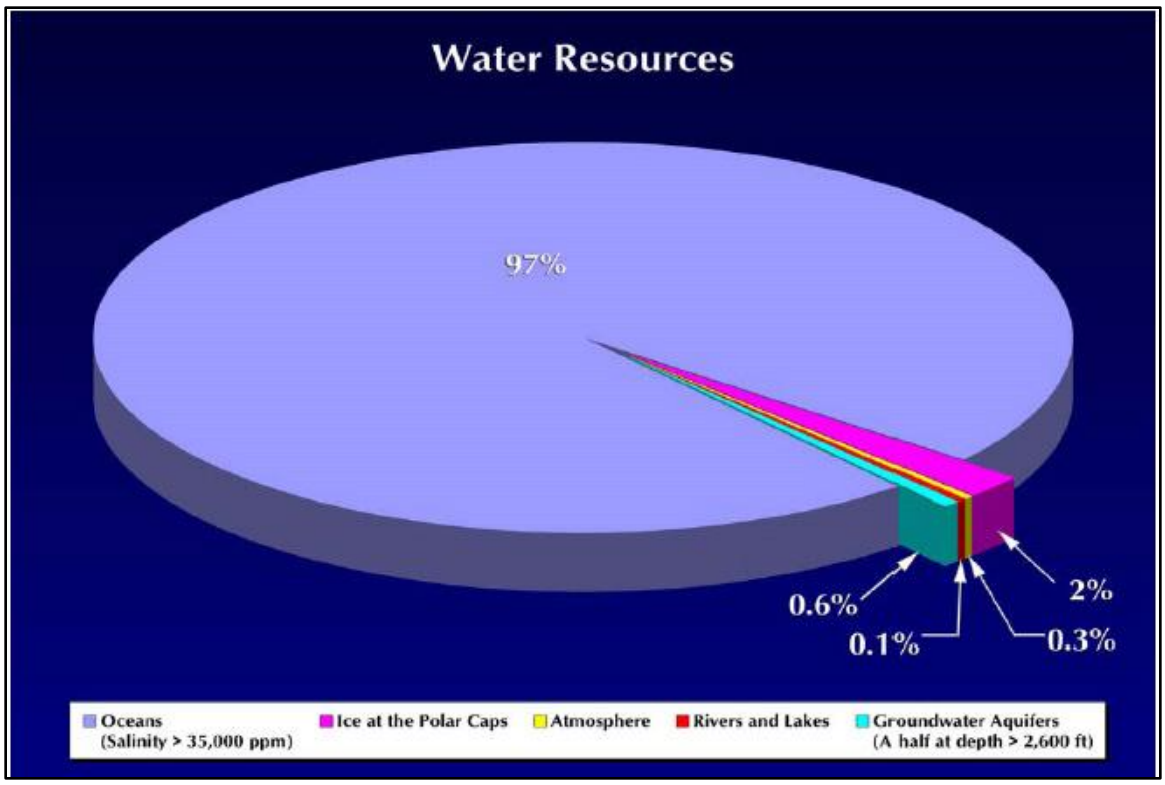

Figure 1.2 Approximate distribution of water on the planet (*Desalination Methods, Technology, and Economics*, Val Frenkel)

1.2 Desalination

Desalination is the process by which excess salts and minerals are removed from water to make it potable and fit for human consumption. Throughout the world a trend to intensified use of desalination as a means to reduce current or future water scarcity can be observed. Exploitation of natural fresh water resources combined with higher water demand has led to an increased demand for alternative fresh water resources. Desalination provides such an alternative source, offering water otherwise not accessible for irrigational, industrial and municipal use.

Desalination technologies can be classified by their separation mechanism into thermal and membrane-based desalination. Thermal desalination separates salt from water by evaporation and condensation, whereas in membrane desalination water diffuses through a membrane, while salts are almost completely retained.

Membrane-based desalination

Membranes are used in a wide range of commercial applications spanning from drinking water purification to gas separations, with a market that is expected to grow to over $10 billion by 2010 [6]. Membrane-based desalination has and is rapidly replacing thermal desalination primarily due to its lower capital and operation costs. In terms of desalination plant capacity, it is now at par with thermal desalination (Fig.1.3). In general, membranes offer many advantages over conventional technologies including a smaller footprint, lower capital costs, and simpler maintenance requirements [7].

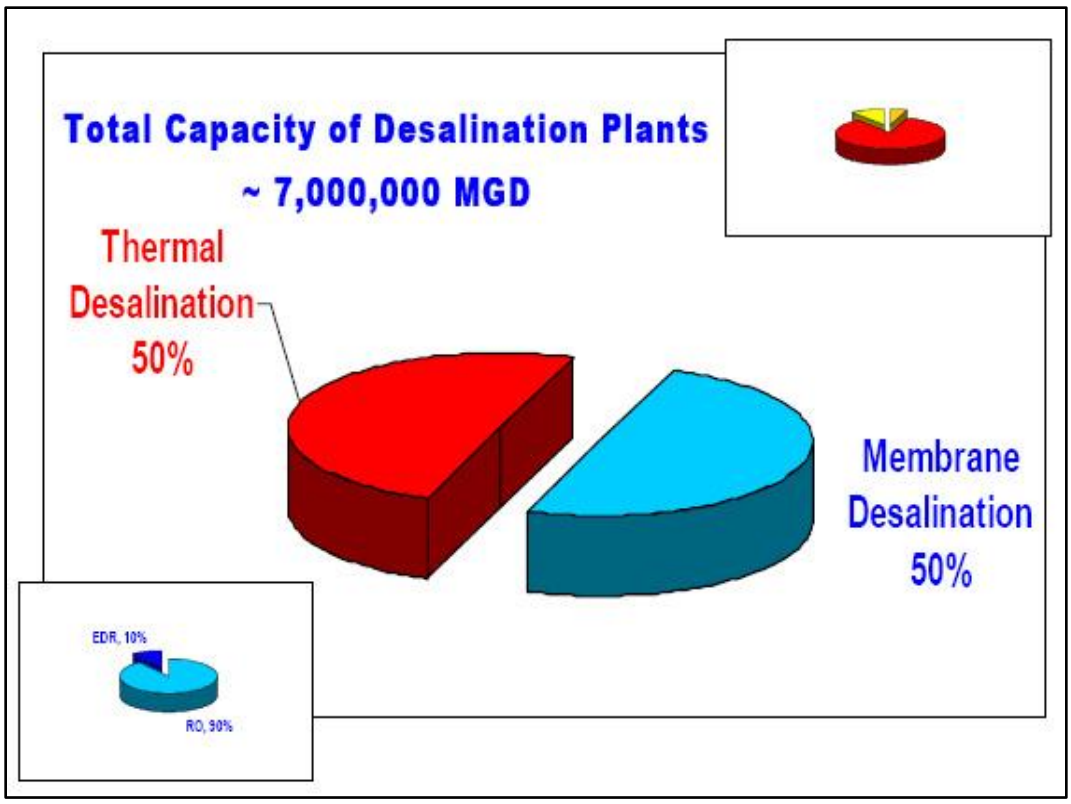

Figure 1.3 Relative distribution of thermal and membrane-based desalination techniques (*www.idswater.com)*

Water treatment processes can employ several types of membranes that are often classified according to the size of the species they reject (Figure 1.4). Microfiltration membranes have the largest pore sizes and typically reject large particles and various microorganisms. Ultrafiltration membranes have smaller pores than MF membranes and therefore, in addition to large particles and microorganisms, can reject bacteria and soluble macromolecules such as proteins. RO membranes are considered to be effectively nonporous and are able to exclude particles and many low molar mass species such as salt ions. Nanofiltration membranes are sometimes called "loose" RO membranes because they are porous membranes, but their pores are on the order of ten angstroms. Consequently, their rejection capabilities fall between those of RO and UF membranes.

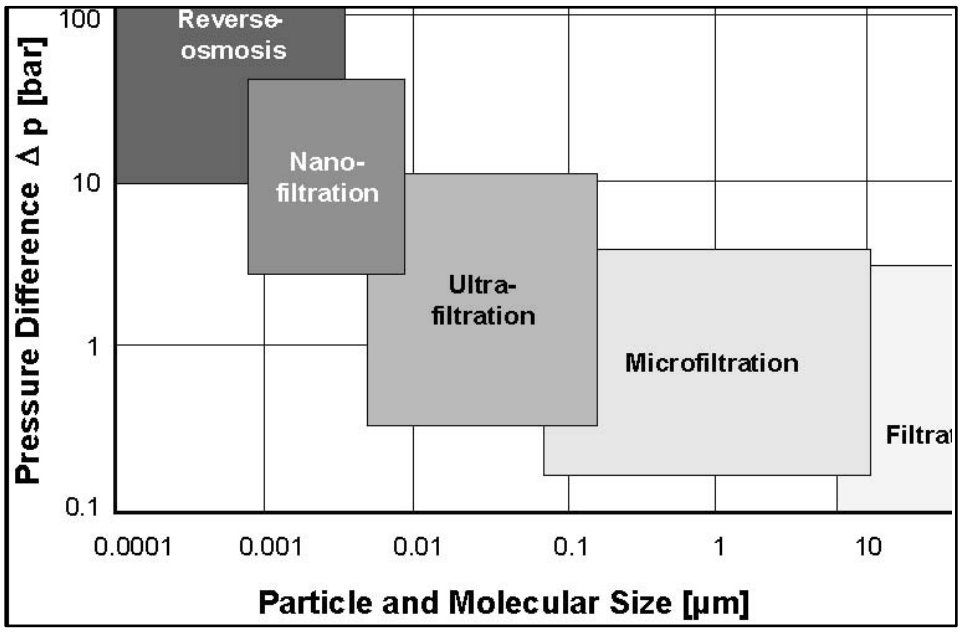

Figure 1.4 Separation capabilities of pressure driven membrane separation processes (*Fritzman et al*. 2007)

1.3 Reverse Osmosis

In recent years, reverse osmosis (RO) has become a critical technology, which promises to greatly increase the supply of clean water through desalination and purification of nontraditional water sources such as brackish, sea, and wastewater[7]. Reverse osmosis is a process that is inherently simple to design and operate compared to many traditional separation processes such as distillation, extraction, ion exchange, and adsorption. Thus RO is considered as the simplest and most efficient technique for seawater desalination purposes [8].

Reverse osmosis is a pressure-driven membrane-based process (Fig.1.5), where the membrane (almost always polymers) acts as the heart of the process in separating the undesired constituents from a feed to obtain the desired pure product. An RO membrane

acts as the semi-permeable barrier that allows selective transport of a particular species (solvent, usually water) while partially or completely blocking other species (solutes, such as salt).

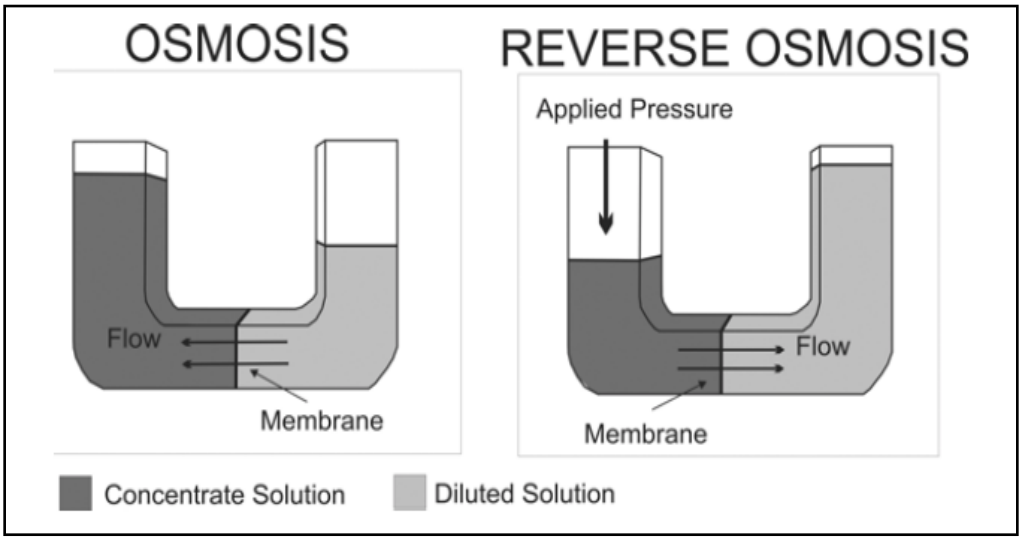

Figure 1.5 Basics of the Osmosis and Reverse Osmosis process (*Fritzman et al*. 2007)

Separation, most importantly, depends upon the properties of the membrane used in the process. These properties depend on the chemical nature and the physical structure of the membrane material. An ideal RO membrane should be resistant to degradation by chemicals and microbes have good mechanical and structural stability over long operating periods, and possess desired separation characteristics.

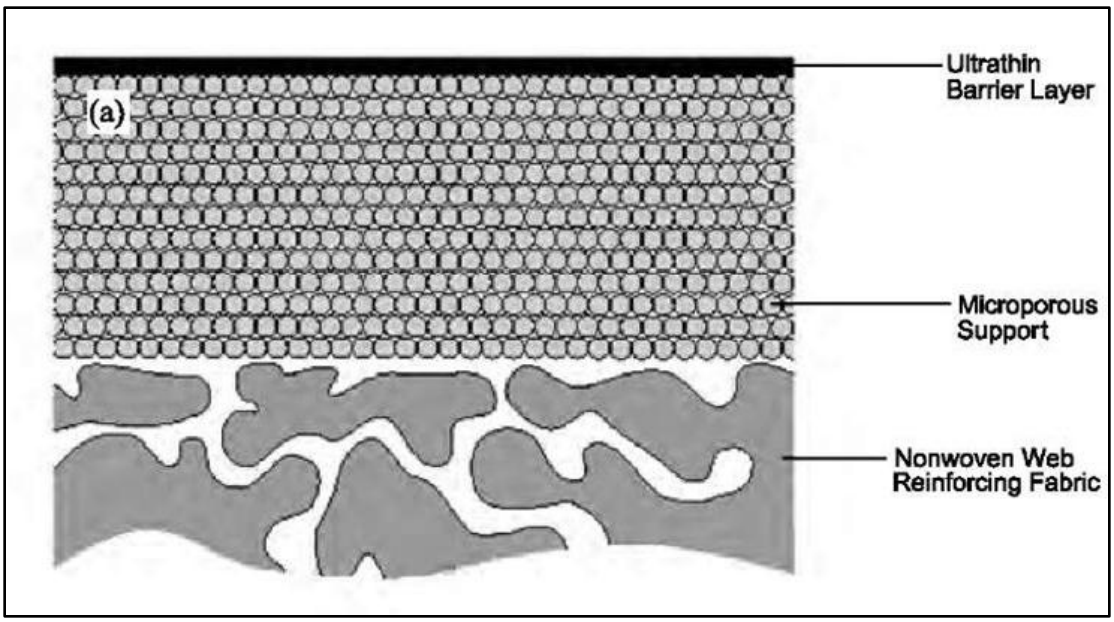

Figure 1.6 Typical structure of an RO membrane showing the different layers

A typical RO membrane consists of three different layers (Fig.1.6): a dense non-porous layer at the top, a microporous support in the middle and a nonwoven fabric at the bottom to provide the mechanical strength. The top layer is the one that separates salt and other solutes from feed water to purify it. Made from polyamide (Fig.1.7), the thickness ranges from 50 – 200 nm.

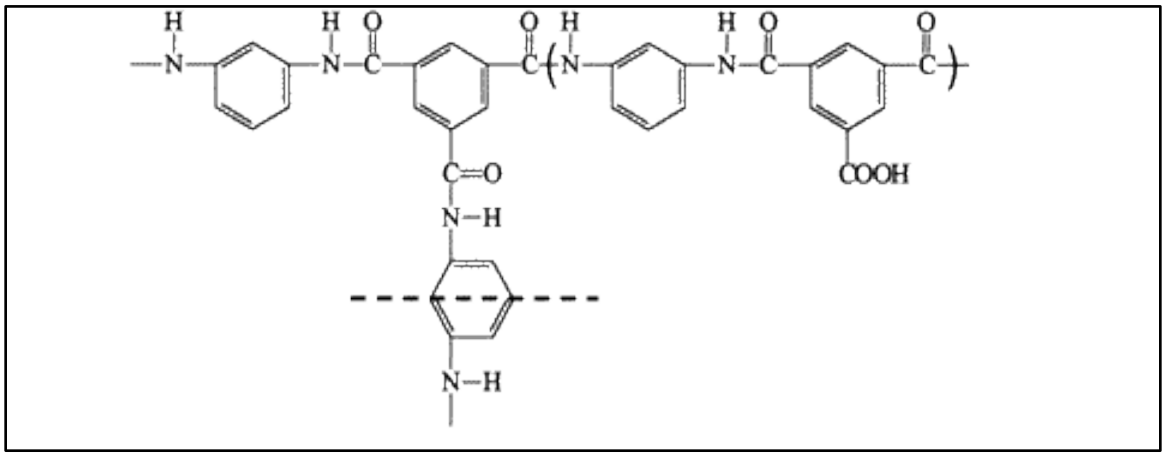

Figure 1.7 Molecular structure of polyamide

1.4 Goals & Organization of the Dissertation

A fouling-resistant RO membrane could increase the efficiency of produced water treatment. Some attempts to surface modify membranes for produced water purification have been reported in the literature (*ref*). These attempts, explained in more detail later, serve as a launching point for the research presented in this dissertation. The goals of this research were three-fold. First, the aim was to modify the surface of RO membranes by the deposition of amphiphilic copolymer films. The second objective was to explore the feasibility of these films as potential antifouling coatings on RO membranes. Last but not the least, was the performance evaluation and characterization of the modified membranes.

This dissertation contains 8 chapters including this introductory chapter. Chapter 2 details the background and theory underlining this research, such as the Biofouling problem and previous work in the literature on fouling-resistant materials. Chapter 3 gives an overview of the Chemical Vapor Deposition process with special emphasis on initiated CVD. Chapter 4 describes the materials and experimental methods used. Chapter 5 discusses the permeation studies performed on the commercial as well as the surface-modified membranes. Chapter 6 details biopolymer adsorption and bacterial adhesion studies. Chapter 7 presents the results of all experimental work and provides a thorough discussion on them. Chapter 8 closes with conclusions and recommendations for future work.

Chapter 2. Background & Theory

2.1 Reverse Osmosis Membranes

Reverse osmosis (RO) membranes are primarily used in water treatment processes to remove salt from water [9]. Effectively nonporous, RO membranes are the most selective of all water filtration membranes. Typically, microfiltration and ultrafiltration membranes remove particulate matter, proteins, and other large species, and then RO is employed to remove dissolved ions.

Currently, the most widely used RO membrane is the polyamide thin film composite (TFC) RO membrane. Pioneered by John Cadotte in the early 1970's, the polyamide TFC offers higher water flux and NaCl rejection relative to early cellulose acetate-based RO membranes [10]. As illustrated in Figure 2.1, the TFC membrane consists of a polysulfone (PSf) ultrafiltration membrane that supports an ultrathin crosslinked polyamide layer. A highly porous nonwoven backing provides additional mechanical strength. The ultrathin polyamide layer is the selective layer of the TFC and dictates the water and salt transport properties of the composite membrane. The chemistry of the fully aromatic polyamide is shown in Figure 2.2.

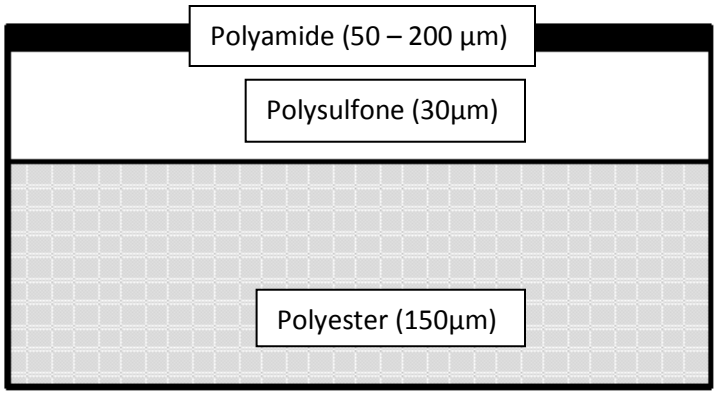

Figure 2.1 Different layers of the commercial RO membrane

Formation of the polyamide layer proceeds via an interfacial polycondensation reaction between meta-phenylene diamine (MPD) and trimesoyl chloride (TMC), shown in Figure 2.2b and c [11]. First, the microporous PSf support membrane is immersed in an aqueous amine solution (typically about 2% w/v MPD) [12]. Next, TMC is dissolved in an aliphatic solvent such as Isopar (a commercial aliphatic solvent), because it is insoluble in water. The TMC solution (typically about 0.1% w/v TMC) is coated onto the top surface of the amine-saturated PSf support membrane4. Organic solvents and water are immiscible, so contact between the two solutions does not result in mixing, but instead produces a reaction at the oil-water interface. A thin crosslinked polyamide film is formed at this interface, which is on the surface of the support membrane. This polymerization method results in film thicknesses ranging between 0.05 to 1 μm [13].

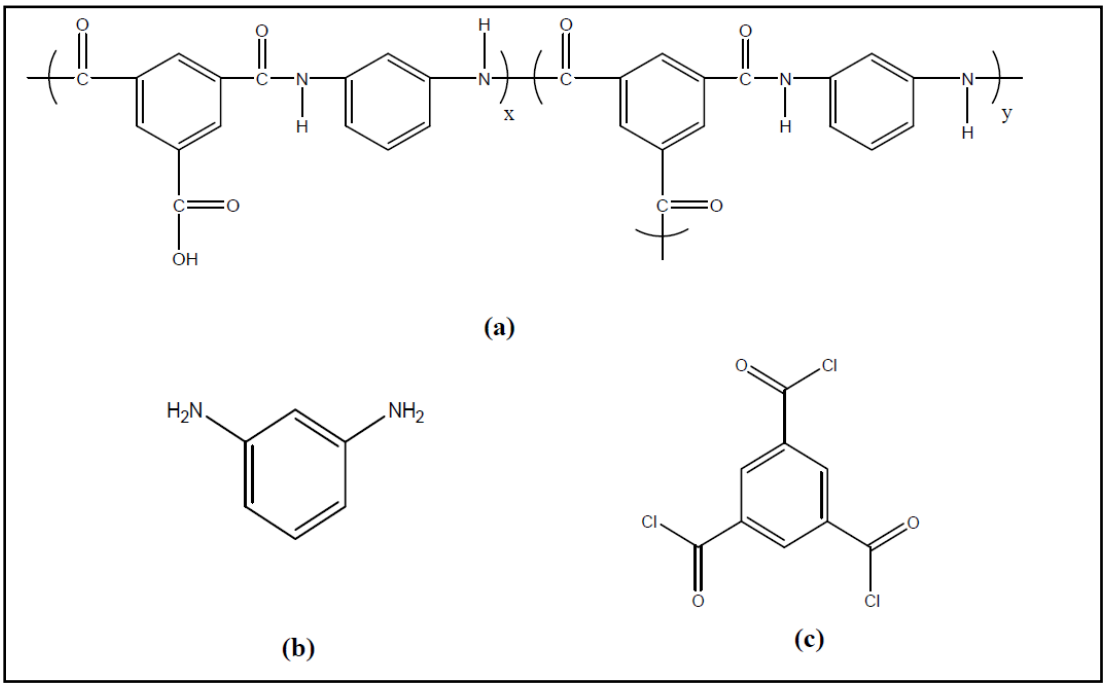

Figure 2.2 Chemical structure of (a) polyamide (b) phenylene diamine (c) trimesoyl chloride

The majority of RO membranes commercially available are based on crosslinked aromatic polyamides, but the membranes are tailored for different applications, resulting in a wide range of membrane properties. For example, one commercially-available brackish water RO membrane is designed to operate at a pressure difference of 15.5 bar(225 psig), producing 44 L/(m^2hr) of permeate at this pressure difference, with 99.5% NaCl rejection from a feed containing 2000 mg/L of NaCl [14]. On the other hand, a commercially-available seawater RO membrane operates at 55.2 bar (800 psig), and produces 26 L/(m^2hr) of purified water, with 99.8% of NaCl rejected from a 32,000 mg/L NaCl feed[8].

Clearly, despite the similarity in membrane chemistry, a wide variety of membrane transport properties can be achieved. Several means of customizing RO membranes include varying the concentration of the aqueous MPD and organic TMC solutions and mixing in chemical additives. For commercially-available membranes, these additives are often proprietary in nature.

2.2 Membrane fouling

The membrane-based RO desalination, like other desalination technologies, is also not free from some serious concerns. A major problem related to reverse osmosis applications in desalination is membrane fouling. Membrane fouling is a phenomenon that is ubiquitous in pressure driven membrane processes. Fouling is caused by solute adsorbing irreversibly or reversibly onto the surface of the membrane or within the pores of the membrane [15,16] (Fig.2.3).

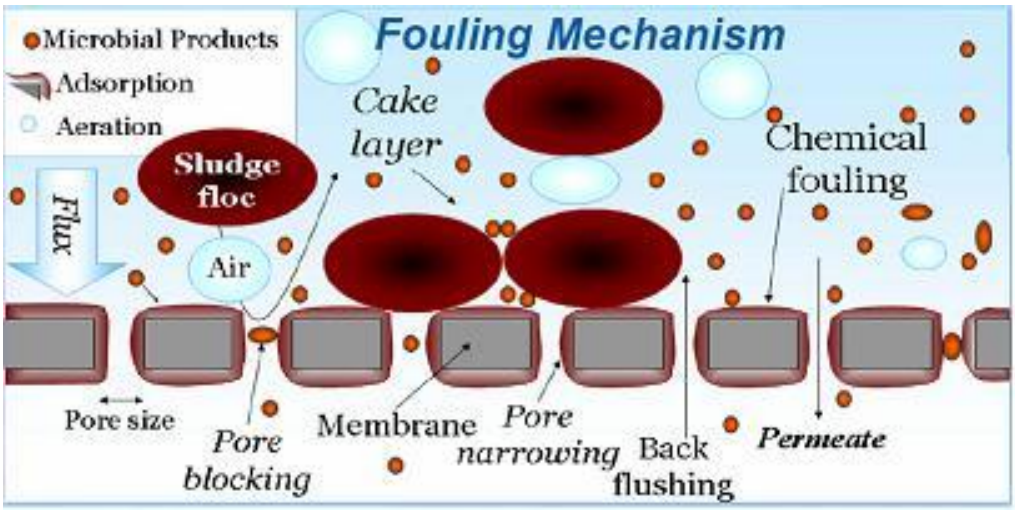

Figure 2.3 Schematic of different mechanisms in membrane fouling (*www.ete.wur.nl*)

Fouling always worsens the membrane performance, shortens its life, and reduces the flux and salt rejection [17]. Although the term fouling can be used to describe both reversible and irreversible solute adsorption, it is the irreversible portion that is most problematic. Irreversible adsorption produces a long-term flux decline that cannot be fully recovered by hydraulically cleaning the membrane [18]. Fouling requires frequent chemical cleaning and ultimately shortens membrane life, thus imposing a large economic burden on RO membrane plant operation (up to 50% of the toal costs) [19].

The major types of fouling in RO membranes are (Fig.2.4) [20]

1. Crystalline fouling: deposition of inorganic material precipitating on a surface
2. Organic fouling: deposition of organic substances (e.g. oil, proteins, humic substances)
3. Particle and colloid fouling: deposition of clay, silt, particulate humic substances, debris, silica

4. Microbiological fouling: biofouling, adhesion and accumulation of micro-organisms, forming biofilms [21]

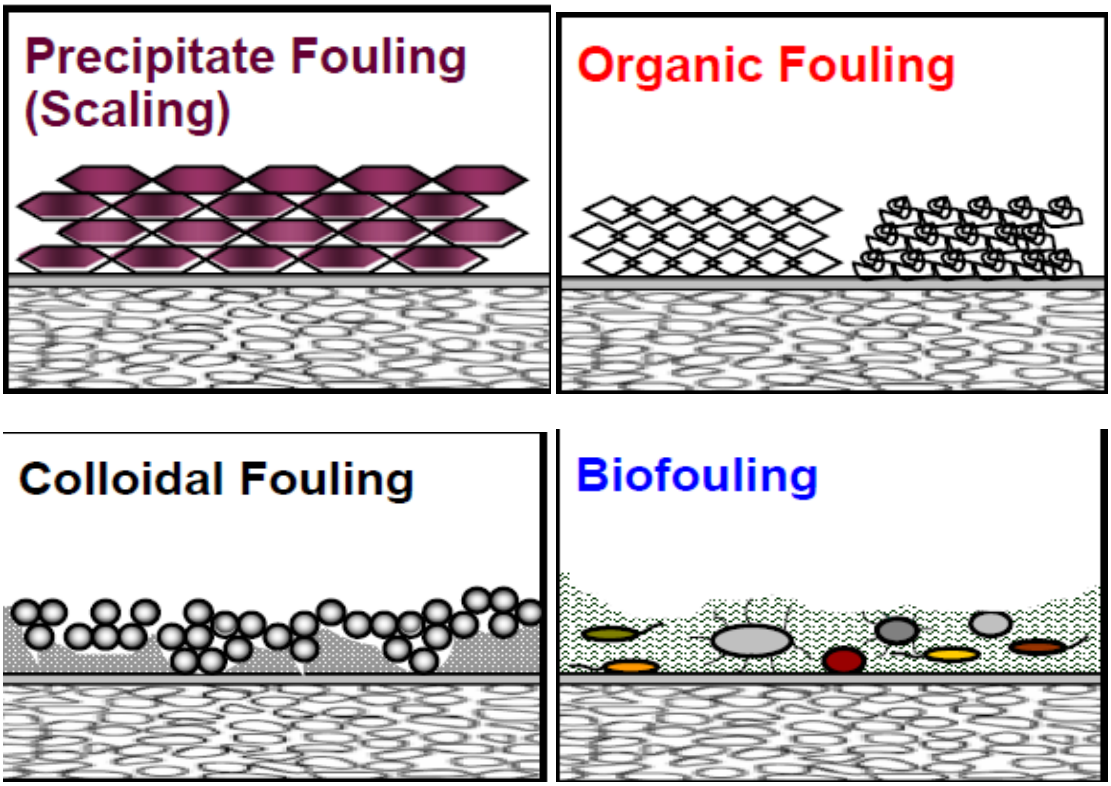

Figure 2.4 Schematic illustration of different fouling types in membranes (*Elimelech 2006*)

While the first three types of fouling can be reduced to a great extent through pretreatment, biofouling cannot be reduced by pretreatment alone [22], because deposited microbial cells can grow, multiply and relocate. Even if 99.99% of all bacteria are eliminated by pre-treatment (e.g. microfiltration or biocide application), a few surviving cells will enter the system, adhere to surfaces, and multiply at the expense of biodegradable substances dissolved in the bulk aqueous phase. Therefore, membrane

biofouling has been found to occur extensively on RO membranes even after significant pretreatment of the influent stream and the addition of disinfectants such as chlorine [23].

2.3 Biofouling

Biofouling is usually referred to the accumulation of microorganisms such as bacteria, algae and fungi on the membrane surfaces forming the biofilms (Fig. 2.5), via multi-step and complex formation process. Micro-organisms are present in nearly all water systems and are capable of colonizing almost any surface and have been found at extreme conditions such as temperatures from -12ºC to 110ºC and pH values between 0.5 and 13 [24]. They tend to adhere to surfaces and grow mainly at the expense of nutrients accumulated from the water phase. The attached micro-organisms excrete extracellular polymeric substances (EPS), in which they are embedded, and form biofilms. Thus, the originally dissolved nutrients are now locally immobilized and converted from solution into a semisolid state [25].

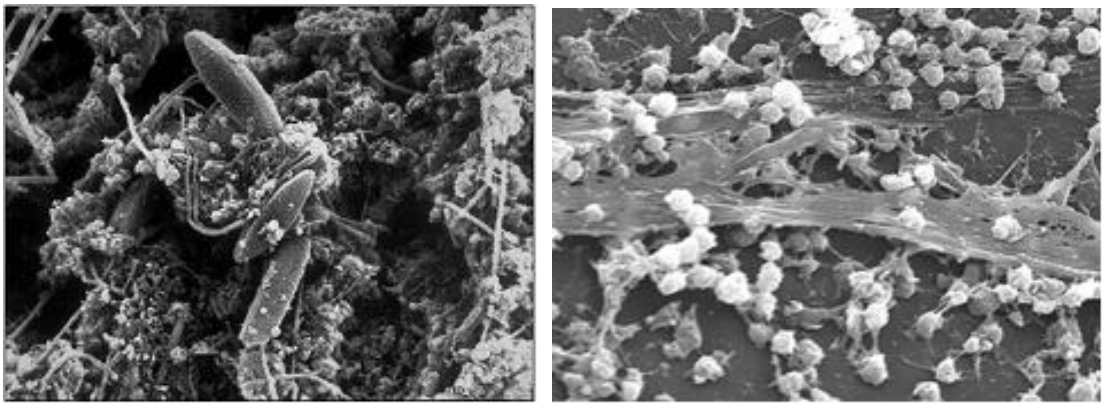

(a) (b)

Figure 2.5 SEM images of biofilms that developed on (a) a mild steel surface in an 8-week period in an industrial water system b) the inner surface of an indwelling medical device (Biofilms: Microbial Life on Surfaces, Rodney M. Donlan, *Emerg Infect Dis*. 2002)

Biofilms are composed primarily of microbial cells and EPS. EPS may account for 50 – 90% of the total organic carbon of biofilms and can be considered the primary matrix material of the biofilm. EPS may vary in chemical and physical properties, but consist primarily of polysaccharides, proteins, glycoproteins, lipoproteins and other macromolecules of microbial origin [21]. The physical properties of the biofilm are largely determined by the EPS, while the physiological properties are determined by the bacterial cells [26].

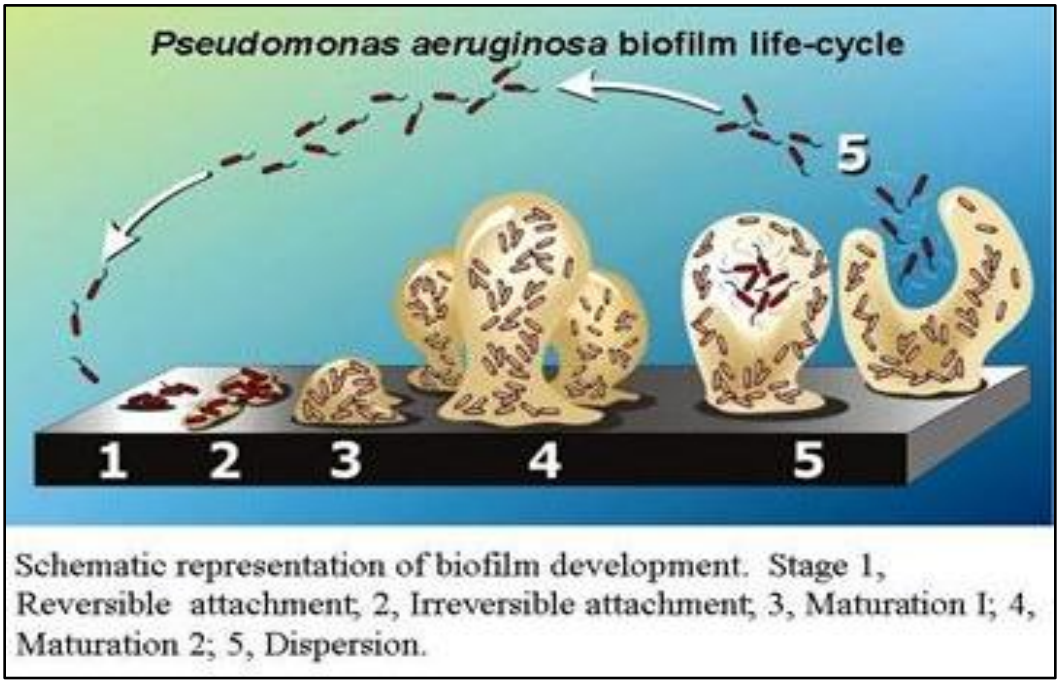

Schematic representation of biofilm development. Stage 1, Reversible attachment; 2, Irreversible attachment; 3, Maturation I; 4, Maturation 2; 5, Dispersion.

Figure 2.6 Different stages in the formation of a Biofilm (*www.biofilm.montana.edu/)*

Biofouling occurs through a cascade of events including the transport, deposition and adhesion of cells followed by exopolymer production, and cell growth and proliferation – all contributing to biofilm formation (Fig.2.6). Within seconds, surfaces immersed in water become covered with a so-called conditioning film consisting of both

organic macromolecules (humic substances, polysaccharides and proteins), and inorganic compounds [27]. The transport and attachment of suspended bacterial cells to a solid-liquid interface is the next step and probably the most crucial in biofilm formation. The next biofilm formation stage takes place by auto-aggregation of the attached cells and formation of microcolonies [28]. Once attached, cells begin to produce exopolymers, grow and multiply at the expense of soluble and sorbed feed water nutrients [29].

Biofouling occurs when biofilms are present in the wrong place and at the wrong times. In other words, biofouling may be considered as a "biofilm reactor in the wrong place". For example, in water purification membrane systems, biofilms participate in the separation process as a secondary membrane and give rise to many deleterious consequences (Fig.2.7) that include increased hydraulic resistance, decreased membrane permeability, enhanced concentration polarization, and decreased salt rejection [25].

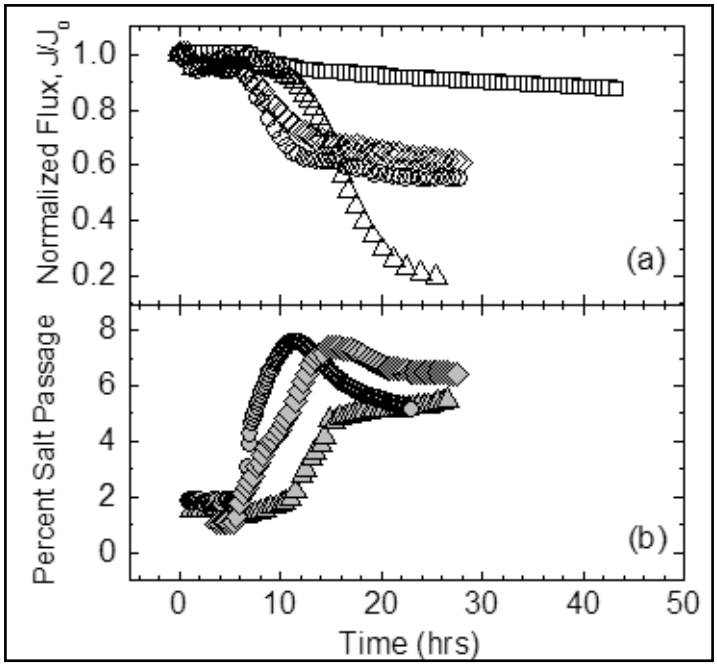

Figure 2.7 Consequences of membrane Biofouling (a) Permeate flux decline (b) Increase in salt passage (*Herzberg et al.* 2007)

Biofouling is operationally defined as biofilm formation resulting in an unacceptable degree of system performance loss e.g. excessive loss of thermal conductivity in cooling systems or increased fluid frictional drag in flow systems, etc. For a given performance parameter (e.g. water transport) a threshold value may be defined below which system performance is considered unacceptable. Characklis and Marshall defined biofouling as that amount or extent of biofilm formation that causes unacceptable operational problems.

An operational problem of a membrane installation is at hand when the increase in normalized pressure drop (NPD) across the membrane at constant flux is around 15-30%, or the decrease in normalized flux while operating at constant temperature and pressure exceeds 10% of the start-up values[9]. In either case, corrective actions are recommended by the manufacturers of membrane elements [30].

The critical issue of biofouling occurs because microbes are able to grow with tiny amounts of nutrients [31]. Moreover, biofouling has more significant impacts on decreasing the membrane flux, deteriorating the membrane structure, and increasing salt passage[32]. Current studies revealed that biofouling can cause more problems in membrane module, such as biofilm-enhanced osmotic pressure [33], feed spacer channel pressure drop [34] in conjunction with the well-known trans-membrane pressure drop. For these reasons, the means to minimize biofouling in RO membranes are always considered as high priority concerns in RO desalination plants from both engineering and fundamental viewpoints.

2.4 Effects of Biofouling on Membrane Processes

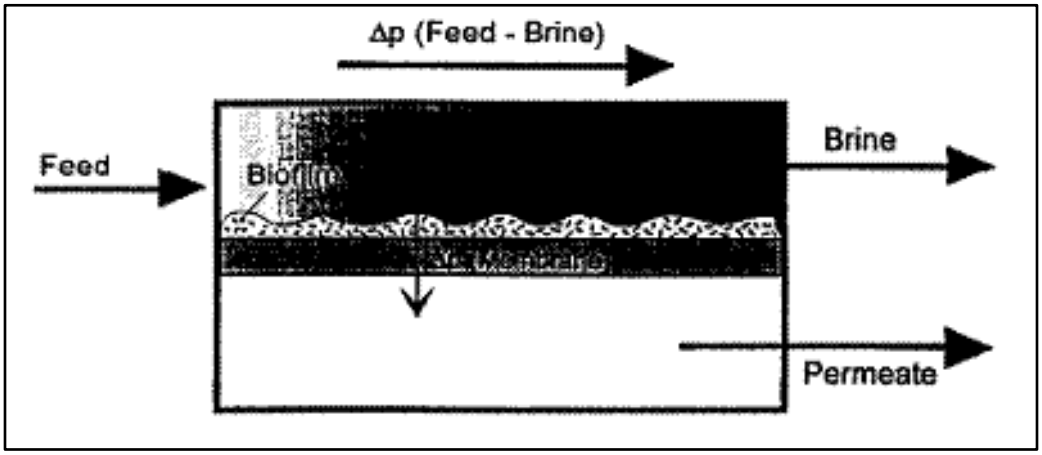

Figure 2.8 Schematic sketch showing the biofilm acting as a secondary membrane (Flemming, *Exp Therm Fluid Sci* 1997)

On a separation membrane, the biofilm matrix is a secondary membrane that participates dominantly in the separation process (Fig.2.8). The gel-like structure of the EPS matrix reduces the efficiency of convectional transport processes and causes a transmembrane pressure (TMP) drop that result in flux decline. Moreover, the rough, viscoelastic surface of the biofilm increases fluid frictional resistance and causes a feed-brine-pressure (FBP) drop.

Ridgway [35,36] and Flemming [29], after collecting several case histories, have summarized the consequences of biofilm development on membranes. In terms of process efficiency, the main concerns are the decline in permeate flux and decrease in salt rejection and are discussed in detail below.

2.4.1 Membrane Flux Decline

Flux decline may be rapid (e.g. several days) or more gradual (weeks to months), depending on the physicochemical and microbiological properties of the feed water,

membrane polymer, and biofilm. The kinetics of flux decline usually exhibit two phases (Fig.2.9); an initial rapid decline followed by a more gradual decay [37]. The initial rapid decline is typically correlated with the early attachment and proliferation of microorganisms on the membrane surface. The slow decline (plateau) phase results from establishment of an equilibrium condition in which biofilm growth and EPS production are balanced by biofilm loss (cell detachment or sloughing) caused by hydrodynamic shear at the solution-biofilm interface [29].

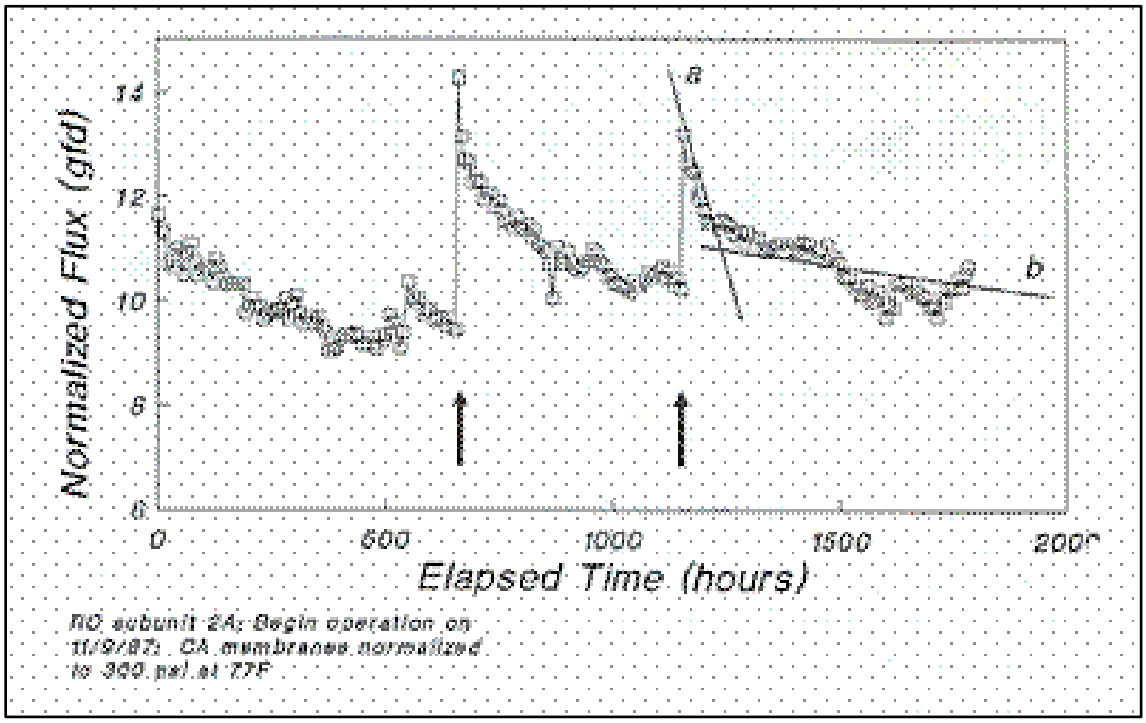

Figure 2.9 Flux decline data showing the two phases (*Ridgway & Flemming 1996*)

In most cases, the system pressure will be increased by an increase of the pump performance in order to compensate the flux decline due to the biofilm. This will result in an increase in energy consumption especially in large separation facilities (>$4x10^6$ L/day

capacity) where high electrical (pumping) costs are needed to maintain operating pressures and constant product output.

Although the molecular basis of flux decline is not very well understood uptil now, it is most probably related to water transport impedance (hydraulic resistance) offered by the biofilm itself, rather than to some modification of the inherent transport characteristics of the separation polymer. The biofilm functions as an independent diffusional transport barrier which retards convective fluid motion proximal to the membrane surface, a concept which is consistent with the hydrated gel nature of microbial biofilms.

2.4.2 Decrease in Salt Rejection

Separation processes based on the pressure-driven transport of water through a membrane inherently lead to accumulation of dissolved substances retained by the membrane at the raw water side. This phenomenon is known as 'concentration polarization' and is primarily responsible for a gradual increase in solute concentration of the RO permeate water. The development of a surface biofilm, consisting of an EPS matrix that suppresses turbulent mixing at the membrane surface, could be expected to extend and stabilize the viscous sublayer (i.e. boundary layer), where dissolved solutes tend to accumulate, thereby leading to an enhanced opportunity for concentration polarization (Fig. 2.10)

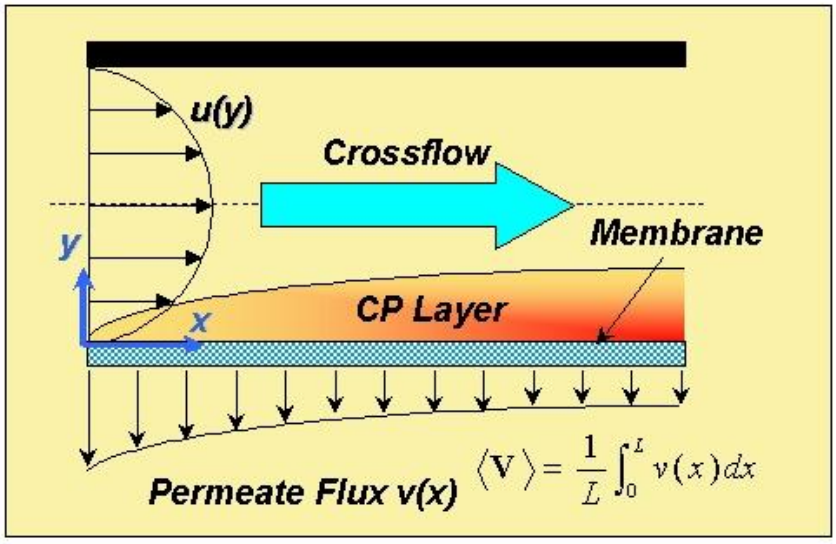

Figure 2.10 The phenomena of concentration polarization (*Bhattacharjee et al. 1999*)

As a result, solute transport through the membrane increases in response to greater ionic activity in the boundary layer. The increase in salt passage deteriorates the quality of the permeate water, making it unfeasible for drinking purposes. Another possible reason for the decrease in salt rejection is biodegradation or biodeterioration of the RO membrane. Bacteria, fungi and other microorganisms comprising biofilms may directly (via enzymes) or indirectly (via localized pH or redox potential changes) degrade the membrane polymer. Evidence for direct biodegradation of cellulose acetate membranes has been reviewed extensively by Cantor [38] and several other authors [39,40].

Murphy et al. [41] showed that (i) fungi identified and isolated from the RO industry, (ii) biofilms associated with field RO systems, and (iii) microorganisms introduced through contamination, were all capable of degrading CA membranes. Beverly et al.[42] confirmed biological deterioration of cellulose acetate RO membranes

by a combination of the FTIR spectra before and after exposure: the hydroxyl groups present initially were absent and amino groups had been introduced.

2.4.3 Module Elements

Biofouling of the feed channels and spacers (Fig. 2.11) in spiral wound elements increases fluid frictional resistance as water is transported tangential to the membrane surface, resulting in a higher module differential pressure (ΔP_{mod}) [43]. If the allowable differential pressure is exceeded, adjacent membrane leaves within the module may shift relative to one another, causing telescoping, or the element may collapse along its longitudinal axis. Even minor telescoping may cause abrasion of semipermeable membrane surfaces resulting in solute leakage.

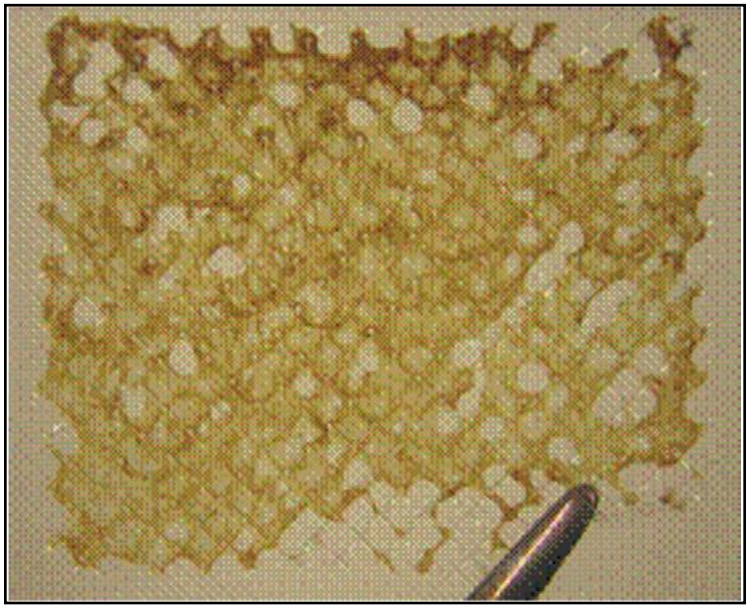

Figure 2.11 Feed spacer taken during autopsy of spiral-wound membrane module from a full-scale installation suffering from a prolonged elevated feed channel pressure drop. (*Vrouwenvelder et al. 2009)*

In a spirally wound element there is the possibility for some sections of the flow channel to become blocked such that the water flow will be concentrated in other parts of the feed channel. Channelling problems also arise in hollow fiber bundles when the individual fibers become bound together by foulant. Channelling causes rapid salt concentration in the affected areas. This leads to the precipitation of sparingly soluble salts such as $CaCO_3$ and $CaSO_4$, the latter being a specific problem with H_2SO_4 dosed feed waters.

2.5 Economic Consequences

A detailed assessment of the costs of Biofouling was made for the RO plant at Water Factory 21 in Orange County, CA [44]. In this plant, wastewater is reclaimed for reuse. It was assumed that the membranes at Water Factory 21, owing to the additional hydraulic resistance of the Biofouling layer, operate at about 150% of their initial operating pressure (about 200 psi) over 80% of their 4-year life to compute the added energy cost due to flux decline. This is probably a fairly realistic assumption.

It was further assumed that the $1 million membrane inventory should theoretically last 8 years instead of the observed 4 years. This amounts to an added cost of $125,000 per year due to Biofouling. About 8mg/L of combined chlorine is added continuously to the feed water. That amounts to about 77 tons per year at $25,000, all of which is for Biofouling control. Membrane cleaning was quite inexpensive, but that is only because the plant formulates its own cleaning solutions. The “bottom line” is $727,816 spent each year to control membrane Biofouling. That represents about 30% of the total operating costs for Water Factory 21.

2.6 Occurrence

Many seawater desalination facilities have been affected by membrane biofouling, including the large desalination plants at Ras Abu Jarjur, Bahrain [45] and at Saint Croix, US Virgin Islands [46]. Among 70 US reverse osmosis membrane installations surveyed by Paul, 58 reported having "above average" problems with membrane fouling, with biofouling representing the most common operational problem experienced [47]. In the Middle East, the region which produces the largest amount of desalted water in the world, about 70% of the seawater RO membrane installations suffer from biofouling problems [48].

2.7 Prevention & Control

Control of membrane biofouling is necessary not only during continuous plant operation, but also during extended periods of plant inactivity due to system repair or modifications. Biofouling must also be controlled when newly manufactured membrane modules are packaged and stored for long periods prior to shipping or installation. Figure 2.12 shows schematically the potential points of intervention in the membrane biofouling process:

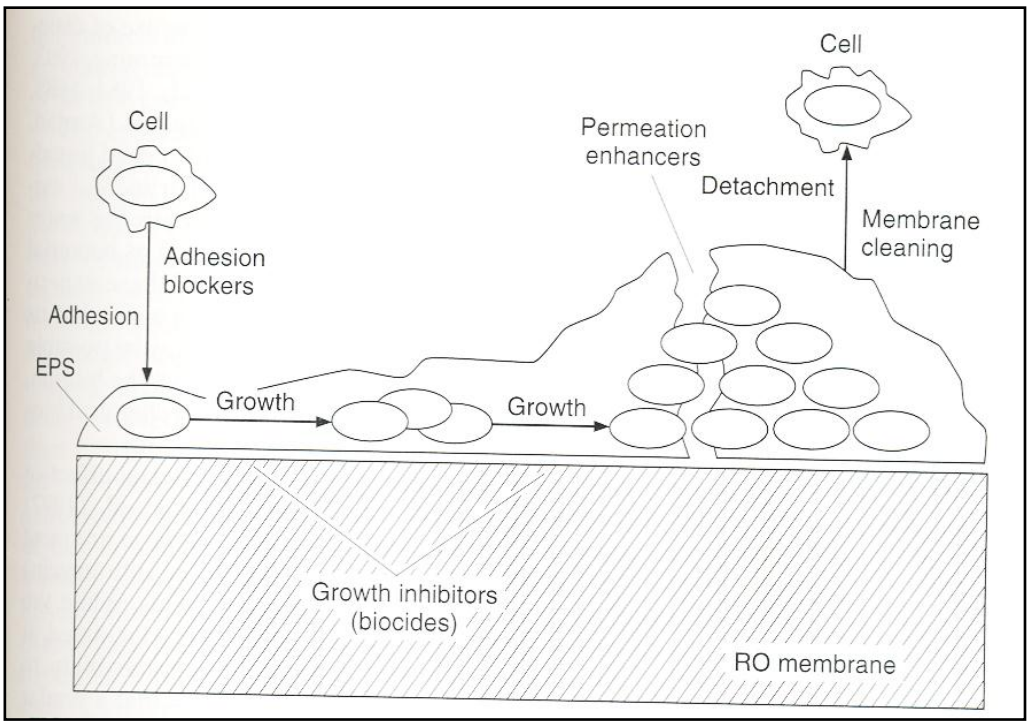

Figure 2.12 Schematic illustration showing potential points of intervention in the membrane biofouling process (*Water Treatment Membrane Processes*. McGraw – Hill, New York, pp. 6.1-6.62 1996)

Biofouling control strategies fall into the following general categories:

1) Selection and optimization of effective feedwater pretreatment methods,
2) Application of biocides or disinfectants,
3) Selection of most appropriate or desired surface modification of existing membrane

Biofouling and its control remains a major operating problem for many reverse osmosis (RO) plants, particularly those in tropical and sub-tropical regions. In the late 1990s, the following two strategies were strongly proposed for the prevention and control of membrane biofouling:

1. Physical removal of bacteria from the feed water of membrane systems (for example by microfiltration or ultrafiltration pretreatment), and

2. Metabolic inactivation of bacteria by applying biocide dosage or UV irradiation [49]

2.7.1 Feed Pretreatment

Processes involving the use of RO membranes (e.g. desalination) are generally composed of intake, pretreatment, reverse osmosis, and post-treatment. Pretreatment systems for RO plant are designed to produce feed water with a reduced fouling potential, by removing particulates, micro-pollutants and micro-organisms as well as preventing the formation of inorganic scales. Pretreatment is one of the most critical processes for successful operation of RO from previous experience since it may reduce the substances and bacteria which may cause membrane biofouling. Failure in pretreatment is incorporated into reduced flux, frequent chemical cleaning, and shortenend membrane life.

Pretreatment is carried out using either conventional or MF/UF membrane processes. A conventional process is composed of coagulation/flocculation, dissolved air flotation, granular media filter, and a dual media filter. Membrane pretreatment is known to be more effective than the conventional one as the former is able to obtain a lower silt density index (SDI) to inhibit biofouling [50]. In addition to obtaining feed water of superior quality (i.e. lower SDI), membrane pretreatment systems generally require less space and chemicals compared to the conventional pretreatment systems [51,52,53].

Achieving stable RO water quality with conventional pretreatment systems on complex feedwaters is difficult [54]. Schneider et al. [55] investigated the efficiency of each unit operation of a conventional pretreatment system in the removal of the major parameters contributing to biofouling. They found that none of the treatment stages

achieved a significant log-scale reduction of microbial numbers. Infact, the Granular Activated Carbon (GAC) filters were a major source of microbial contamination and chlorination was the most important contributor to Assimilable Organic Carbon (AOC) in the plant.

A major limitation of pretreatment is its inability to eliminate microorganisms present in the feed water intake. This means that even if a handful of bacteria are present, they will ultimately attach to the membrane surface, grow and multiply, produces the EPS matrix and result in membrane Biofouling.

2.7.2 Biocide Application

The conventional antifouling strategy is to use continuous dosage of biocides. Biocides are disinfecting agents which are capable of inactivating micro-organisms. There are two main applications of biocides in membrane systems. First, a biocide may be added continuously or intermittently (e.g., via a metering pump) to the system feedwater in an attempt to suppress or otherwise control the unrestricted growth of biofilm microorganisms on the membrane surfaces.

A second general application of biocides is in the preservation of the polymer membranes and related module components (e.g., glues, plastic spacers, other materials of construction) during extended periods of membrane storage or plant shutdown. The most popular and effective biocides that have recently gained attention are chlorine, ozone and UV radiation.

It has been standard practice to control biological growth in the feedwater by the use of chlorine. Free chlorine (i.e. HOCl, OCl^-) has been dominantly used to inactivate

microbial growth for the SWRO process. It has been reported that biofilm formation was related to the depletion of residual disinfectant concentration, and that no biofilm was formed using chlorinated water containing a residual of 0.04-0.05 mg/L free chlorine [56]. Other forms of chlorine that have been successfully used to control microbial growth include chloramines [57] most notably monochloramine (NH_2Cl) and chlorine dioxide (ClO_2) [58].

The challenges using free chlorine as a biocide are related to its strong oxidation potential and possible chemical attack of the amide functional group in the polyamide RO membrane [59,60,61]. Moreover, chlorine addition and dechlorination processes are known to occasionally enhance severe Biofouling [62,63]. In addition, chlorination results in the generation of carcinogenic by-products such as trihalomethanes (THMs) and halo acetic acids (HAA) [64].

Ozone has been widely used as a disinfectant for drinking water treatment because it has a very strong oxidation potential, produces fewer halogenated disinfection by-products, and oxidizes iron and manganese dissolved in water. It has been shown to be effective against biofilms and toxic by-products are formed comparatively to a much lesser extent [65]. Ozone weakens the biofilm matrix and thus, facilitates the removal of biomass by shear forces [66]. Koyuncu et al. [67] found that ozonation combined with GAC pretreatment reduced membrane fouling to the greatest extent in both dead end and cross-flow filtration tests.

However, a major disadvantage is that the costs for ozone generation are about fourfold higher than those of chlorine. Moreover, due to its strong oxidizing properties it

is known to break down the membrane surface. Ozonation of seawater has found to generate bromine compounds that are both carcinogenic and deteriorate the membrane surface [68,69]. In a microfiltration study, the presence of ozone caused the breakdown of larger molecular weight organic matter that favored micro-organism growth and thus accelerated biofouling [70].

2.7.3 Membrane Cleaning

Cleaning is defined as "a process where material is relieved of a substance, which is not an integral part of the material" [71]. In general, much of the decline in membrane performance can be corrected by cleaning the membrane [72,73]. The objective of the cleaning processes is to restore membrane performance when it falls below the expected permeate yield typically by about 10%, or feed pressure increase by about 10% and/or differential pressure increase by 15–50% [74,75]. In general, around 5–20% of the operating cost is the cost of cleaning [76].

The mechanical stability of biofilms is overcome in a two-step process [25]: i) weakening of the biofilm matrix by the use of appropriate chemicals that interfere with the bonding, ii) removal of the biofilm from the membrane surface by shear forces. A large number of chemical cleaning agents are commercially available, and the commonly used ones fall into six categories: alkalis, acids, metal chelating agents, surfactants, oxidation agents and enzymes [77,78,79].

Although usually effective in Biofilm removal and the restoration of the baseline flux levels, membrane cleaning has the following disadvantages:

i. It is very expensive due to the chemicals used

ii. Consumes a lot of time

iii. Shortens membrane life and hence accelerates the need for replacement

2.7.4 Membrane Surface Modification

As mentioned earlier, the important stages in biofilm formation are bacterial adhesion, microcolony formation, and biofilm maturation. Membrane surface modification is done primarily to prevent or retard one or more of these stages. For example, bacterial adhesion has been found to decrease significantly by making the surface more hydrophilic (Fig.2.13), negatively charged and/or smooth [80 , 81]. Similarly, inactivation of irreversibly adhered microorganisms can be achieved by a few different methods that include the incorporation of antimicrobial nanomaterials (Fig.2.14) [82] and self-assembling peptides that disrupt bacterial membranes [83].

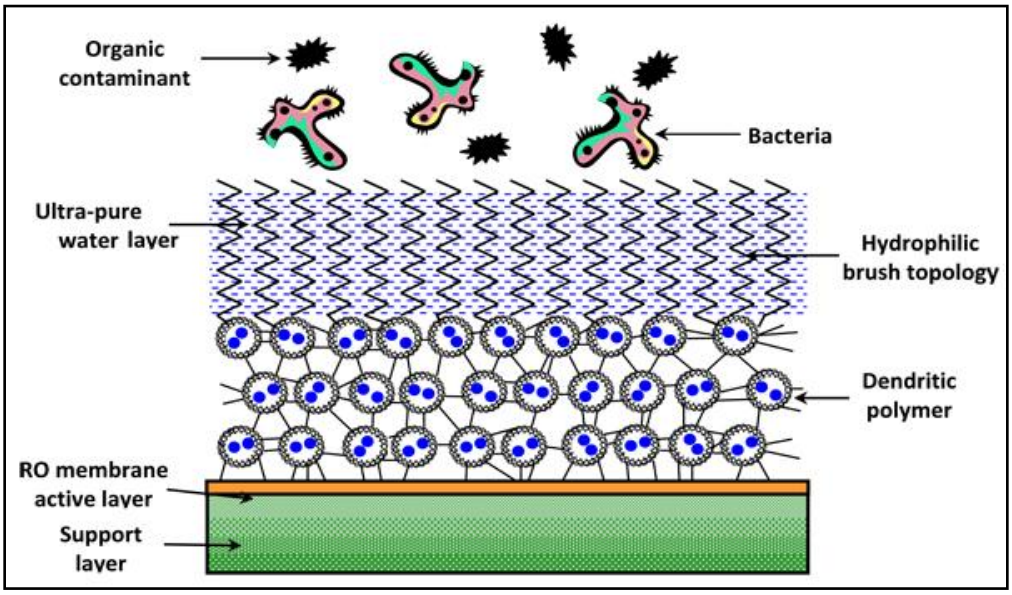

Figure 2.13 Membrane surface modification by increasing hydrophilicity (*www.mmi.org)*

Numerous methods for membrane surface modification have been examined in order to increase surface hydrophilicity [84,85]. These methods include blending with hydrophilic polymers, surface modification by grafting hydrophilic monomers [86] and surface coating. However, most of these requires complex multiple steps, involve the use of chemicals and are time consuming, which restricts their application.

Incorporation of Nanomaterials

The rapid growth in nanotechnology has spurred significant interest in the environmental applications of nanomaterials. In particular, its potential to revolutionize century-old conventional water treatment processes have been enunciated recently [87]. More recently, several natural and engineered nanomaterials have been shown to have strong antimicrobial properties, including chitosan [88], silver nanoparticles [89], photocatalytic TiO_2 [90], aqueous fullerene nanoparticles [91] and carbon nanotubes [92].

Due to the presence of a wide variety of and the diversity in the properties of contaminants in water, multiple stages of treatment (e.g. pretreatment, biocide application, etc.) are essential to minimize/delay fouling. By the proper incorporation of antimicrobial nanomaterials, membranes become more “reactive” instead of a simple physical barrier, making it possible to achieve multiple treatment goals in one reactor while minimizing fouling.

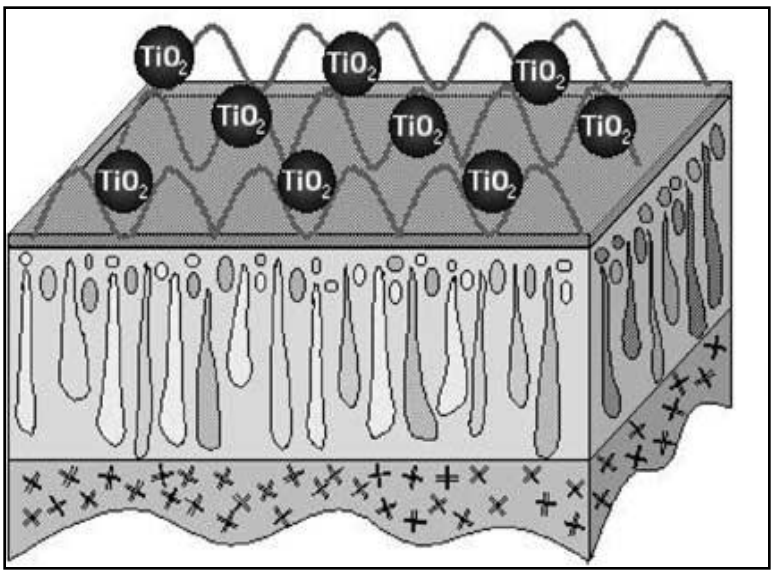

Figure 2.14 Self-assembly of a layer of TiO_2 nanoparticles on the membrane surface (*Kim et al. 2003*)

Titanium dioxide (TiO_2) has been the focus of numerous investigations in recent years, particularly because of its photocatalytic effects that decompose organic chemicals and kill bacteria [93]. TiO_2 photocatalysis is known to generate various active oxygen species, such as hydroxyl radical (OH), hydrogen peroxide (H_2O_2), etc. by reductive reactions or oxidative reactions under light [94]. These active oxygen species further destroy the outer membrane of the bacterial cells and decompose the endotoxin from them.

Kwak et al. [95] fabricated hybrid organic/inorganic RO membranes composed of aromatic polyamide thin films underneath TiO_2 nanosized particles by a self-assembly process, with the aim of discouraging biofouling problems. The antibacterial fouling potential of the hybrid membrane was examined and verified by measuring viable cell numbers and survival ratios of the *E. coli* as a model bacterium, both with and without UV illumination. The photocatalytic bactericidal efficiency was remarkably higher for

the TiO_2 hybrid membrane under UV illumination, compared to that of the same membrane in darkness, as well as those for the neat membranes under either light condition.

Kim et al. [96] prepared a similar hybrid membrane with TiO_2 nanoparticles and in addition to that also introduced the nanoparticles on an actual commercial RO membrane (Fig. 2.14). The results of the survival ratios of *E. coli* in both the hybrid and bare membranes with and without UV illumination showed that the TiO_2 nanoparticles accelerate the sterilization effects of UV light. In addition, comparison of relative flux declines showed that the bare membrane lost around 30% of its original water permeability whereas the decrease is a mere 10% for the hybrid membrane under UV illumination.

Silver compounds and ions have long been known to possess strong inhibitory and bactericidal effects as well as a broad spectrum of antimicrobial activities [97,98,99]. It is generally believed that silver ions reacting with thiol (-SH) groups in microbial cells play an essential role in bacterial inactivation [97]. In addition, it has also been shown that Ag^+ ions prevent DNA replication and affect the structure and permeability of the cell membrane [100].

Yang et al. [101] proposed an innovative biofouling control approach by surface modification of not only the actual RO membrane but the feed spacer as well with a coating of nAg. The results showed that both silver-coated membrane (Ag-cM) with uncoated spacer and silver-coated spacer (Ag-cS) with uncoated membrane performed

better than the unmodified membrane and spacer, in terms of much slower decrease in permeate flux.

Several challenges exist for efficient application of antimicrobial nanomaterials in membrane filtration, primarily concerning dispersion and retention of nanomaterials and the sustainability of antimicrobial activity. Retention of nanomaterials is critical not only because ofthe cost associated with loss of nanomaterials, but also, and more importantly, because of the potential impacts of nanomaterials on human health and ecosystems [102,103].

Because most studies on antimicrobial activities of nanomaterials were conducted in relatively simple and clean solutions, the sustainability of their antimicrobial activities in natural or waste water, whose constituents may interfere with the nanomaterial–microbe interactions, is unclear. When coated on surfaces to prevent microbial attachment and biofilm formation, antimicrobial nanoparticle coatings may rapidly lose their effectiveness due to adsorption of extracellular polymeric material and occlusion by precipitating debris [104].

Confusing surfaces

It is believed that surfaces with compositional heterogeneities on the length scale of the foulant of interest may discourage thermodynamically favorable interactions between the foulant and the surface, which in turn would limit adsorption events. Such heterogeneities are usually presented by amphiphilic films incorporating components with very different surface energies. For example, hyperbranched fluoropolymers (HBFP) crosslinked with polyethyleneglycol (PEG) phase segregate when cast as a thin

film; the HBFP-rich phase presents a low surface energy domain, and the PEG-rich phase presents a high surface energy domain.

Recently, Baxamusa and Gleason [105] demonstrated that copolymerization of the hydrophilic hydroxyethylmethacrylate (HEMA) with the hydrophobic perfluorodecylacrylate (PFA), resulted in a dynamic surface structure with nanoscale compositional heterogeneities (Fig.2.15). Furthermore, they showed that a representative protein, bovine serum albumin (BSA), adsorbed significantly less on an intermediate composition of the copolymer (~40% PFA), than on the HEMA and PFA alone (Fig.2.16). Proteins are an important foulant class, since adsorbed proteins can subsequently recruit cells or microorganisms to the surface, so surfaces that resist protein adhesion can potentially block other foulants as well.

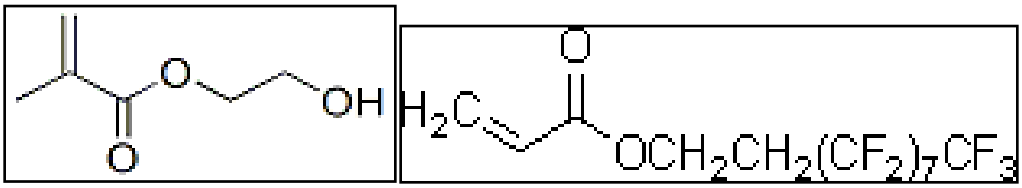

Figure 2.15 Molecular structure of the HEMA-PFA copolymer

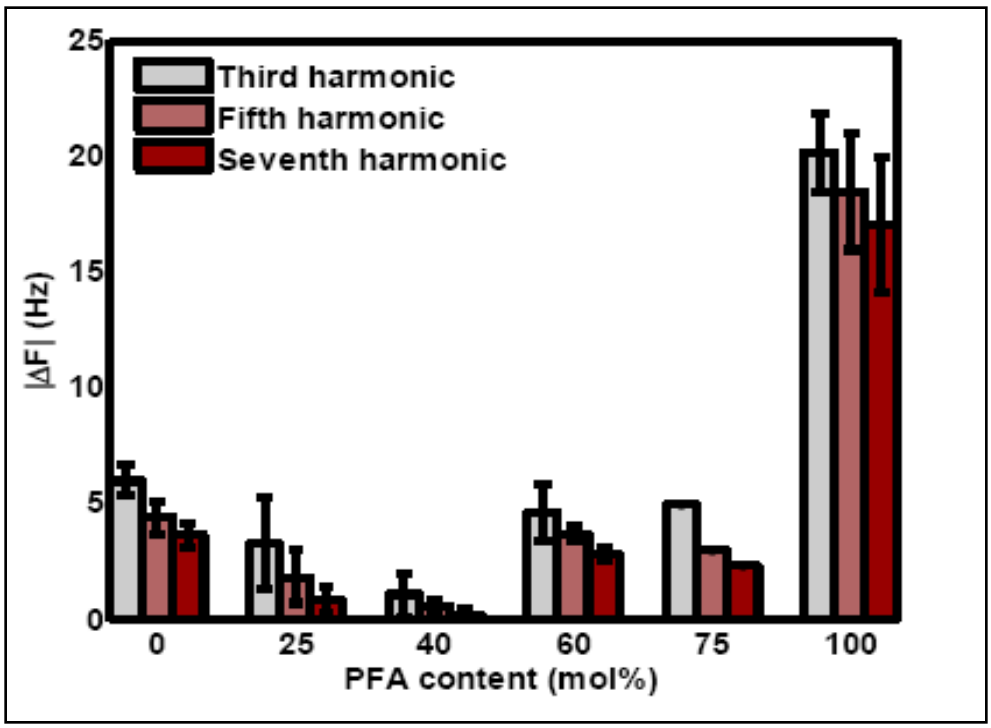

Figure 2.16 QCM results showing the adsorption of protein with varying copolymer chemistry (*Baxamusa et al. 2009*)

Chapter 3. Initiated CVD of polymer thin films

3.1 Introduction

Thin film technologies have advanced significantly over the last several decades, becoming one of the major components of electronic, medical or energy related industries [106,107] . As free standing structures, two-dimensional thin films have advantages over the bulk materials due to their large surface-to-volume ratios, desirable for applications requiring enhanced surface interactions. Thin films can also be employed as coatings over bulk materials to achieve application specific properties that are unattainable in the substrate material.

With the advance of polymer thin film deposition techniques, polymer films continue to garner more recognition in the thin film industry that historically has been dominated by inorganic films [108]. A polymer is a long chain organic molecule composed of one or more type of monomer. The organic nature of the polymer thin films makes them invaluable for biomedical applications and the ability to tune the response of the films by functionalization significantly expands the application areas of the polymer thin films [109,110]. Furthermore, the mechanical robustness, ease of processing and the low cost of the polymer thin films are desirable characteristics for industrial applications.

Liquid-phase techniques for polymer synthesis, such as ink-jet printing, spin-coating or dip-coating are widely employed due to the ease of scaling up and low cost of the overall process [111]. However, these processes generally require the use of solvents that may have adverse effects on the deposition process, such as the degradation of the underlying layers or alteration of the mechanical properties of the delicate substrates.

Coating high-aspect ratio structures poses additional challenges arising from de-wetting and surface tension, leading to non-uniform coatings, in which the coating solution runs down sidewalls, pools at the bottom of features, and pulls away from edges, leaving them uncoated. Furthermore, the impurities introduced to the system by the solvent leads to defective films that are not suitable for high-purity applications. The drying process of solvent droplets can also lead to the inhomogeneous deposition of solutes, often in regions at the edge of the drop [112].

The challenges caused by the liquid-phase techniques can be overcome by using chemical vapor deposition (CVD) technique where the precursors are introduced to the surface in the vapor phase and the polymerization takes place directly on the surface [113].

The CVD technique has been the most commonly employed thin film deposition technique in the industry for the deposition of inorganic thin films, due to the robustness and the low cost of the process [114]. CVD of inorganic films requires high substrate temperatures and high powers which would damage the functional groups of the polymer and lead to undesirable cross linking, therefore, CVD is traditionally not compatible with polymer thin film deposition. However, through modifications on the CVD reactants or reactor designs, polymer depositions at low temperatures and low energy inputs can be achieved, making CVD a widely used technique for polymer deposition [115].

CVD polymerization utilizes the delivery of vapor-phase monomers to form chemically well-defined polymeric films directly on the surface of a substrate. CVD polymers are desirable as conformal surface modification layers exhibiting strong retention of organic functional groups, and in some cases, are responsive to external

stimuli. Traditional wet-chemical chain- and step-growth mechanisms guide the development of new heterogeneous CVD polymerization techniques.

3.2 Initiated CVD

Initiated CVD is a one-step film-growth method which draws on the chemistry of free-radical chain-growth polymerization (Fig.3.1). An initiating species is introduced through the gas phase along with the monomers. The initiator is selectively decomposed to free radicals through gas-phase heating [116]. High-rate deposition of true linear free-radical polymer chains can be achieved by iCVD with essentially 100% functional retention.

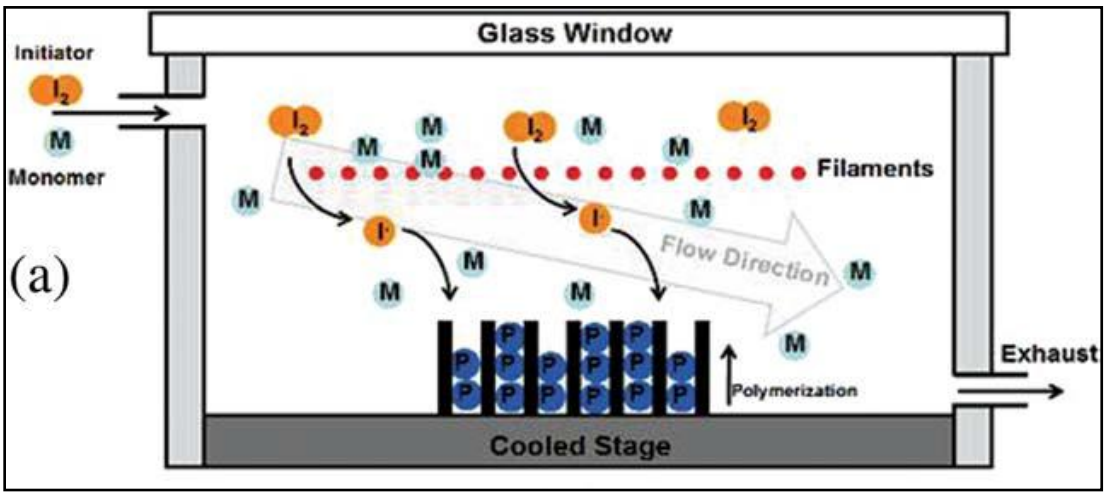

Figure 3.1 Side-view schematics of a typical iCVD reactor configuration showing the mass transfer and reaction processes during iCVD (Lau et al. *2008*)

The iCVD method conformally coats high-aspect-ratio structures at high deposition rates (Fig.3.2), enabling conformal layers to be deposited using a wide range of polymers. Microparticles and nanotubes were conformally encapsulated with iCVD PGMA [117]. The related method of piCVD, produced conformal hydrophilic coatings on microspheres [118].

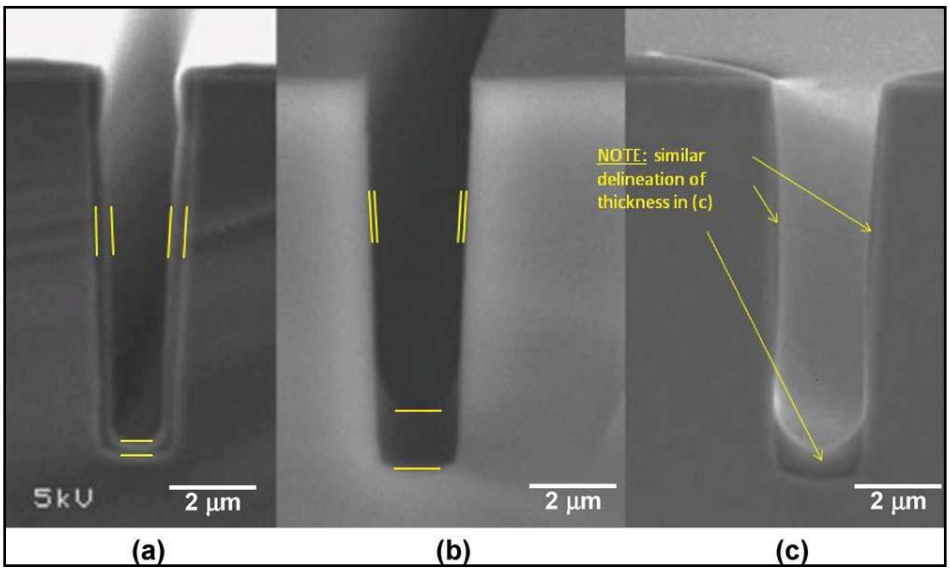

Figure 3.2 Conformality of an iCVD film (left) is better than both spin-casting (middle) and plasma deposition (right). (*Montero et al. 2008*)

The iCVD method, which is capable of synthesizing linear polymeric chains at high deposition rates from commercially available monomers, has successfully been used to synthesize many distinct homopolymers, random copolymers, and alternating copolymers using free-radical polymerization. Ultra-hydrophobic, hydrophilic, chemically resistant, hydrogel- and peptide-functionalized polymer surfaces have all been produced via iCVD.

The method of initiated CVD provides a close translation of free-radical polymerization to heterogeneous, solventless chemistry [119]. The monomer(s) and the initiator, both in the vapor phase, flow into a reactor held at mild vacuum [116]. The first step is the dissociation of the initiator to create free radicals, which occurs in the vapor phase. These radicals are transported to the surface where they initiate the free-radical

polymerization reaction with the adsorbed monomers. The chain is terminated upon contact with another free radical, whether it is another live chain or a dissociated initiator molecule (Fig.3.3)

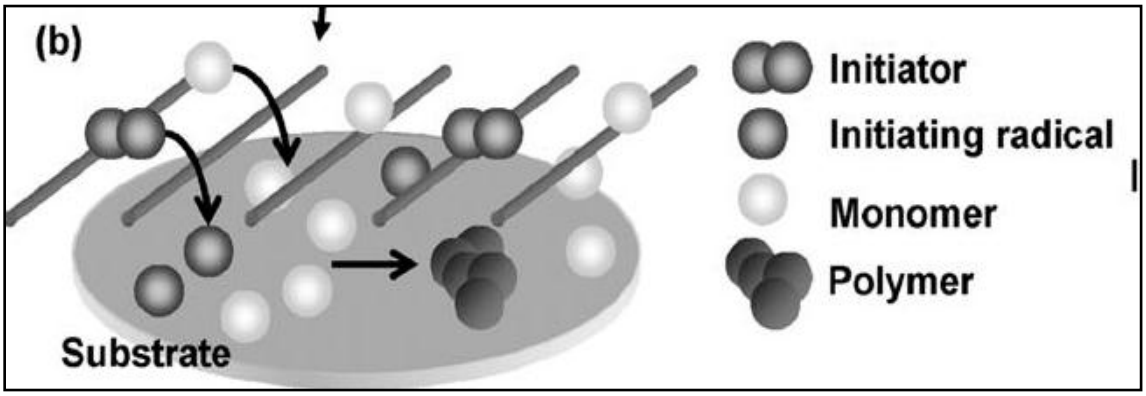

Figure 3.3 Depiction of the iCVD mechanism. The initiator passes through the hot zone around the filaments and thermally dissociates to form two initiating radicals. The monomer passes through the hot zone unaffected and adsorbs on the surface. The initiating radicals combine with surface-adsorbed monomer to form polymer. (*Baxamusa et al. 2009*)

iCVD follows the mechanism and kinetics of free-radical polymerization, but as a surface reaction that also includes adsorption/desorption equilibria. Infact, using the surface concentrations, the propagation and chain termination rate constants are very similar to those measured in solution-based systems. Additionally, *i*CVD copolymerization results in similar reactivity ratios as those observed in solution systems when the surface concentrations of the comonomers are considered.

Most iCVD takes advantage of the thermal decomposition of the initiator, achieved upon contact with a resistively heated filament array in the vacuum chamber. Thermal initiators for iCVD include triethylamine, *tert*-butyl peroxide, and *tert*-amyl peroxide. The filaments are heated to a temperature high enough for the decomposition of

the initiator, but low enough to preserve the integrity and functionality of the monomer. The filament temperature is as low as 200 – 300°C for the initiator TBPO (Fig.3.4).

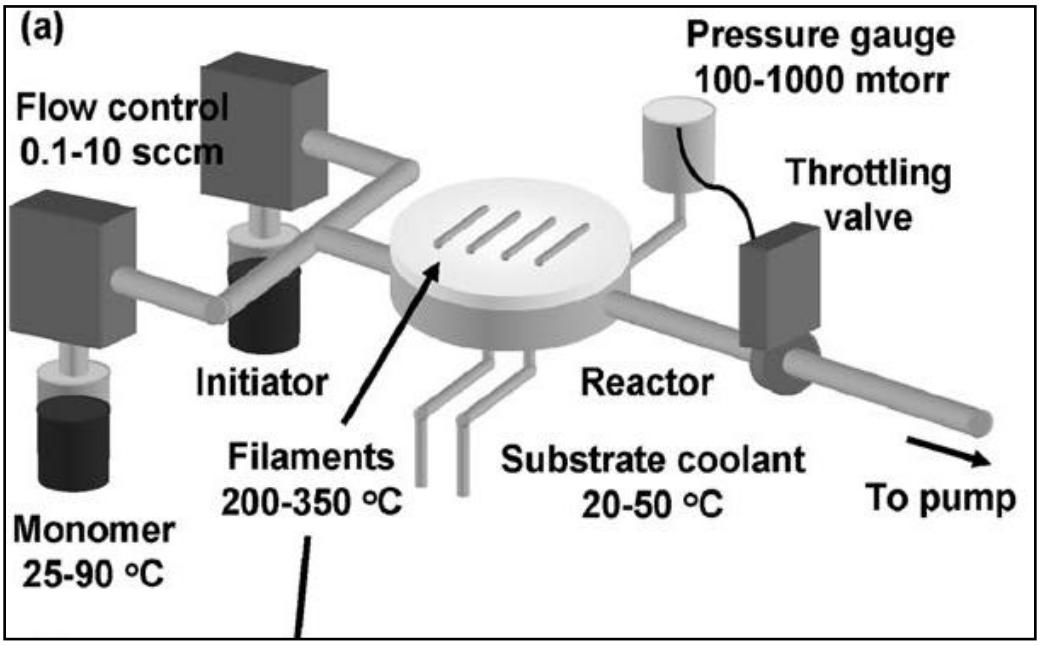

Figure 3.4 Schematic of the iCVD reactor and typical operating parameters (*Baxamusa et al. 2009*)

The advantages associated with the iCVD of thin polymeric films are numerous (Fig.3.5). The most notable of these include, but are not limited to, conformal and continuous coverage, precise control of film thickness and chemistry, negligible damage to the substrates, and almost complete retention of organic functionality. These are directly a consequence of the unique characteristics associated with this particular technique such as solvent-free nature, vapor phase process and operation at ambient temperature and pressure conditions

Process Characteristic	Advantage
Solvent-free	Easy stacking of polymeric films Limited damage to the substrate Copolymerization with immiscible monomers Reduced waste generation
Vapor-phase	Conformal coverage One-step film formation Extremely low level of impurities Tunable film properties
Uniqueness of iCVD/oCVD	Retention of organic functionality Applicability of various monomers Scalable Mild, low power processes
Use of polymeric materials	Low cost Flexible Wide variety of functional groups Well-known structure-property relationships

Figure 3.5 Summary of the advantages associated with the *i*CVD process (*Im et al. 2011)*

Chapter 4. Experimental Materials & Methods

4.1 Materials

Commercial RO Membranes

Commercial thin film composite polyamide RO membranes were kindly supplied by Sterlitech Corporation (Kent, WA). These included TFC-HR from Koch, UTC-80B from Toray and TF-RO-AD from GE Osmonics. The TFC-HR is a brackish water membrane featuring high salt rejection and also used for organics reduction. On the other hand, the remaining two are standard seawater desalination membranes. Table 4.1 outlines the specifications for these membranes as provided by the manufacturer:

Table 4.1 Specifications of the commercial membranes

Designation	**Manufacturer**	**Performance Parameters**		
		Salt rejection (%)	Flux ($L/m^2.h$) at 800psi	pH range
TFC-HR	Koch	99.5	140	4-11
UTC-80B	Toray	99.8	27.1	2-11
TF-RO-AD	GE Osmonics	99.5	25.43	4-11

Monomers

Surfaces of pure poly(HEMA) and poly(PFA) have water contact angles of 17° and 130°, respectively, reflecting their very different surface energies [120]. HEMA is hydrophilic due to its pendant hydroxyl (Fig. 4.1), and PHEMA is commonly used in applications where high water content is important, such as in contact lenses, wound dressings, and other physiological systems. In contrast, the fluorinated alkyl side chain of PFA (Fig. 4.1)

is highly hydrophobic and has a surface energy lower than PTFE, commonly known as Teflon.

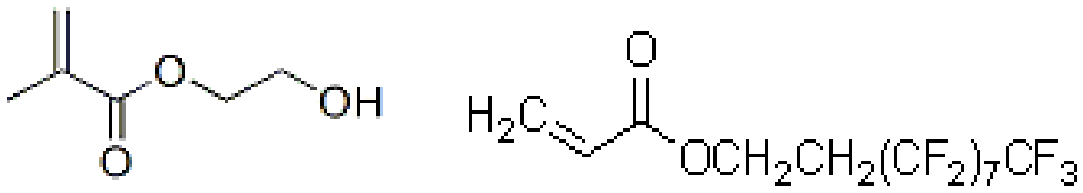

Figure 4.1 Molecular structures of the monomers (a) HEMA (b) PFA

4.2 Methods

4.2.1 Film Deposition

The two monomers, HEMA and PFA, were utilized without further purification. They were heated in separate crucibles to 80°C and 85°C, respectively. Vapors of each monomer were metered through mass flow controllers. Various copolymer chemistries were obtained by adjusting the relative flow rates of the two monomers. Since, the PFA molecule is the heavier of the two, the flow rate for PFA was kept constant around 2 sccm. The flow rate of HEMA was varied according to the copolymer film composition required.

Prior to the actual deposition itself, calibrations of flow rates were performed for both monomers and the initiator, TBPO. This was done by flowing each of the components individually into the reactor and waiting until the pressure inside reached a steady-state value of 2mtorr. The butterfly valve was then opened and the pressure inside recorded after every 5 seconds. The pressure values were then plotted on a graph and an average value of the flow rate determined from the slope. This procedure was repeated until an almost uniform value obtained for a certain opening of the needle valve.

The vapors met and mixed at a common manifold prior to entering the reactor. A throttling butterfly valve (MKS, 653B) was used to control the pressure inside the chamber at 100mtorr (1 Torr = 133.32 Pa). The film was deposited on a silicon wafer (Waferworld) maintained at 35°C by backside contact with a temperature-controlled stage. Film growth was monitored in situ through interferometry, and growth was terminated at approximately 30nm. Typical film growth rate was on the order of 10nm/min.

4.2.2 Copolymer Film Characterization

Ellipsometry

The composition and thickness of the deposited copolymer films were determined by measuring the refractive index at a wavelength of 633 nm, as determined by ellipsometry, and linearly interpolating based on the measured refractive indices of the pure PHEMA and PPFA homopolymers. The silicon wafer sample placed inside the reactor during the deposition was used for this particular measurement.

The ellipsometer is first calibrated using a standardized wafer. After this, the sample is placed on the stage and aligned to the beam. A spectroscopic scan is taken in the depolarization mode. A scan is taken at 3 different angles: 65°, 70°, and 75°. This data is then fit to a specified computer model. The model gives the index of refraction for the sample at different wavelengths of light. A wavelength of 633nm is chosen in this case.

A computer model of the sample is constructed by using predefined substances in the computer database. A silicon wafer has a very thin layer of Silicon dioxide (~2nm) on its surface. The predefined substances used are Silicon, Silicon Dioxide, and Cauchy.

Cauchy simply means any unknown material which is not present in the database. In our case, Cauchy represents the copolymer film.

The model is as follows. Layer 0: Silicon (1 mm), Layer 1: Silicon Dioxide (2.5 nm), and Cauchy (variable thickness in nm). The thickness you input for Cauchy should be the approximate thickness you determined by interferometry. Once the scan data is fit to this model, the actual thickness and index of refraction for the Cauchy will be given.

Copolymer composition is determined using the two homopolymer 633 nm indices of refraction and the copolymer index of refraction.

$$\%PFA = 100 * \frac{\eta_{co} - \eta_{HEMA}}{\eta_{PFA} - \eta_{HEMA}} \qquad \textbf{Equation (4.1)}$$

Atomic Force Microscopy

Surface topology of modified and unmodified membranes was examined by Atomic Force Microscopy (AFM). A Digital Instruments Dimension 3100 with a Nanoscope IV controller (Woodbury, NY) was used in tapping mode to image the surface and collect roughness data. 300 kHz Silicon NCH tips (Veeco Metrology, Inc.) were used to scan a 10 μm x 10 μm area with 256 lines scanned at a rate of 1.0 Hz.

Surface Composition

X-ray photoelectron spectroscopy (XPS) was used to detect the presence of coatings on the membrane surface. Samples were dried under vacuum overnight before analysis. An Axis Ultra DLD XPS, (Kratos Analytical Inc, Chestnut Ridge, NY) equipped with a monochromatic Al Kα1,2 X-ray source performed a surface scan at 0° take-off angle to

detect carbon, oxygen, and/or fluorine. Operating conditions were: $2x10^{-9}$ Torr chamber pressure; 15 kV; 150 W for the Al X-ray source. A charge neutralizer was used to minimize surface charging during testing.

At these operating conditions, the penetration depth was approximately 10 nm, and the spot size analyzed was approximately 300 μm x 700 μm. However, the XPS results were only used to provide relative amounts of C, O, and/or F on the membrane surface. The samples were submitted for analysis to the Center for Materials Science & Engineering (CMSE) at the Massachusetts Institute of Technology. Reported results were based on at least two samples. The typical uncertainty for XPS measurements is ± 1 wt%.

Contact Angle

Hydrophilicity was measured using a goniometer equipped with an automated dispenser (Model 500, Rame-Hart). A droplet of water (20μL) was placed on the surface, and the static angle was measured immediately. In order to probe the effects of surface reconstruction, the receding angle was measured by allowing this droplet to dry in an ambient environment. The contact angle was monitored as the droplet volume decreased. In all cases, the water contact angle initially decreased as the droplet volume decreased.

Scanning Electron Microscopy

Scanning electron microscopy (SEM) was done to image uncoated and coated RO membranes. The samples were sputter coated for 15-20 min using an Au target to deposit a film of 5-10 nm in thickness. Images were taken on an SEM (Philips) at 10 kV and with a working distance of 5-7 mm.

Chapter 5. Permeation Studies

5.1 Solution-Diffusion Theory

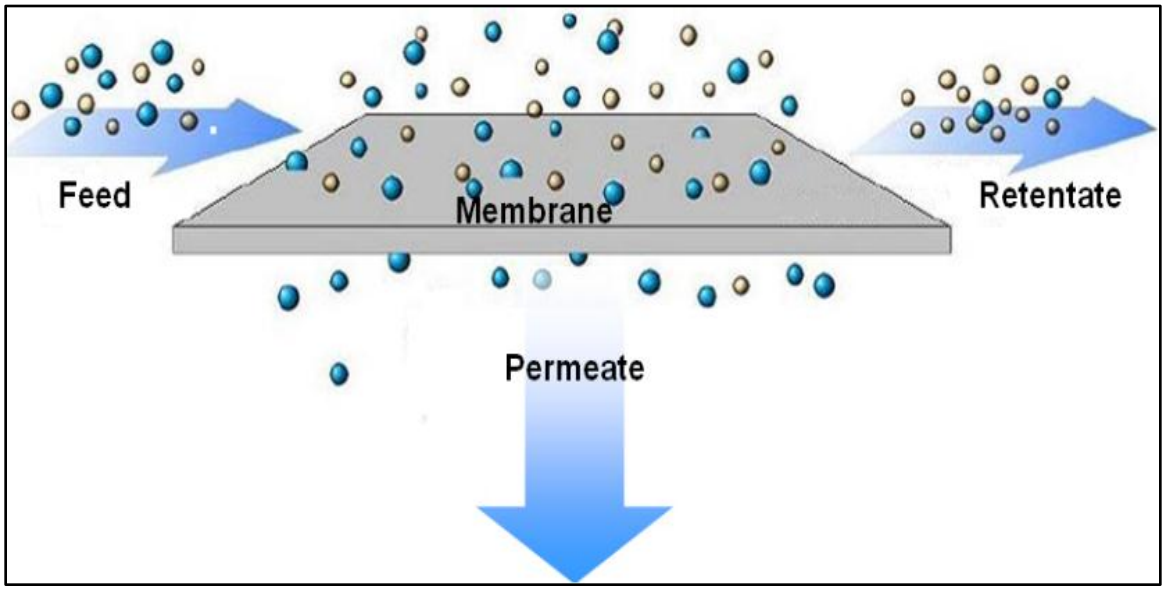

Figure 5.1 Schematic sketch showing cross-flow across an RO membrane

Transport through RO membranes occurs via a solution-diffusion mechanism [121,122]. First, a molecule sorbs from the feed solution onto the upstream face of the membrane. Then, it diffuses down the chemical potential gradient in the membrane. Finally, it desorbs from the downstream face to the permeate solution. The activity gradient is induced by an applied pressure, which is the driving force for transport through RO membranes. The governing equation describing solution-diffusion transport is:

$$\boldsymbol{J_w = L_p(\Delta P - \Delta \pi)} \qquad \textbf{Equation (5.1)}$$

where J_w is volumetric water flux (L/(m^{2}hr)), L_p is membrane permeance (L/(m^2 hr bar)), Δp is the applied transmembrane pressure difference (bar), and $\Delta \pi$ is the osmotic

pressure difference between the feed and the permeate solutions (bar). The flux is defined as the volume of water passing through the membrane across a unit cross-sectional area and in a unit time.

For a nonporous, defect-free RO membrane, L_p is given by [121,122]:

$$L_p = \frac{DS\bar{V}}{RTl} \qquad \textbf{Equation (5.2)}$$

where D is the diffusion coefficient of water in the membrane (cm^2/s), S is the water solubility in the membrane, equivalent to the water volume fraction in the membrane,V is the molar volume of water (18 cm^3/mole), R is the ideal gas constant (83.1 (cm^3bar)/(mol K)), T is the ambient temperature (K), and l is the membrane thickness (cm), taken to be the hydrated thickness.

In membrane-based desalination, purified water is forced through the membrane by the application of high pressure (Fig.5.1). The external pressure is necessary in order to overcome the osmotic pressure present in the system by virtue of the difference in the salt concentration of both sides. The osmotic pressure depends on the solute concentration and, for an ideal solution, with all salt ions being completely dissociated, is given by the following equation:

$$\pi = iMRT \qquad \textbf{Equation (5.3)}$$

i is the dimensionless van 't Hoff factor

M is the molarity

R=0.0821 L atm K^{-1} mol^{-1} is the gas constant

T is the thermodynamic (absolute) temperature

Table 5.1 presents the osmotic pressures of several salt solutions pertinent to water treatment applications. As seen in Table 5.1, the osmotic pressure of salt solutions can be significant. A large osmotic pressure in the feed solution reduces the driving force of the separation process and becomes an important factor in the resulting membrane water flux.

Table 5.1 Typical osmotic pressures for solutions at 25°C (*Freeman 1995*)

Solute	Concentration (mg/L)	Osmotic Pressure (bar)
NaCl	2,000	1.7
NaCl	35,000	27.4
Brackish water	2,000-5,000	1-2.7
Seawater	32,000	23.4

In an analogous fashion, salt transport is also modeled using solution-diffusion principles, and the transport equation is [121,122]:

$$J_s = B(C_f - C_P) \qquad \textbf{Equation (5.4)}$$

where J_s is salt flux (mg/(m^2hr)), B is the membrane salt permeance (L/(m^2hr)), and C_f and C_p are the salt concentrations in the feed and permeate streams, respectively (mg/L).

For a nonporous, defect-free membrane, the salt permeance is described by the following equation [121,122]:

$$B = \frac{D_s K_s}{l} \qquad \textbf{Equation (5.5)}$$

where D_s is the salt diffusivity in the membrane (cm^2/s), K_s is the salt partition coefficient, and l is the hydrated membrane thickness (cm). Salt flux is related to water flux by:

$$J_s = J_w C_p \qquad \textbf{(Equation 5.6)}$$

However, RO membranes are more commonly evaluated in terms of salt rejection, not salt flux. Salt rejection is defined as:

$$R = \left(1 - \frac{C_p}{C_f}\right) \times 100 \qquad \textbf{Equation (5.7)}$$

Rejection can also be expressed by combining Equations 5.1, 5.4, 5.6, and 5.7 into the following form [121,122]:

$$R = \left[\frac{\frac{L_p}{B}(\Delta P - \Delta \pi)}{1 + \frac{L_P}{B}(\Delta P - \Delta \pi)}\right] \times 100\% \qquad \textbf{Equation (5.8)}$$

This equation relates rejection to both the operating conditions and the intrinsic water and salt transport properties of the membrane.

For economical and quality reasons, it is strongly desired to maximize both the flux and salt rejection. In general, membrane fouling will result in a long-term flux decline and increase in salt passage with time. In order to assess the effectiveness of any antifouling strategy, it is imperative to carry out permeation studies with the membranes both after the application of the strategy and before. Therefore, it was deemed necessary to perform both short-term and long-term permeation tests after the deposition of the random copolymer films.

5.2 Series-Resistance Model

Transport through coated RO membranes is also considered. An idealized model for a coated membrane is shown in Figure 5.2. In this model, the coating layer is continuous and uniform across the surface of the underlying RO membrane. Based on this configuration, a series-resistance model can be constructed to estimate the steady state water flux and salt rejection of a coated RO membrane using the fundamental transport properties of the coating layer and the RO membrane [123,124]. In this model, the water flux of a coated membrane is given by:

$$\boldsymbol{J_W = L_{pT}(\Delta P - \Delta \pi)} \qquad \textbf{Equation (5.9)}$$

where L_{pT} is given by:

$$\boldsymbol{L_{pT} = 1 \Big/ \left[\frac{1}{L_p} + \frac{l_c}{P_W}\right]} \qquad \textbf{Equation (5.10)}$$

P_w is the water permeability of the coating ((L μm)/(m^2 hr bar)), and l_c is the hydrated thickness of the coating (μm).

In the same manner, the salt flux of a coated membrane is given by:

$$J_s = B_T(C_f - C_p) \qquad \textbf{Equation (5.11)}$$

Where B_T is given by:

$$B_T = \frac{1}{\frac{1}{B}+\frac{l_c}{P_s}} \qquad \textbf{Equation (5.12)}$$

P_s is the salt permeability of the coating (cm^2/s).

The salt rejection of the coated membrane can be estimated from the following modified form of Equation 5.8:

$$R = \left[\frac{\frac{L_{pT}}{B_T}(\Delta p+\Delta\pi)}{1+\frac{L_{pT}}{B_T}(\Delta p-\Delta\pi)}\right] \times 100\% \qquad \textbf{Equation (5.13)}$$

Equation 5.13 can be used to predict the salt rejection of a coated membrane as a function of membrane and coating water permeabilities, salt permeabilities, and the coating thickness. To the extent that experimental data obey this model, the integrity of the coating and the influence of the coating on water flux and salt rejection of the RO membrane can be assessed.

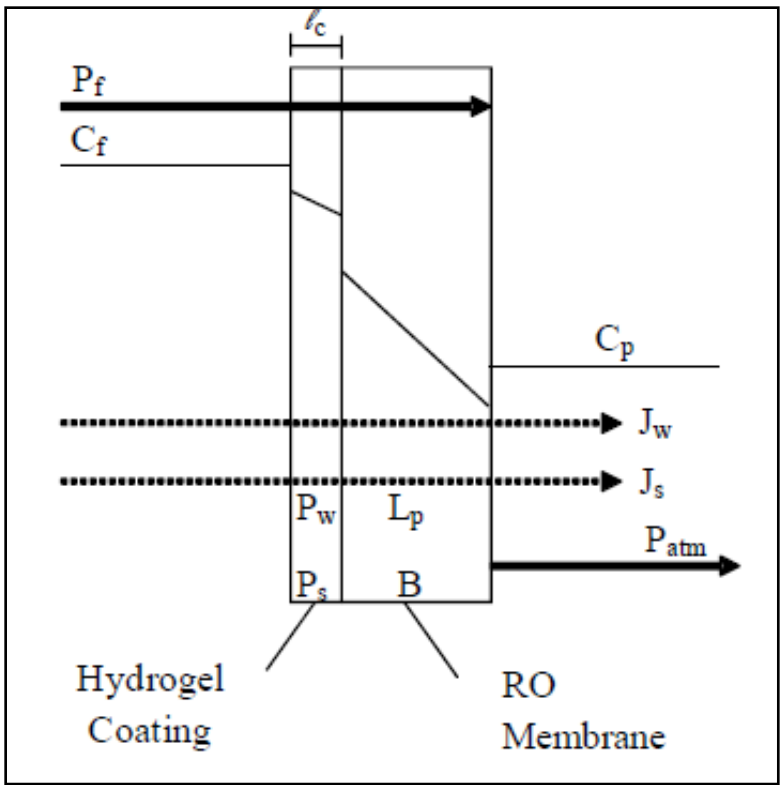

Figure 5.2 Schematic of a coated membrane and related transport properties

5.3 Experimental Setup

The major component of this setup is the permeation cell, a rectangular unit made of either stainless steel or a plastic material (Fig.5.3). It consists of separable top and bottom portions with the membrane sample sandwiched in between them. A rectangular metallic slab with identical dimensions is placed above the upper half to secure the sample in place during the permeation test. Stainless steel tubings a quarter of an inch in diameter connect the cell to the feed tank and other components of the setup. A plastic tube of similar dimensions connected to the upper half of the cell allows the permeate water to flow out that could be either recycled to the feed tank or collected in a separate container.

The feed tank is a large plastic container with a maximum capacity of 30 liters by volume (Fig.5.3). A high-pressure pump draws the feed solution and diverts the

pressurized water towards the permeation cell housing the membrane. The configuration of the cell allows for flow across the membrane which is placed with the active layer of polyamide faced downwards. Second tubing connected to the lower half of the cell carries the retentate back to the feed tank. Pressure gauges with analog readouts of upto 1500 psi were installed in the path of both the feed and the retentate.

Maintaining uniformity in the temperature is essential because the permeation characteristics are influenced significantly by slight variations in temperature. This was accomplished with the help of a chiller whose coils are made of stainless steel. The temperature of the feed solution was continuously monitored by a thermocouple. For safety reasons, a pressure relief valve was inserted into the system with a ceiling value of 1000 psi. The valve was connected to the reject side of the feed.

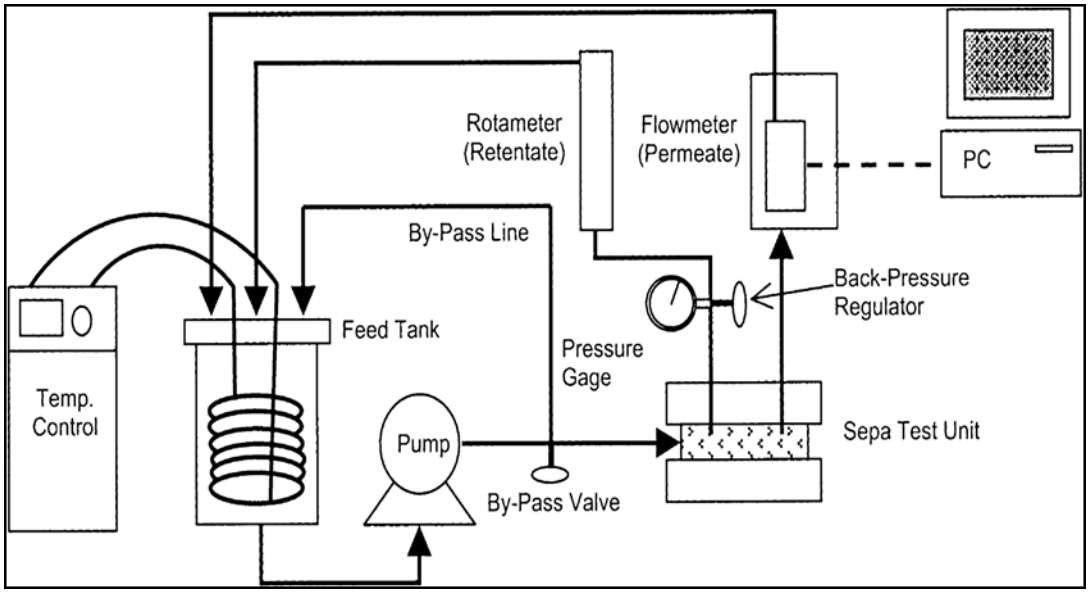

Figure 5.3 Schematic sketch of the permeation setup in the laboratory

Chapter 6. Bacterial Adhesion & Biopolymer Adsorption

6.1 Introduction

Initial microbial cell deposition, a.k.a., "primary adhesion" (Fig.6.1) is a critical early stage event in the overall process of Biofouling [125]. Once deposited, cells can grow, multiply, and produce extra-cellular polymers (EPS), which form a tangled matrix of fibers that provide structure to the assemblage termed a "Biofilm ". Once formed, a Biofilm is difficult to remove because the EPS layer strongly adheres cells to the membrane surface and protects microbes from attack by predators and biocides [126]. Hence, efforts to combat membrane Biofouling by modifying the surface of membrane materials for example must begin with a study of initial bacterial adhesion on membranes.

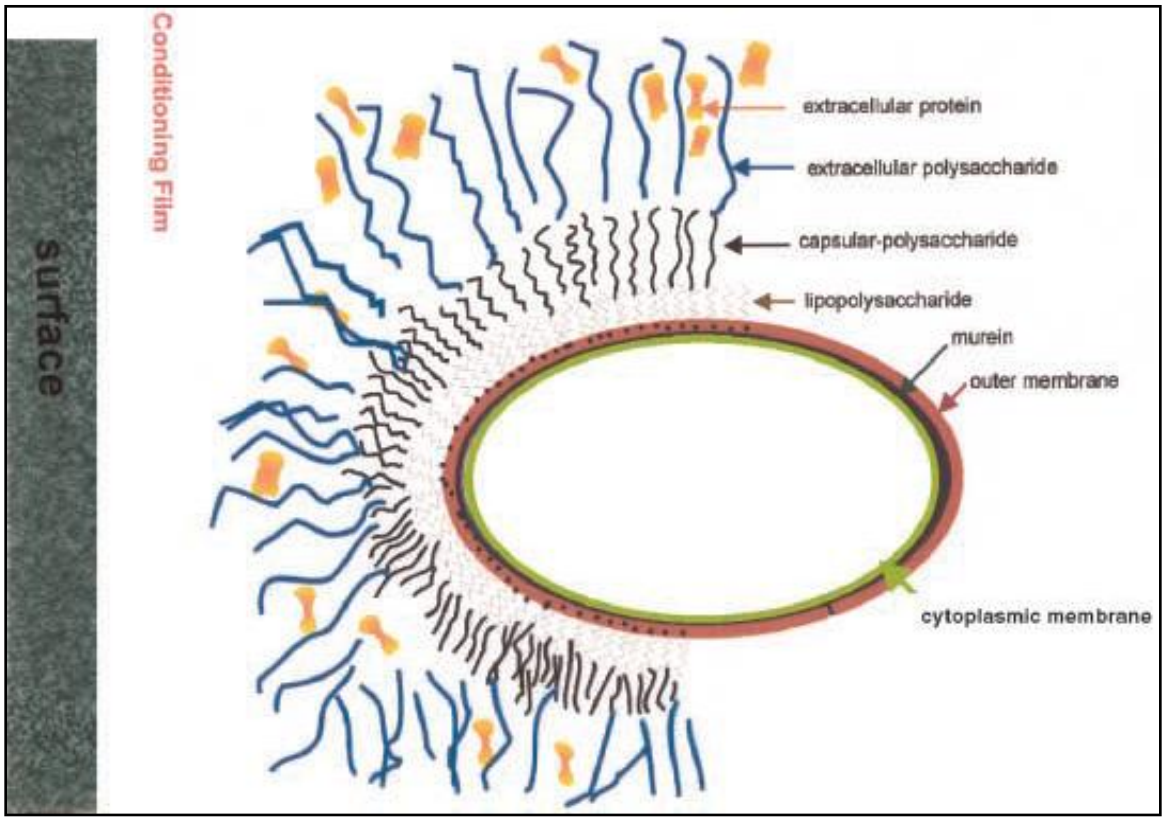

Figure 6.1 A Gram-negative bacterium approaching a membrane surface in water

However, there is another important phenomenon occurring before primary adhesion that needs to be taken into account. Within seconds, surfaces immersed in water become covered with a so-called conditioning film consisting of macromolecules, such as humic substances, polysaccharides and proteins, which are present in trace amounts in water, as was recognized many years ago [127]. The cells do not need to be viable for adhesion – the EPS already present are sufficient for adhesion [128].

Therefore, in addition to bacterial adhesion, it was deemed necessary to study the adsorption behavior of the above-mentioned biopolymers on the random copolymer films being explored as potential antifouling coatings on RO membranes. The Gleason group at MIT has already done adsorption measurements on a model protein, Bovine Serum Albumin [105]. Hence, it was decided to continue similar studies with the other biopolymer types i.e. polysaccharides and humic substances.

6.2 Quartz Crystal Microbalance

The quartz crystal microbalance with dissipation (QCM-D) is a useful tool to study the adsorption of macromolecules, such as polysaccharides and proteins, on a substrate in situ, in real time (Fig.6.2). The adsorption could be studied as a function of one of several variables such as solution chemistry [129] and substrate chemistry. The principles of this instrument have been extensively described elsewhere [130].

Figure 6.2 The complete setup for the Quartz Crystal Microbalance

The piezoelectric quartz crystal microbalance (QCM) is an ultrasensitive weighing device, consisting of a thin disk of single crystal quartz, with metal electrodes deposited on each side of the disk (Fig.6.3). The crystal can be made to oscillate at its resonant frequency, f, when connected to an external driving oscillator circuit.

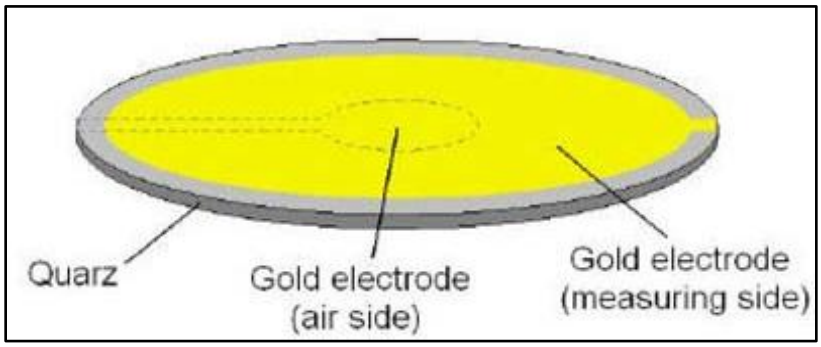

Figure 6.3 A sketch of the quartz crystal showing the gold electrode

The principle of operation as a balance is that any mass added to, or removed from, the electrode(s) induces a frequency shift, related to the mass change (Fig.6.4). A quartz crystal microbalance (QCM) measures a mass per unit area by measuring the change in frequency of a quartz crystal resonator. The resonance is disturbed by the addition or removal of a small mass due to oxide growth/decay or film deposition at the surface of the acoustic resonator.

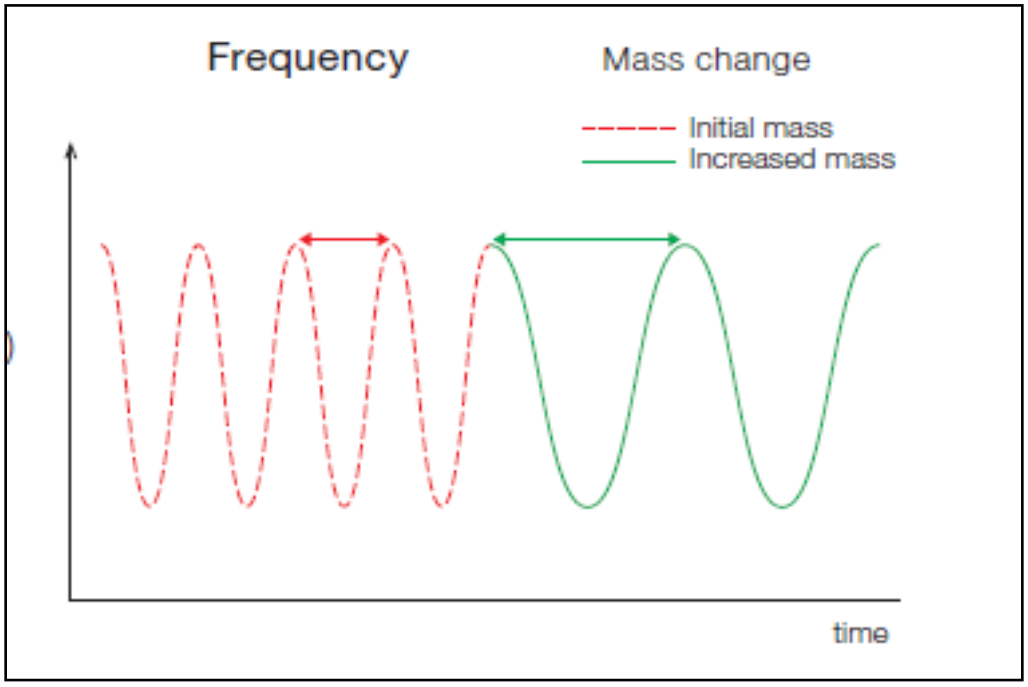

Figure 6.4 Principle of operation of the QCM-D

6.3 Model Biopolymers

Sodium alginate

Alginates are unbranched polysacchraides produced by brown algae as the principal component of their cell wall [131]. Alginates are also produced by Gram-negative bacteria, such as *Pseudomonas aeruginosa*, and play an important role in the cohesion and protection of the microorganism in biofilm matrices [132]. Adsorption and

accumulation of alginate cause the fouling of engineered biomedical devices that are by alginate-producing bacteria [133].

Alginates have unique chemical and physicochemical properties, influenced by their composition and the solution chemistry of their surrounding environment. These polyelectrolytes are made of pattern blocks of homopolymeric regions of two residues: mannuronic (M) and guluronic (G) acids (Fig.6.5) [134]. The specific chemical and physical properties of alginates create major difficulties in understanding variations in the nature of inter- and intramolecular associations. The high negative charge of alginates due to the deprotonated carboxylic functional groups at near neutral pH induces repulsive inter- and intramolecular electrostatic forces.

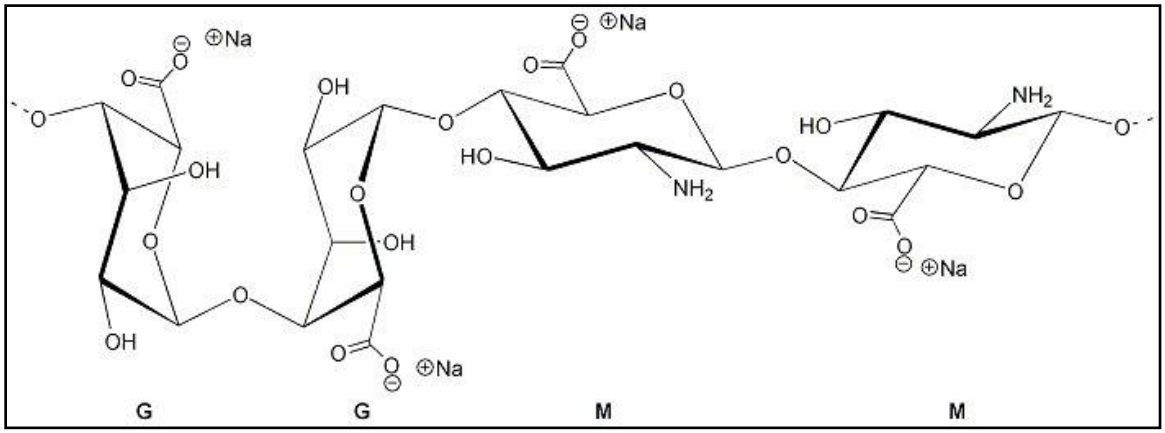

Figure 6.5 Molecular structure of sodium alginate

Humic Acid

Humic substances are abundant in natural waters. They are the result of chemical and biological degradation of plant and animal residues and the synthesis activities of microorganisms [135]. Humic and fulvic acids represent the major fraction of dissolved natural organic matter (NOM) in aquatic environments. These substances are also important constituents of the organic colloidal phase and are one of the major fouling

agents during filtration of surface waters in reverse osmosis [136], Nanofiltration [137], ultrafiltration [138] and microfiltration [139].

Humic acid is a subclass of humic substances and generally displays macromolecular characteristics. It contains both hydrophobic and hydrophilic moieties as well as many chemical functions such as carboxylic, phenolic, carbonyl, and hydroxyl groups connected with the aliphatic or aromatic carbons in the macromolecules (Fig.6.6) [140]. The presence of carboxylic and phenolic groups results in humic acid predominantly carrying negative charges in aqueous solutions [135]. This charge also varies with the physic-chemical properties of the solution such as ionic strength and humic concentration.

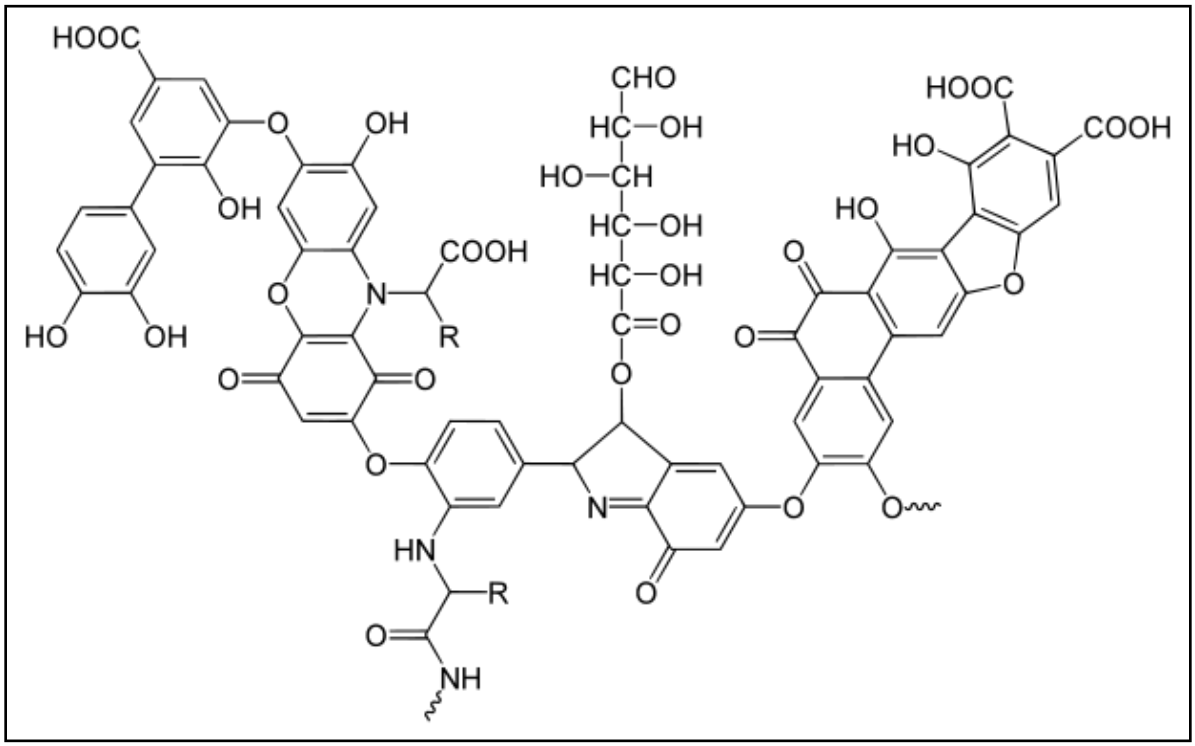

Figure 6.6 Molecular structure of humic acid

6.4 Experimental Procedure

Sodium Alginate and Humic Acid were selected as the model polysaccharide and humic substance respectively. Both of these chemicals were obtained from Sigma Aldrich Inc. with a high degree of purity. Stock solutions of concentration 10g/L were prepared by dissolving 1g in 100mL of DI water and overnight stirring with a magnetic stirrer.

The quartz crystals for the adsorption measurements were purchased from Q-Sense, Sweden. Copolymer films with a variety of chemistries were deposited on the crystals using the iCVD reactor in the Gleason laboratory. For stability and uniform deposition, the crystals were fixed to the reactor surface using commercial scotch tape. Both the homopolymers, HEMA and PFA, and several compositions in between (17, 28, 40, 60, 80 %PFA) were deposited on the crystals.

The crystals with the copolymer films were carefully placed in the cells of the QCM with the coating side face downwards. The resonant frequencies were determined for multiple harmonics (1-13). DI water at a flow rate of around 200 µL/min was flown through the cells until the frequencies stabilized. In general, this step took about 15-20 minutes. Thereafter, the DI water was replaced by the solution of interest while maintaining a similar flow rate. Just before the replacement of the feed solution, the flow direction was reversed for a few seconds and then normalized.

6.5 Model Bacteria

Escherichia coli K12 MG1655 was used as a model bacterial cell (Fig.6.7) [141]. The strain was kindly received from Buie Lab in the Mechanical Engineering department at MIT and from Prof. Amjad Khalil of the Physics department at KFUPM. To allow live cell detection under fluorescent microscopy, bacterial strains were tagged with a plasmid

coding for green fluorescent protein (MG1655 was introduced with the suicide plasmid pSM1696). The *E. coli* cells were incubated and harvested at midexponential growth phase in Luria Bertani (LB) broth with 50 mg/L kanamycin at 37°C.

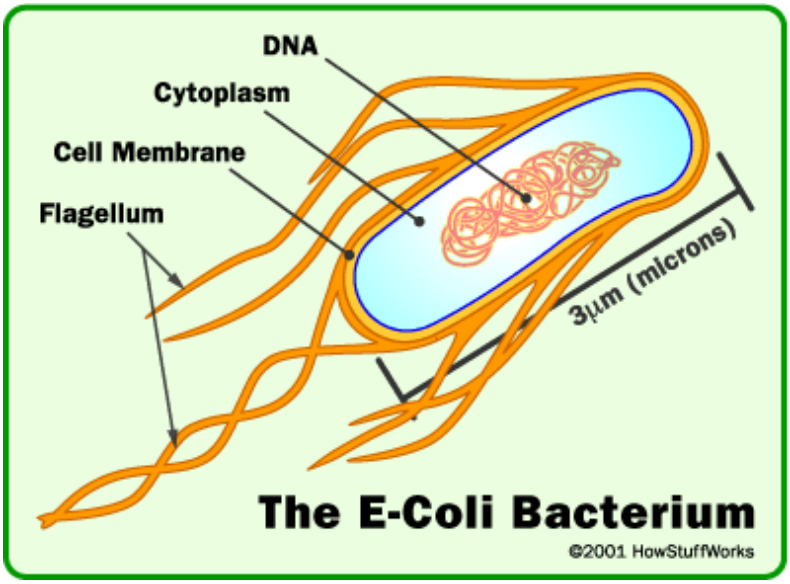

Figure 6.7 An E.coli bacteria showing the different components (*science.howstuffworks.com*)

6.6 Static Bacterial Adhesion Tests

Fluorescence Microscope

Membrane coupons (each with dimensions of 1cm by 1cm) were placed in 20mL cell suspension (4×10^7 cells/mL) in a test tube. The cells and the membranes were incubated in a shaker (Lab-line 4631 Maxi Rotator) at 20 rpm and room temperature (22°C) for 1 h. The membrane coupons were then rinsed gently with a bacteria-free broth to remove weakly bound cells. The samples were then observed under a fluorescent microscope at two different magnifications (10x, 20x) of the objective lens. A total of 10 images were

taken from different areas of the membrane surface. The bacterial colonies were manually counted and the average taken for each sample.

SEM

Similarly, membrane samples coated with copolymer films of different compositions were placed in 10mL cell suspension for 4-5 hours at 37°C. Upon removal, they were rinsed in bacteria-free TT media for a few seconds to remove reversibly attached microorganisms. The next step was complete drying: the first batch in vacuum for a couple of hours and the next group with dry nitrogen for a few minutes only. Finally, the dried samples were observed under the SEM with different magnifications.

A total of 20 images from different locations were taken for each sample at identical magnification e.g. 2500x. Images in multiple of five were selected randomly for each sample and the average no. of bacterial cells calculated. This procedure was repeated until a steady value was obtained.

Chapter 7. Results & Discussion

7.1 Copolymer Film Depositions

Table 7.1 summarizes the depositions performed on different commercial RO membranes as well as QCM-D quartz crystals. As can be seen, a wide range of compositions were covered including the pure homopolymers, PHEMA and PPFA. The copolymer coating chemistry was varied by increasing the amount of PFA monomer added in the mixture. The target value for the copolymer film thickness was 30 nm as this was considered optimum for maintaining permeate flux and provide the antifouling functionality. Thicker films can result in significant flux decline, whereas, thinner coatings do not provide adequate coverage needed to create a uniform film which is necessary for preventing biopolymer adsorption and bacterial adhesion.

Table 7.1 Coating chemistries and film thickness deposited on commercial RO membranes and the QCM quartz cyrstals

S. No.	Chemistry (%PFA)		Thickness (nm)	Membrane	QCM crystals
	Target	Actual			
1	0	0	30	√	√
2	20	17	26.7	√	√
3	35	35	29	√	
4	40	40	32.4	√	√
5	50	50	27	√	
6	60	58	32	√	
7	70	70	29.5	√	
8	75	76	32.7	√	√
9	90	90	35	√	
10	100	100	50	√	√

Table 7.1 and Figure 7.1 provide the chemistries and the thicknesses of the deposited films. As can be seen the iCVD is indeed a very accurate and precise technique which provides a good control on the film composition and thickness. The maximum deviation in the copolymer film composition was a mere 3% (in the case of 20% PFA). On the other hand, except for the pure PFA deposition where the deviation in thickness was around 20 nm, the thickness values were very close to the targeted thickness of 30 nm.

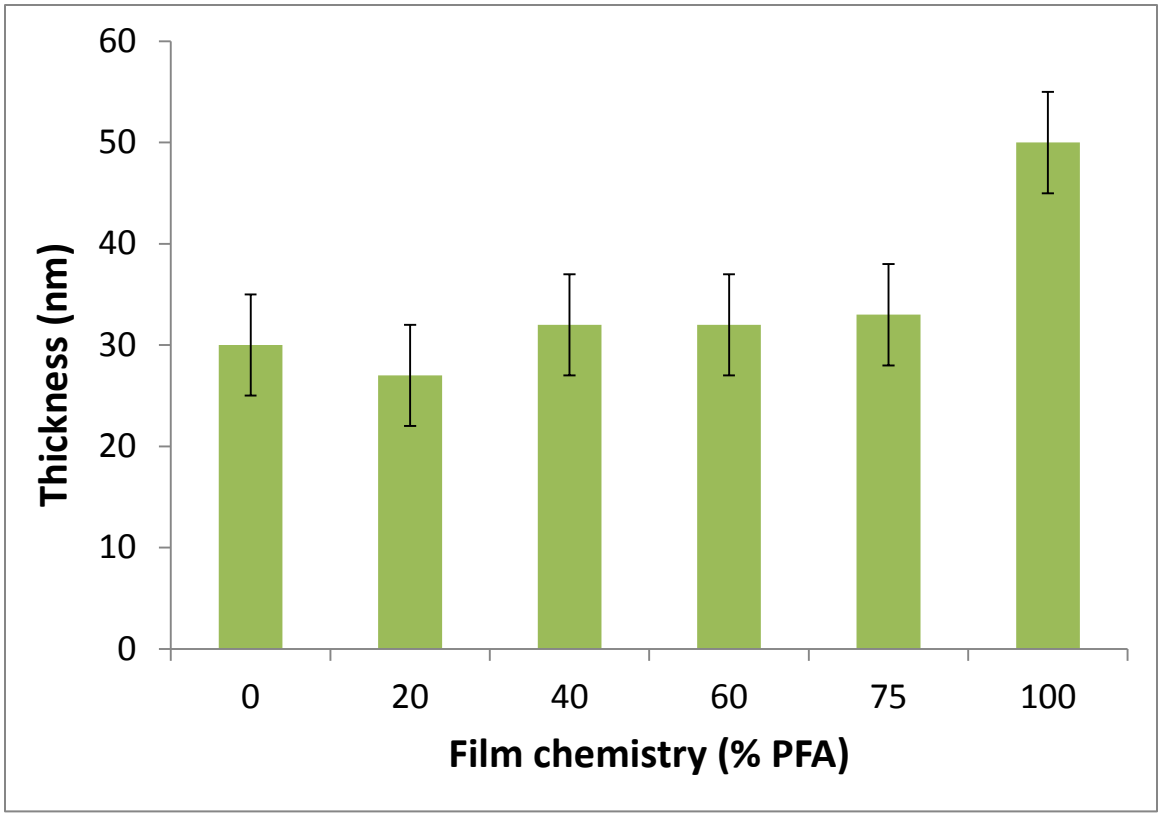

Figure 7.1 Thickness values for films of different chemistries as measured by variable angle ellipsometry

In addition to *in situ* laser interferometry and post-deposition ellipsometry, TEM images of the cross-section confirmed the thickness of the deposited film. The figure below (Fig.7.2) shows a high resolution image for a sample deposited with a copolymer film of composition 60% PFA. The thickness determined from ellipsometry was 32.2 nm (Table 7.1) and the approximate value from the TEM image to be 29 nm. The TEM images are also a proof of the conformality of these coating as found in several previous studies [142].

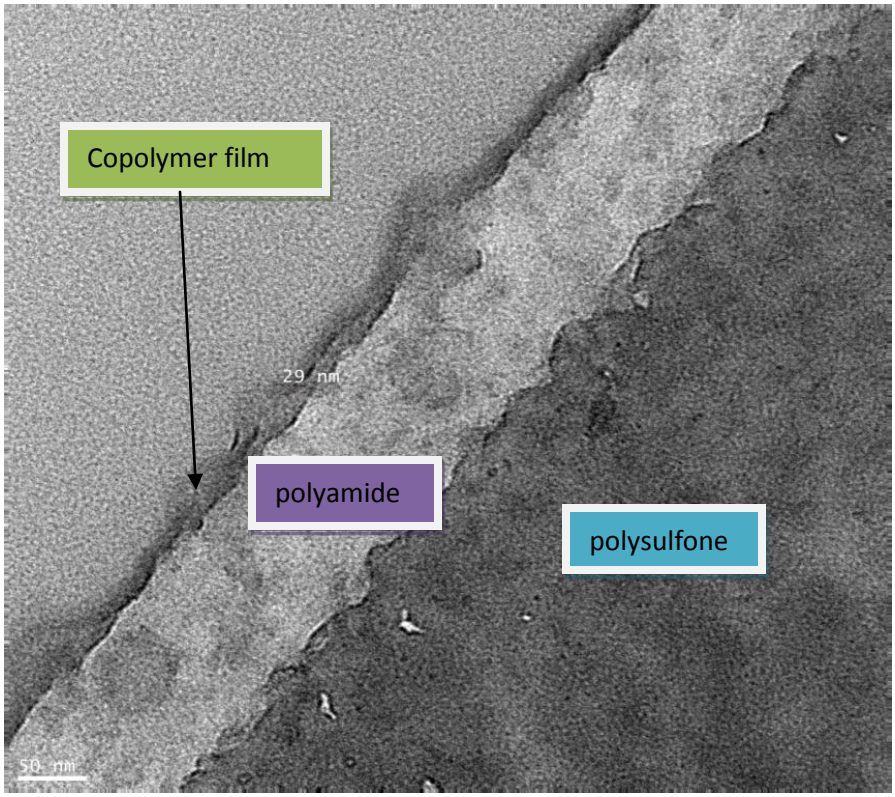

Figure 7.2 TEM image of cross-section of a membrane sample coated with a copolymer film of chemistry 60% PFA showing the thickness measurement to be around 30 nm

The high degree of conformality can be readily explained by the low sticking coefficient of the vapor-phase molecules of the initiator in the iCVD process. The sticking coefficient for a molecule is defined as the probability that a reactive vapor-phase molecule irreversibly adsorbs to the substrates. For conformal deposition on non-planar substrates, the sticking proabability should be as low as possible. For iCVD technique, measured sticking probabilities range from 0.011 to 0.050, which are low enough to result in conformal coverage [142].

In addition, the solvent-free characteristic and the vapor phase nature of the process allows for easy stacking of polymeric films. Control of the flow profiles inside the process chamber enables uniform film growth over relatively large-sized substrates; additionally, precise, real-time control of film thickness is possible at the nanometer scale [143].

7.2 Surface Roughness

First, the commercial membrane samples without any copolymer film were analyzed for surface roughness. The average roughness values for the commercial membranes are given in Figure 7.3. The TFC-HR membrane from Koch Membrane systems has the smoothest of all surfaces with the rms roughness in single digits as shown in our relevant studies [144]. The roughest surface belongs to the TF-RO-AD membrane from GE Osmonics with an average value close to a hundred nanometers. The UTC-80B from Toray has an intermediate roughness with a mean value around 50 nm. These are typical values for commercial polyamide membranes, which can range from 10 to 100 nm [145,146,147,148]. Many studies have linked surface roughness to water flux and flux decline. For example, higher surface roughness often leads to larger flux declines [147].

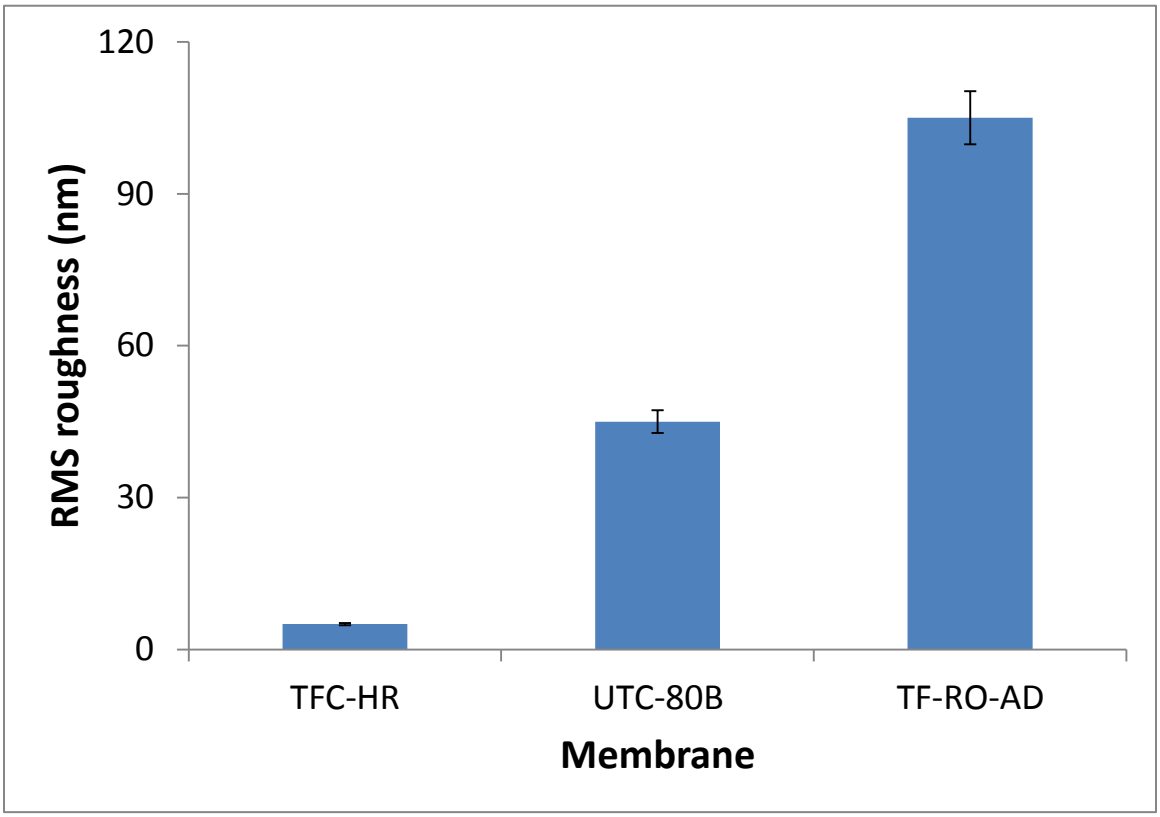

Figure 7.3 Average roughness values for commercial membranes

The roughness measurements were also performed for membrane specimens coated with copolymer films of different chemistries. Figure 7.4 shows three-dimensional images of the surface topology of coated samples. It was found that the coatings did not add to the inherent surface roughness of the commercial membrane. Infact, in majority of the cases, the coated membranes showed somewhat less surface roughness than the uncoated counterpart. These observations can be readily explained by the conformal nature of these films deposited using the iCVD technique. The copolymer films seem to acquire the peak and valley structure of the polyamide surface as can be seen in TEM images of the cross-section.

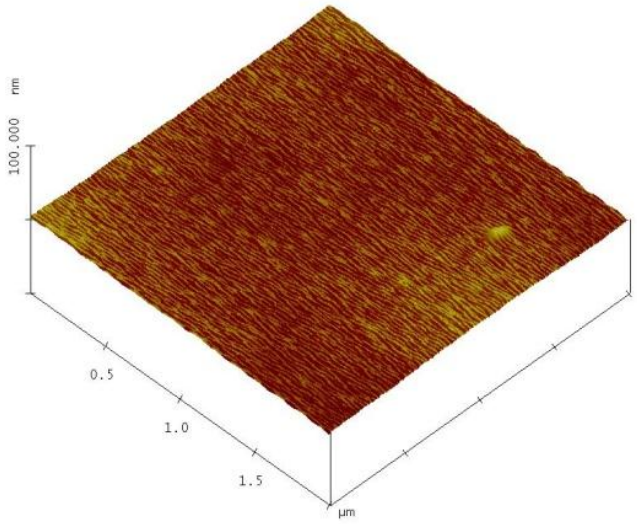

(a)

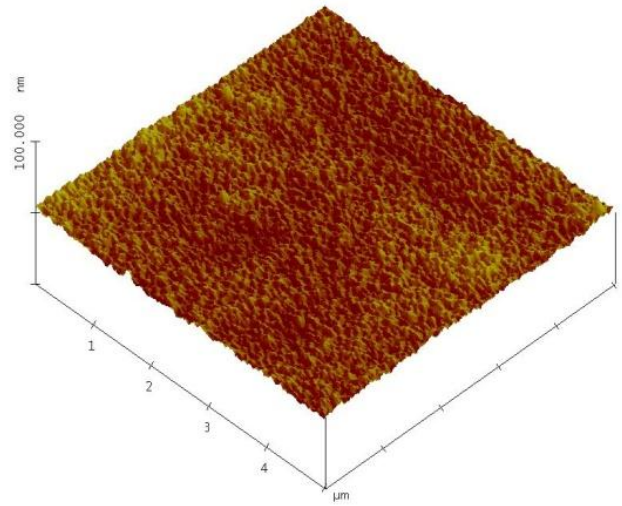

(b)

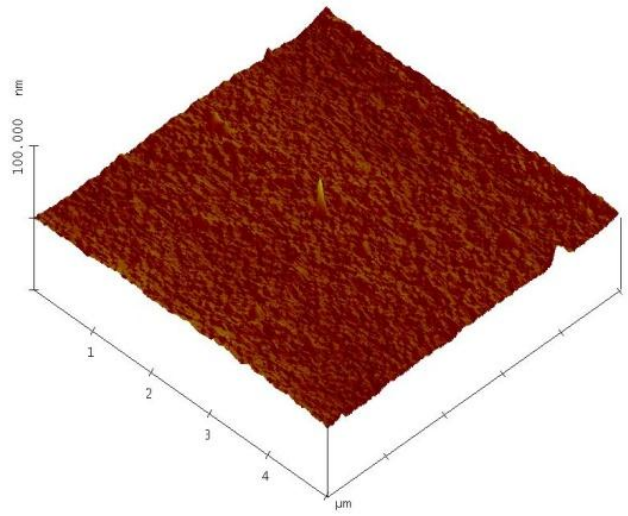

(c)

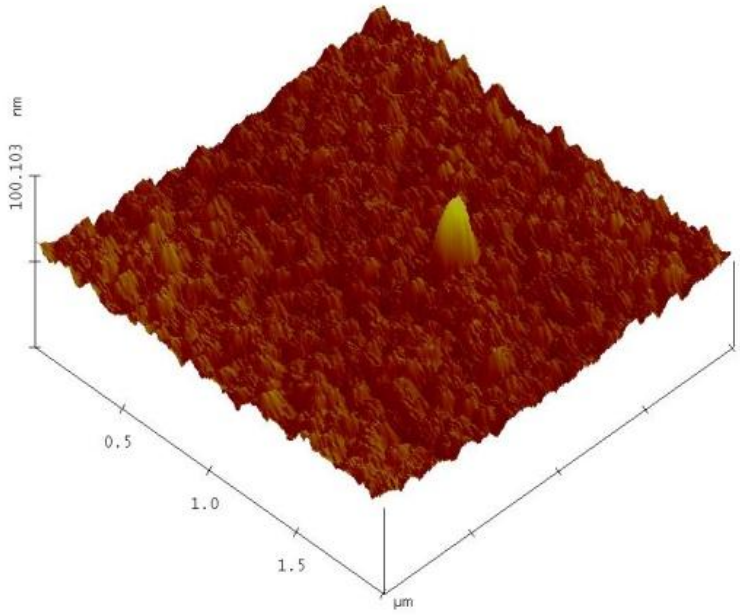

(d)

Figure 7.4 TFC-HR membrane with copolymer films of different chemistries (a) 10 (b) 17 (c) 35% and (d) 75% PFA

Atomic force microscopy (AFM) images of the coated membranes showed only nanoscale roughness. Figure 7.5 shows the effect of the copolymer film chemistry on the root-mean-square (RMS) roughness of the TFC-HR membrane. The roughness increases almost linearly with the PFA content in the copolymer film as shown earlier by Gleason and co-workers [105]. This trend is atleast partially a consequence of the respective glass transition temperatures (T_g) of the homopolymers: 80°C for PHEMA and -20°C for PPFA. As more PFA is incorporated into the copolymer, the film becomes increasingly amorphous, resulting in greater mobility of the polymer chains and therefore higher surface roughness.

However, the more important observation is the very low roughness values for all the chemistries investigated. For very hydrophilic compositions such as 10% PFA, the rms value is less than a nanometer which implies a perfectly smooth surface. Even for the hydrophobic chemistries e.g. 75% PFA, the mean value is less than 5 nm which also is a very smooth surface. For the amphiphilic chemistry i.e. 40% PFA its almost a couple of nanometers.

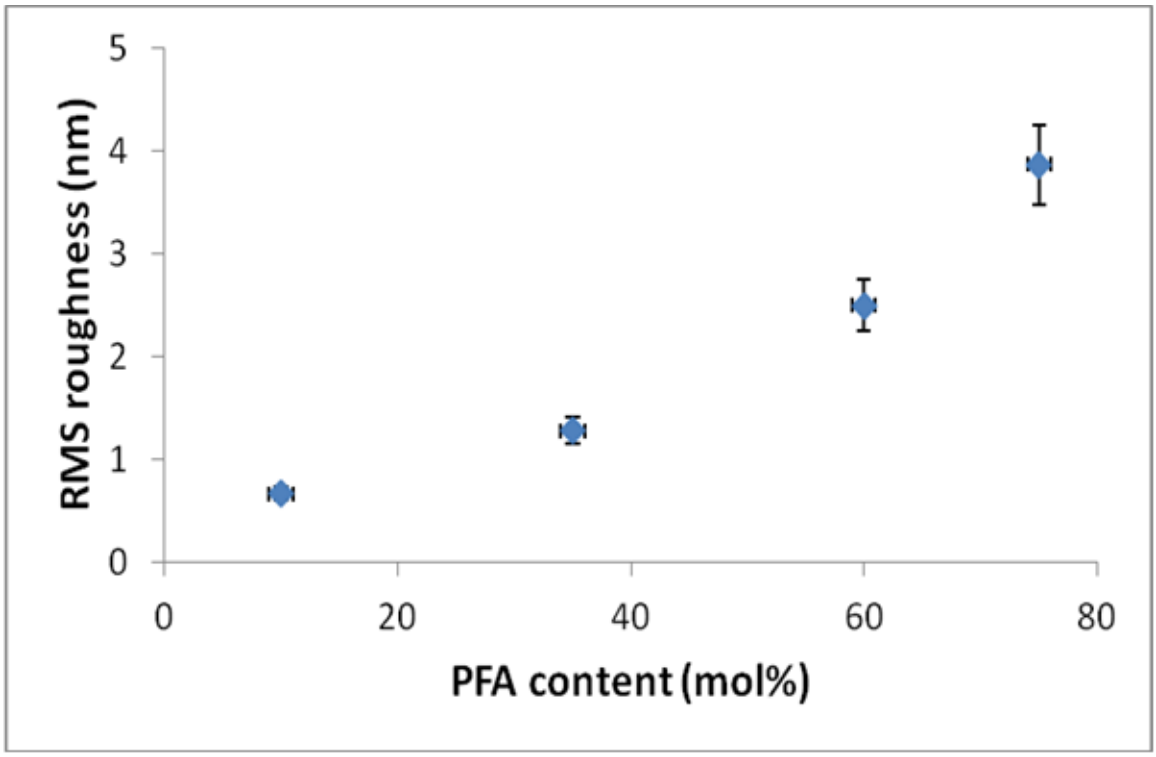

Figure 7.5 Variation of surface roughness with copolymer film chemistry for TFC-HR membrane

Several studies have shown the initial adhesion rate of bacteria to be much lower on smooth surfaces as compared to very rough surfaces [149]. In fact, surface roughness is a major factor affecting other fouling types as well such as colloidal [150] and organic [151] fouling. Thus the roughness results indicating a very smooth surface for the copolymer HEMA/PFA films augur well for ts use as antifouling coatings for RO membranes. Fouling due to biopolymers is relevant in our case because the conditioning film formation precedes initial microbial attachment.

The hypothesis on the effect of surface roughness on biopolymer adsorption is illustrated in Fig. 7.6. Since the scale of the membrane surface roughness features (tens to hundreds of nanometers) is much larger than the size of the foulant molecules, a rough membrane surface provides more surface area for the foulant molecules to attach to compared to a smooth surface. More importantly, the foulant molecules deposited in the "valleys" are less subject to the hydraulic shear force, resulting in faster accumulation of foulants in these "valleys".

.

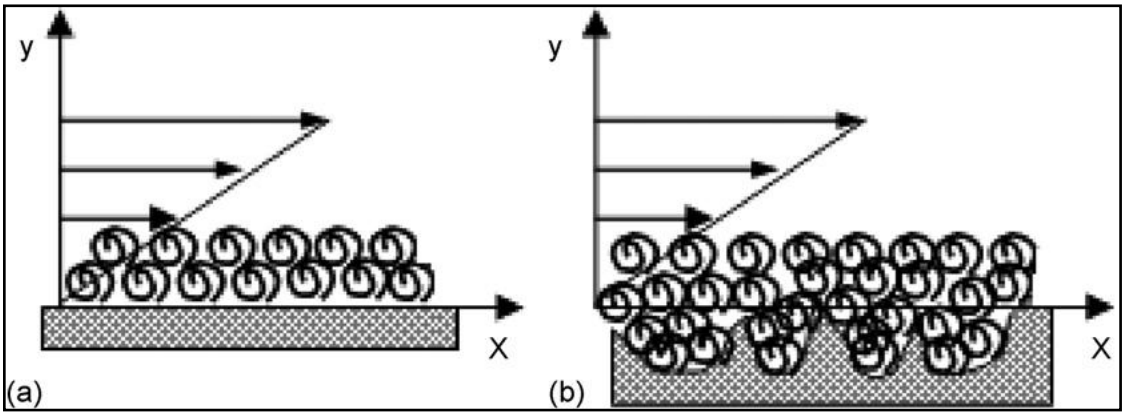

Figure 7.6 Schematic illustration of the effect of surface roughness on membrane fouling (a) perfectly smooth surface (b) rough surface with "peaks" and "valleys" (*Li et. al 2007)*

7.3 Surface Morphology

RO membranes are assumed to be effectively nonporous. Although these membranes are often cited as having "pore" sizes ranging from 1 to 10 Å [121], the "pores" are more accurately described as transient free-volume elements. These elements are not rigid unchanging structures, but instead fluctuate in size and location with time [121]. Conversely, porous membranes, such as ultrafiltration membranes, have permanent pore structures and are, therefore, governed by a different transport mechanism.

SEM was used to visually verify the nonporous nature of RO membranes, at least within the resolution limits of SEM. Figure 7.7 shows some representative SEM images for both commercial and modified membranes. The top-down SEM images in both of these figures display the nonporous nature of the RO membrane surface. At the given scale, pores on the order of 0.1 μm or larger (typical for ultrafiltration membranes) would be visible.

The top-down SEM images display the nodular structure (peaks and valleys) of the RO membrane surface. This is more apparent in the images taken at higher magnifications (Figs. 7.7 c & d). Cadotte attributed this topology to the interfacial reaction mechanism8; he proposed that the initial reaction between the aqueous amine solution and the organic acid chloride produces a porous polyamide network. Subsequently, the aqueous amine solution diffuses through pores in the newly-formed polyamide layer to react with the top organic layer, eventually creating a continuous polyamide barrier. However, since this barrier is created not in one instantaneous

moment, but rather in a series of subsequent (albeit very fast) reactions, the resulting surface structure is not perfectly smooth and, in fact, has significant surface features.

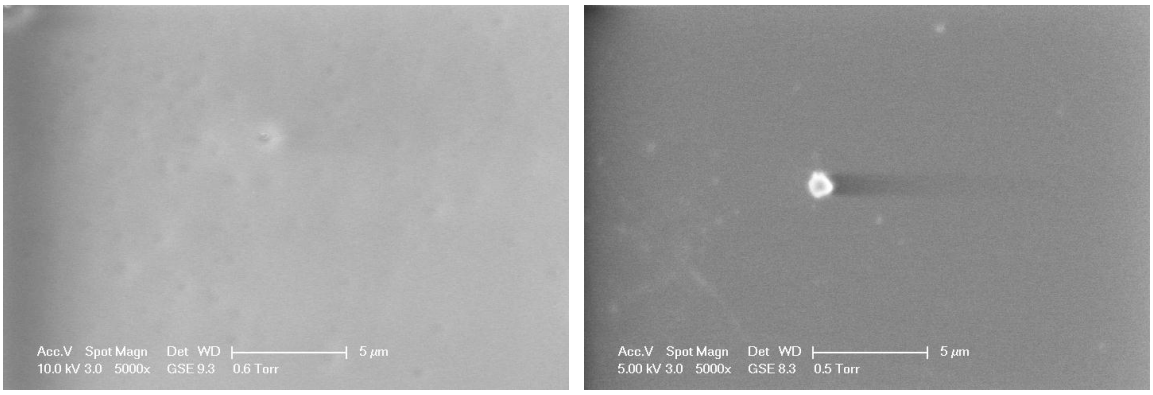

(a) (b)

.

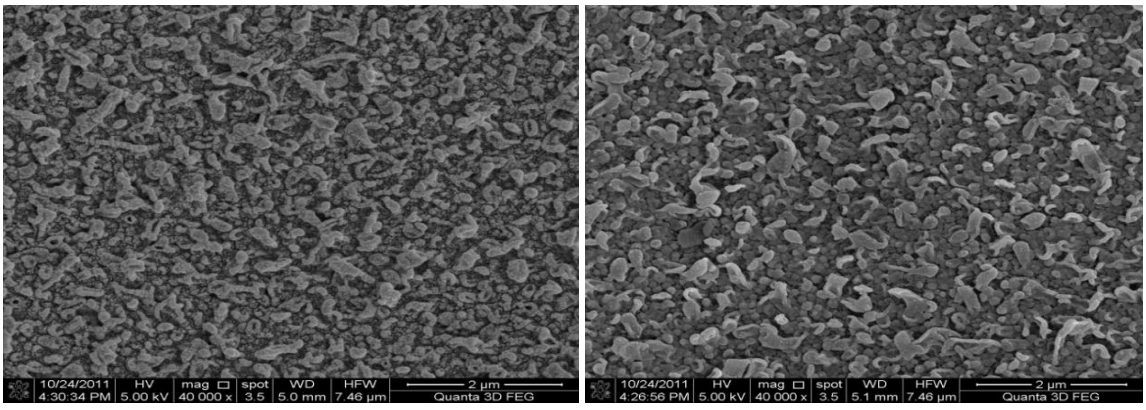

(c) (d)

Figure 7.7 SEM images of TFC-HR membranes at different magnifications (a) uncoated at 5k (b) coated with 40% PFA at 5k (c) uncoated at 40k (d) coated at 40k

7.4 Cross-section Examination

High resolution TEM was used for observing the cross-section images of the coated membrane sample. Several images of the cross-section were taken at very high magnifications. Different layers of the RO membrane as well as the ultra-thin copolymer film are clearly visible in all of the images. The thickness of the coating and polyamide layer was also measured at different locations and the coated film thickness was found to be consistent with the values obtained from *in situ* laser interferometry and variable angle ellipsometry.

The TEM images confirm the conformal and smooth nature of the copolymer films deposited using the initiated CVD technique. The low magnification image (Fig. 7.8a) shows the continuous presence of the coating on the polyamide layer. The images at higher magnifications (Figs.7.8c&d) corroborate the earlier findings from AFM measurements regarding the ultra-smooth surface of the copolymer film. In addition, the difference in porosity of different layers is clearly visible: the micro porous polyester support at the bottom followed by the intermediate layer of polysulfone with average pore size in tens of nanometers, and finally the virtually non-porous polyamide.

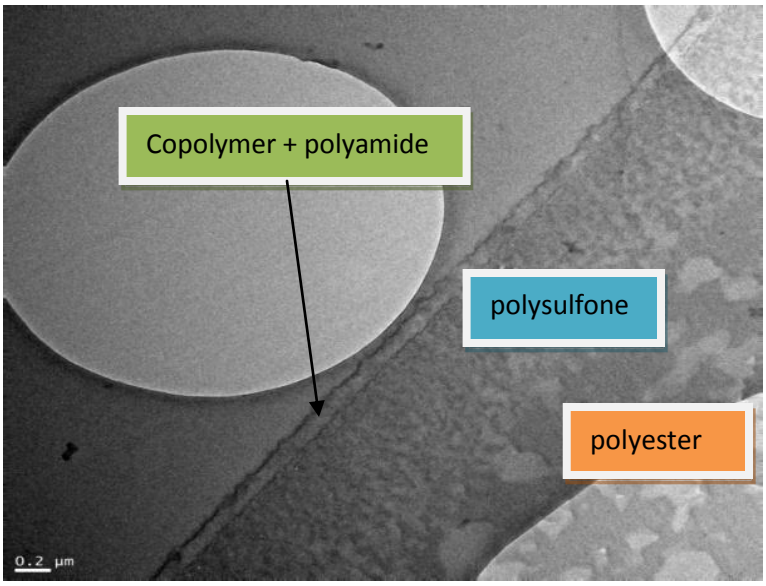
Copolymer + polyamide
polysulfone
polyester
0.2 µm

(a)

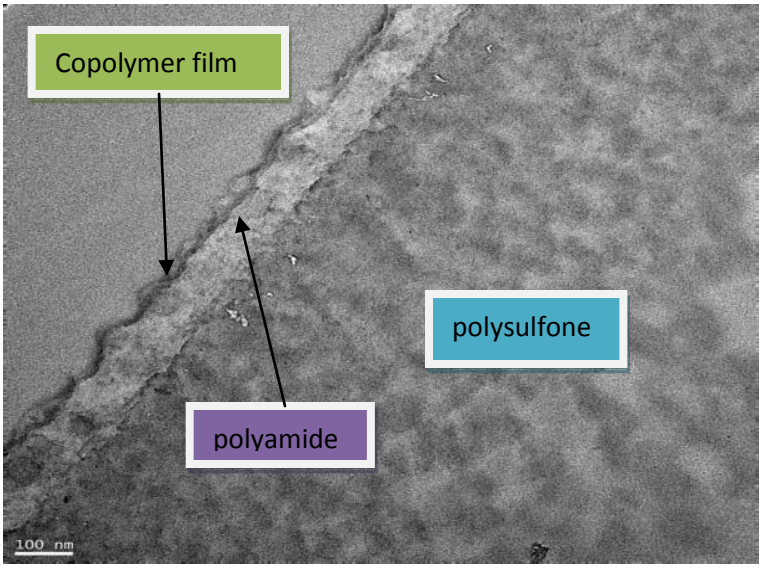
Copolymer film
polysulfone
polyamide
100 nm

(b)

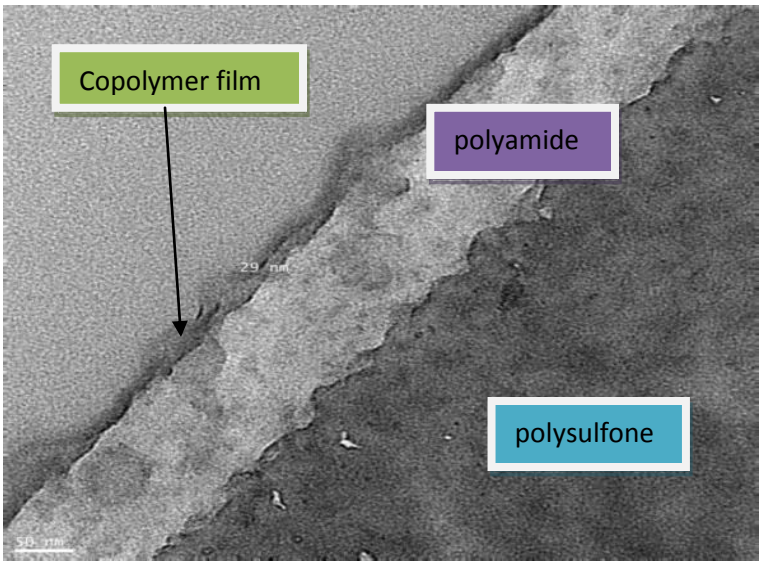

(c)

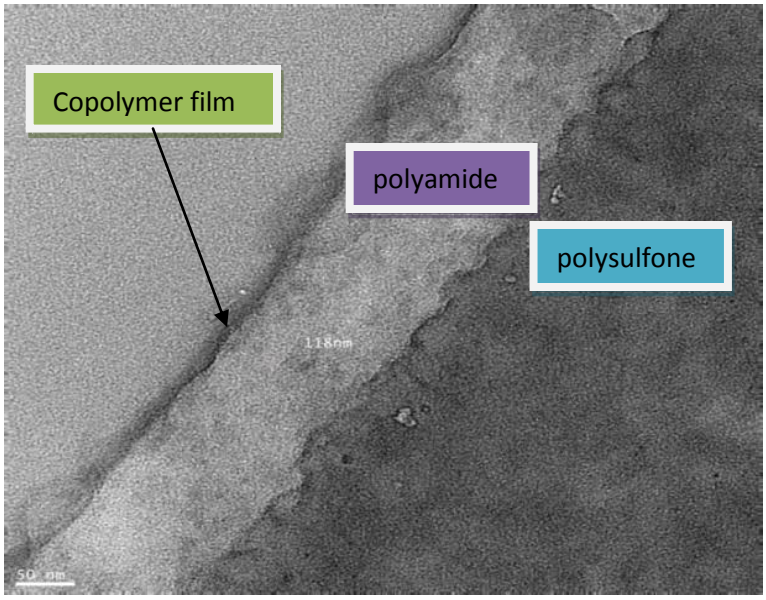

(d)

Figure 7.8 TEM images of cross-section showing the different layers of TFC-HR membrane covered with 60% PFA film (a) all the layers including the microporous polyester (b) the top three layers (c,d) polyamide and copolymer film

7.5 Contact Angle Measurements

Static contact angle measurements were performed initially on the virgin membranes. The static angle was measured immediately after placing a droplet of water (20µL) on the surface. Both the right and left angles were measured and their average calculated. The hydrophilicity of the membranes can be verified by images of the water droplet taken on the surface of the different commercial membranes (Fig.7.9).

The results (Fig.7.10) show the UTC-80B membrane to possess the most hydrophilic surface of the three membranes with a mean value of 20°. The TFC-HR appears to be the least hydrophilic with an average contact angle value of 35° with the TF-RO-AD not far away with 32°.

In general, a hydrophilic surface is desired for achieving high permeate flux and discouraging fouling by microorganisms. Several studies have shown bacterial attachment to be favorable on relatively hydrophobic surfaces [152,153]. Therefore, one approach for the control and prevention of Biofouling is to modify the membrane surface to make it more hydrophilic [154].

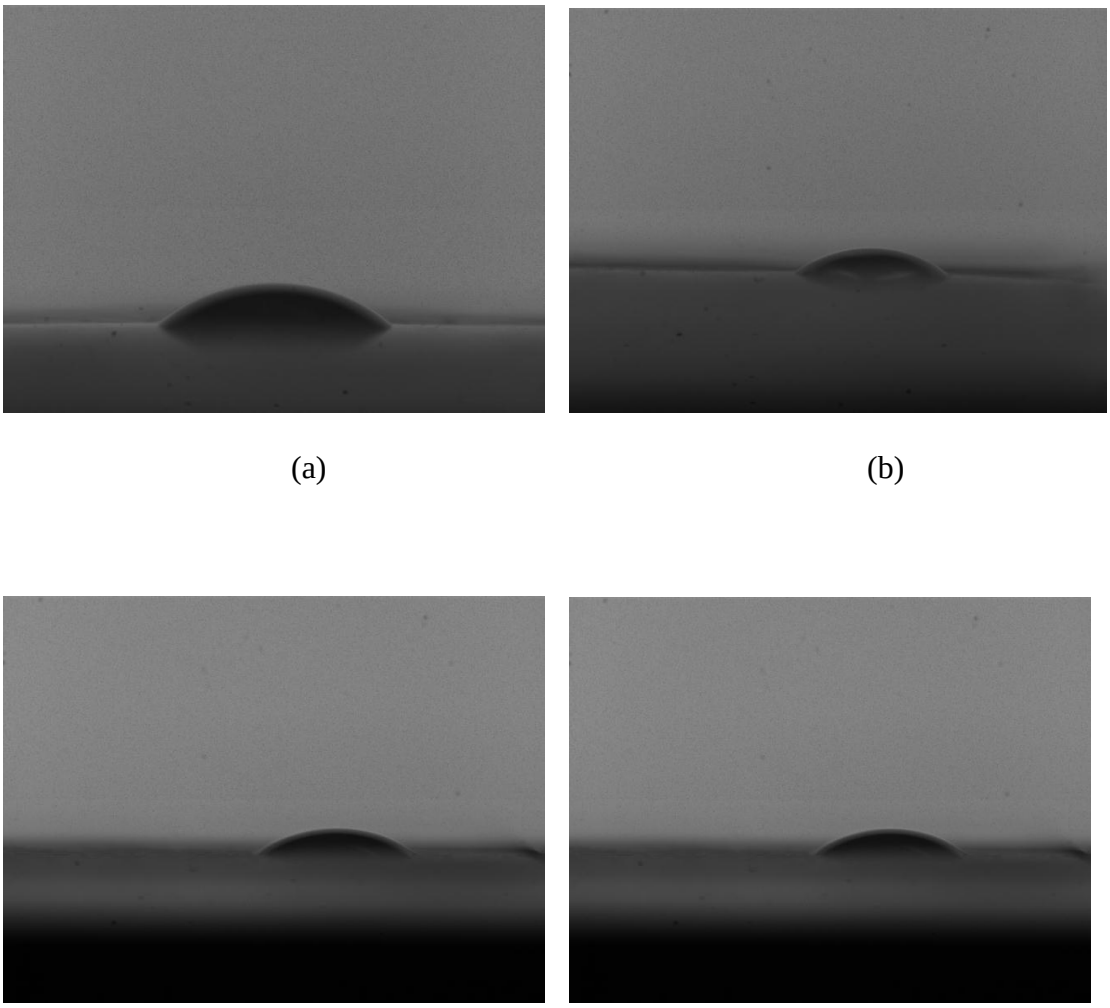

(a) (b)

(c) (d)

Figure 7.9 Representative contact angle images for membranes (a) TFC -HR (b) TF-RO-AD (c) SWC1 (d) UTC-80B

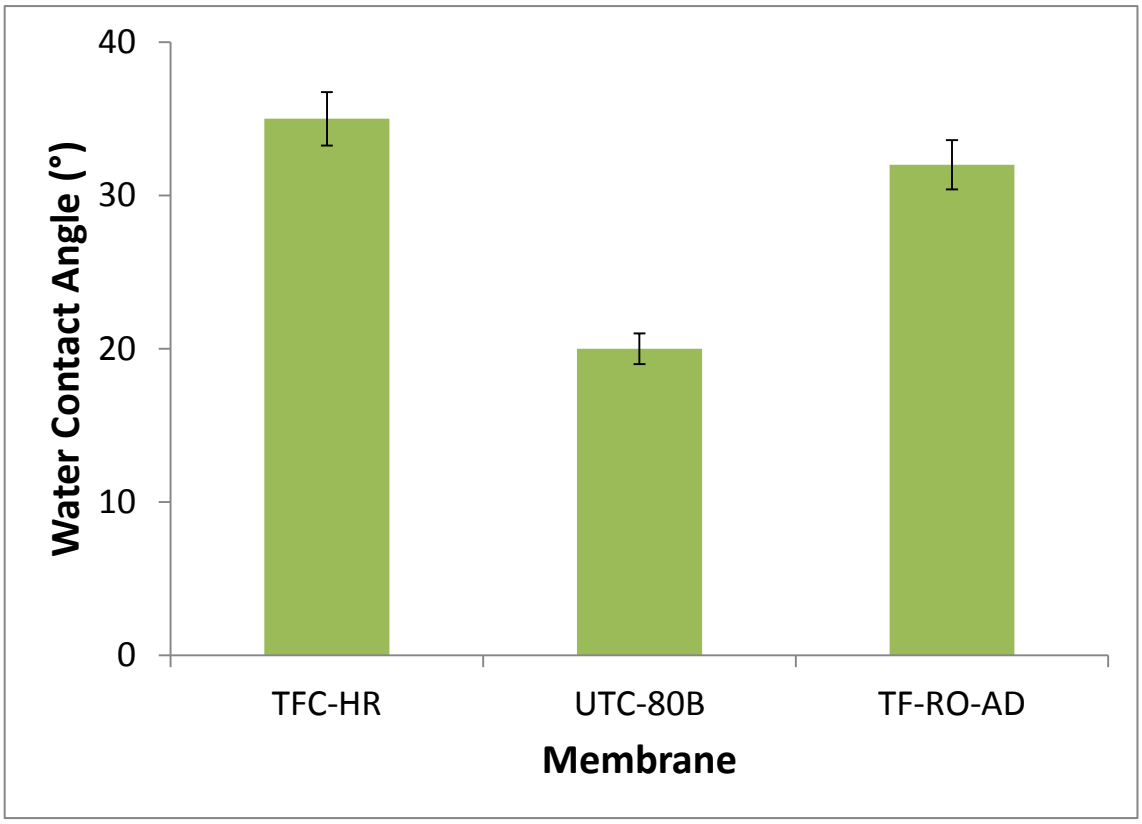

Figure 7.10 Average contact angle values for commercial membranes

To study the effect of the copolymer film chemistry, measurements were performed on TFC-HR membranes coated with films of different compositions. The static angle was used to probe the dry, fluorinated state of the film. Figure7.11 shows the droplet images captured on copolymer films of different chemistries. The droplet on the sample with 10% PFA coating has a very small contact angle (~15°) that confirms the hydrophilic nature of HEMA. On the other hand, the water droplet on the 75% PFA specimen has a very large angle value (~65°), courtesy of the hydrophobic PFA.

Fig. 7.12 shows the variation of the contact angle with increasing PFA content of the deposited copolymer film. The static contact angle increases rapidly with increasing hydrophobic content and saturates near the value for the PPFA homopolymer. For example, an amphiphilic chemistry of around 40% PFA, shows a water angle of more than 50° which is not far from the value for 75% PFA.

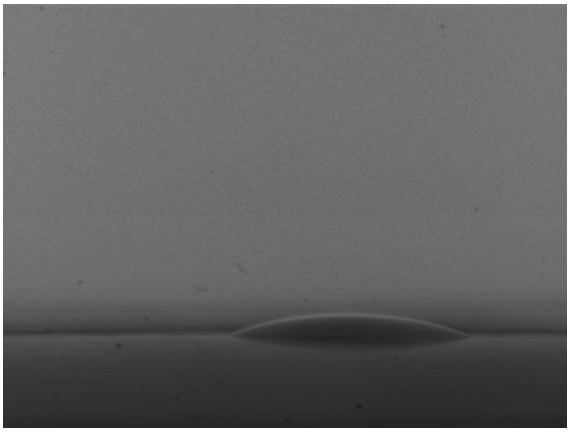

(a)

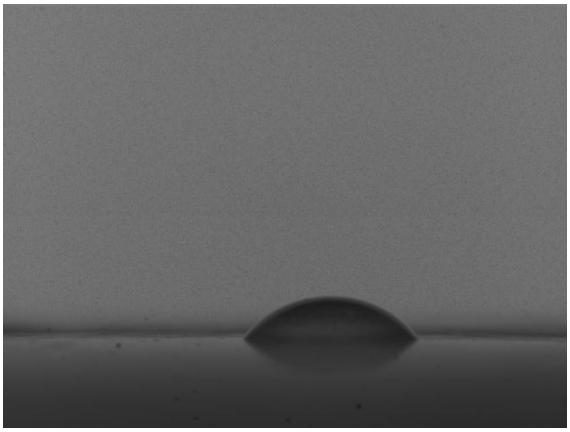

(b)

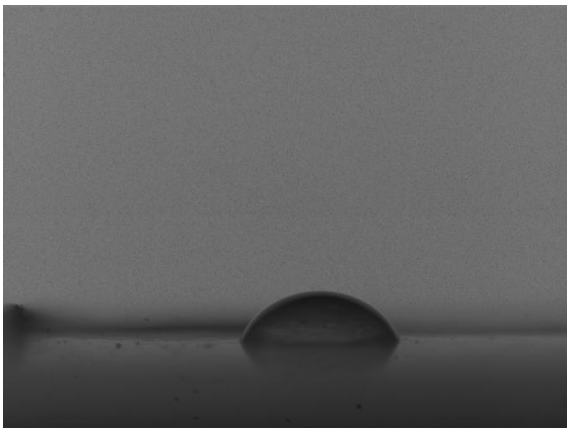

(c)

Figure 7.11 Water droplet images on the surfaces of TFC-HR membranes deposited with copolymer film of different chemistries (a) 10 (b) 37 (c) 75% PFA

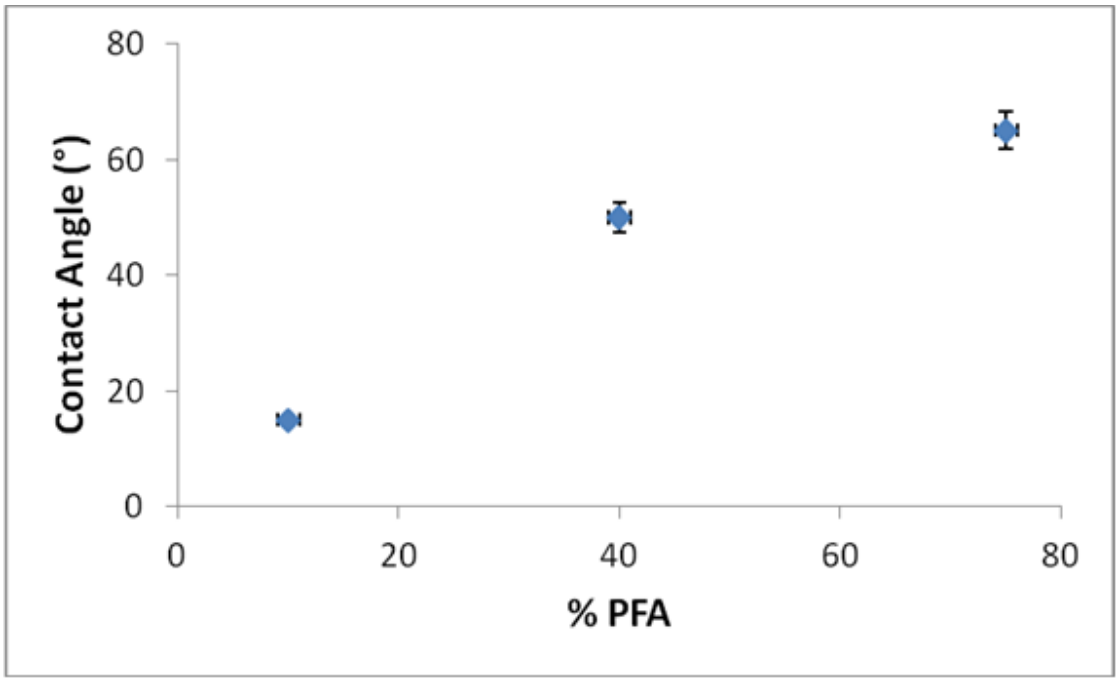

Figure 7.12 Variation of static contact angle with increasing PFA content

7.6 Surface Composition

Although the films are only 30nm thick, the bulk composition of the film does not reflect the surface composition of the film. In air or vacuum, the hydrophobic fluorinated alkyl chains of PFA will preferentially orient outward at the surface while the hydrophilic hydroxyl moiety of HEMA will preferentially orient inward.

The surface composition of the copolymer films was quantified using XPS survey scans, which have a sampling depth of approximately 5nm. As shown in Figure 7.13, the surface was always enriched in PFA as compared to the bulk for all film compositions except the pure homopolymers. In vacuum, the surface was over 50% PFA at bulk PFA concentrations below 20%.

As XPS probes only the near-surface depth of the film, this result confirms the preferential outward orientation of the hydrophobic side chains and the inward orientation of the hydrophilic side chains in vacuum. Similar fluorine enrichment at surfaces has been observed previously in copolymer films [155]. These results corroborate the earlier findings with the contact angle measurements (Figs.7.11 & 7.12)

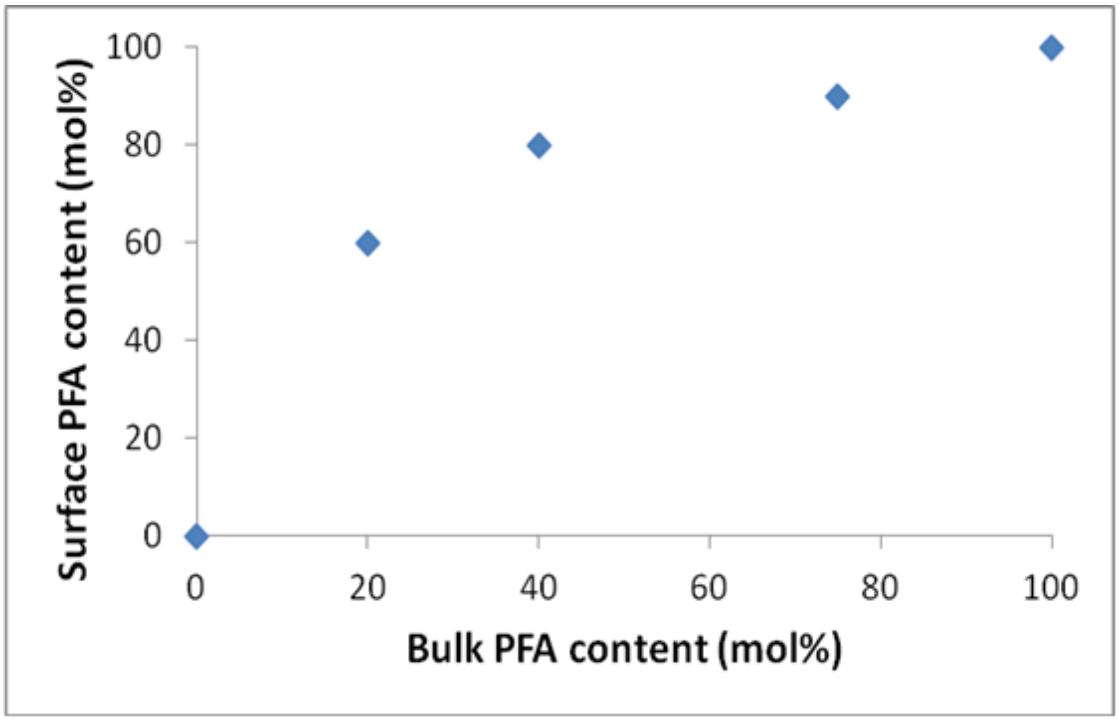

Figure 7.13 XPS measurements of the surface composition of the film as a function of the bulk film composition

7.7 Quartz Crystal Microscopy

Sodium Alginate

Representative QCM-D time traces corresponding to three different copolymer compositions in Figure 7.14 show a negative shift in the fifth harmonic frequency (24.8 MHz) of the crystal when the copolymer-coated sensor was exposed to a solution of sodium alginate, a model polysaccharide. These shifts occurred very rapidly upon introduction of the alginate into the sensor flow chamber. Similar negative shifts were observed for the third (14.9 MHz) and seventh (34.7) harmonics. A decrease in the harmonic frequency of a QCM-D sensor indicates a mass increase at the surface [156].

Because the films were allowed to fully hydrate in DI water prior to alginate exposure, this mass increase can be readily associated with the rapid adsorption of sodium alginate to the polymer films. Hydrophilic surfaces are known to have a strong affinity for hydrophilic macromolecules, and Figure 7.15 shows that sodium alginate adsorbs readily to the hydrogel PHEMA homopolymers. The magnitude of the frequency shift is much less for the PPFA homopolymer, consistent with previous observations that hydrophobic surfaces tend to discourage adsorption of hydrophilic macromolecules.

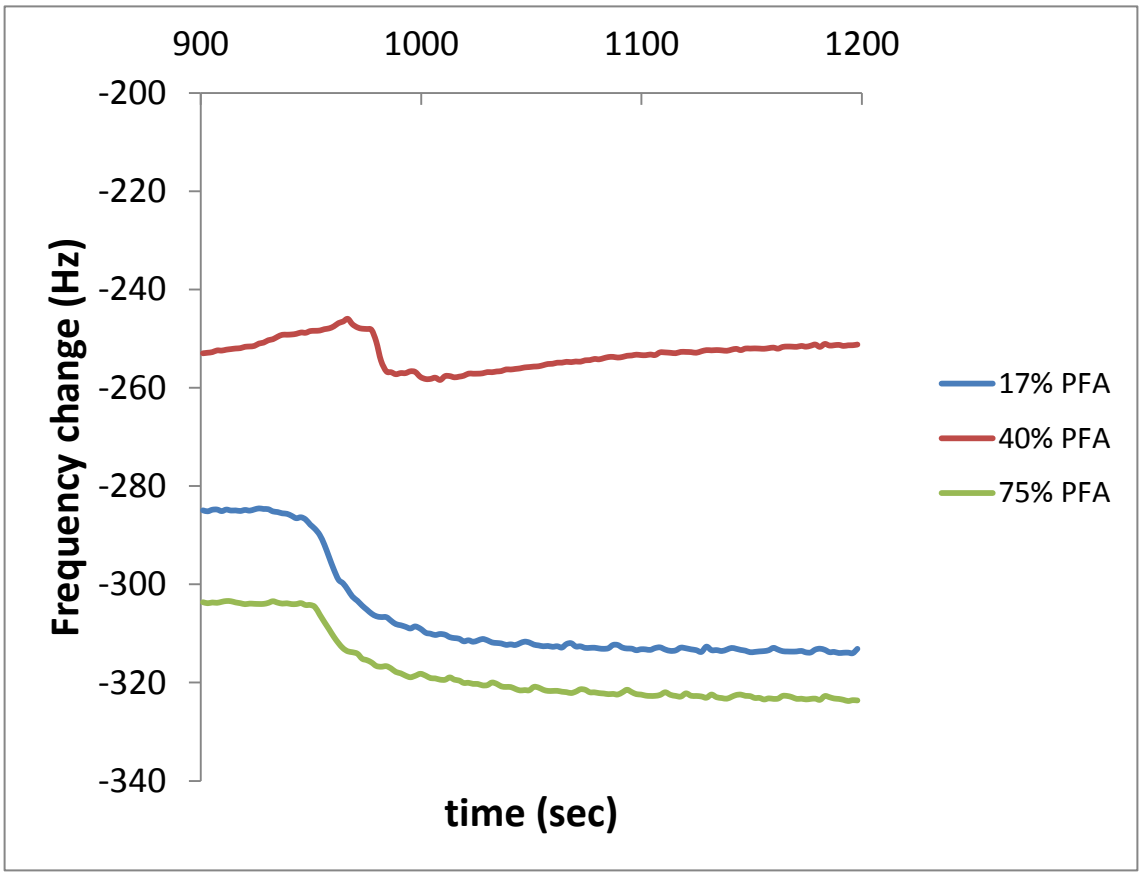

Figure 7.14 Representative time traces of the frequency shifts in the fifth harmonic of a QCM-D crystal sensor coated with copolymer film of compositions 17, 40 and 75% PFA

The magnitudes of the frequency shifts at the third, fifth and seventh harmonic frequencies are shown as a function of composition in Figure 7.15. In the case of protein adsorption, many studies employed a rinsing step to remove reversibly bound protein [157,158,159]. However, in the current work, no rinsing was used. Thus, these data represent the total alginate adsorption (reversible and irreversible) immediately after the introduction of alginate to the copolymer surfaces.

Understanding the initial adsorption event is critical for understanding the behavior of the copolymer films. As the PFA content of the copolymer film increases, the frequency shift, and therefore the adsorbed alginate mass, decreases quite significantly. This can be readily explained by the increasing hydrophobicity of the coating which tends to discourage the adsorption of the hydrophilic sodium alginate. A minimum is observed at a composition of 40% PFA that corresponds to an amphiphilic surface.

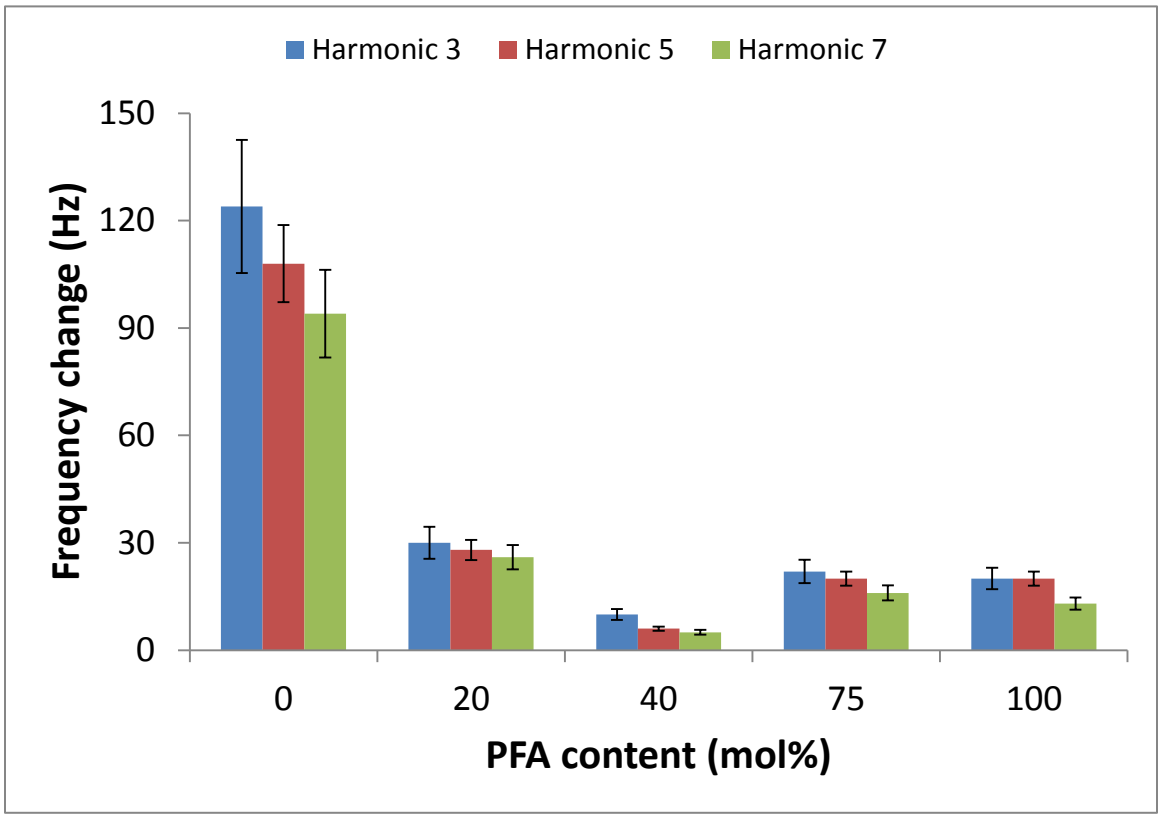

Figure 7.15 Harmonic shifts for different copolymer film compositions upon the introduction of sodium alginate in the flow cell of QCM-D

As the PFA content is increased further, the frequency shift, and hence the adsorbed mass, increases and then remains almost constant in the composition range 75-100% PFA. Hydrophobic surfaces discourage adsorption of hydrophilic materials because it is thermodynamically unfavorable. Thus, it is counterintuitive that increasing the hydrophobic content should increase alginate adsorption (Fig. 7.15). How then, can increased hydrophobic content (40-75% PFA) actually increase the amount of alginate that adsorbs to the surface?

This apparent contradiction can be explained by the fact that specific interactions, between some functional groups present in the copolymer film and the alginate, play an important role in alginate adsorption in addition to the nonspecific electrostatic and hydrophobic interactions. Li and coworkers [160] reported a similar observation while studying the role of common membrane surface functionalities on adsorption of organic foulants. They found that hydrophobic groups such as $–CH_3$ and –OPh showed more alginate adsorption than some of the hydrophilic groups such as $–EG_6OH$ and $–CONH_2$.

Humic Acid

Fig.7.16 shows the representative time traces of the frequency shifts in the fifth harmonic for two different copolymer film chemistries. The humic acid solution of known concentration was introduced around the half-hour mark and a sudden decrease in frequency is witnessed for both compositions around that time.

A summary of the results is presented as a bar chart in Fig.7.17 for the identical harmonic frequencies. Similar to the alginate, adsorption appears to be enhanced on hydrophilic surface as compared to hydrophobic and amphiphilic ones. However, the difference is that the adsorption remains almost constant upon increase in the PFA content beyond the intermediate chemistry.

The above trend can be readily explained by the molecular structure of humic acid. Although amphiphilic in characteristics, the hydrophilic groups such as hydroxyl, phenolic, etc. are present on the outside of the macromolecule and are first ones to interact with nearby molecules. On the other hand, the hydrophobic groups such as amine are present on the inside and are able to interact with neighboring molecules after a considerable delay.

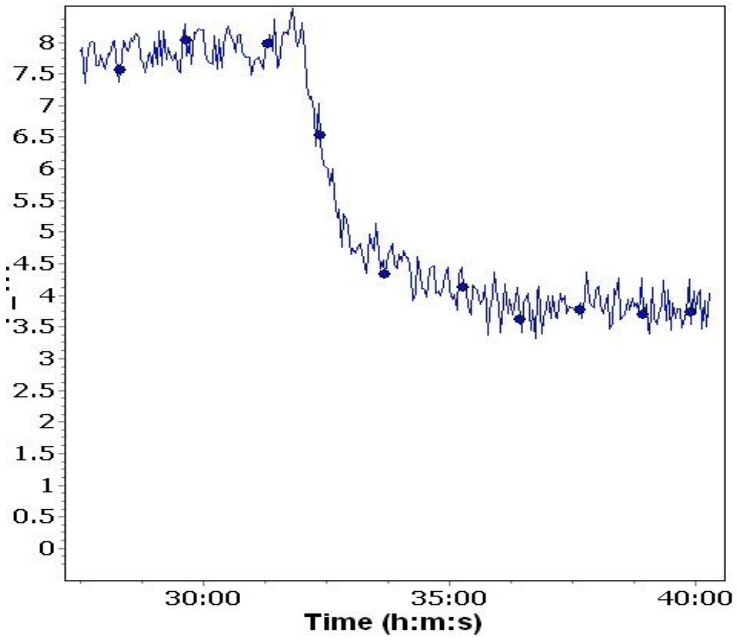

(a)

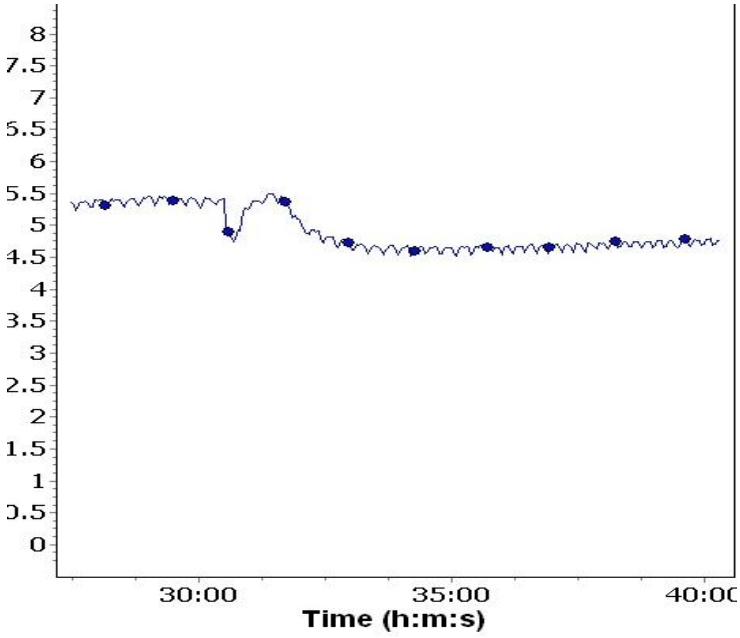

(b)

Figure 7.16 Representative time traces of the frequency shifts in the fifth harmonic of a QCM-D crystal sensor coated with copolymer film of composition (a) 20% PFA (b) 40% PFA

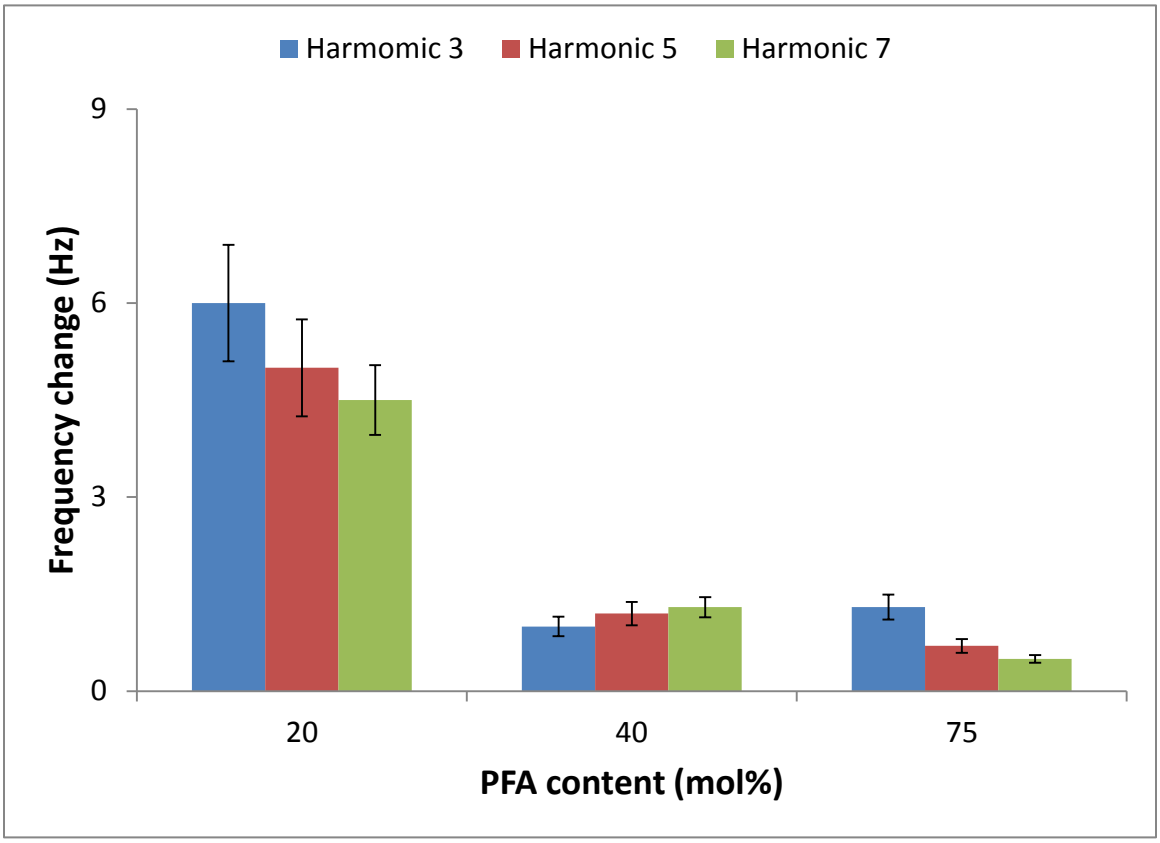

Figure 7.17 Harmonic shifts for three different copolymer film compositions upon the introduction of humic acid in the flow cell of QCM-D.

7.8 Bacterial Adhesion

SEM

To enable quantification of the bacteria attached irreversibly on the membrane surface, a total of 20 images were taken from different regions of the sample and at identical magnifications. Some of the representative images for both the virgin and the coated membrane are shown in Figure 7.18. They clearly reveal the greater susceptibility of the virgin membrane to bacterial attachment as can be seen from the quantity of bacteria. On the other hand, hardly any microorganisms are visible on the membrane covered with a copolymer film of intermediate chemistry i.e. 48% PFA.

Figure 7.19 shows the quantitative analysis of the bacteria carried out on the membranes. For each image, the total no. of bacteria were counted manually and divided by the sample area to give the no. of cells per unit area. The results show that bacterial adhesion to the copolymer film surface is negligible and hence confirms the antifouling capabilities of the amphiphilic chemistry.

To make the quantitative analysis as accurate as possible, the bacterial count was done for different number of images (5, 10, 15 and 20) selected at random. This was done until a plateau was reached for the cell density and a significant change was no longer visible. For better coverage of the samples, the images were taken at locations far away from each other. Some images were also taken at very high magnifications (20k, 40k) that clearly show the rod shape of the *E.coli* (Fig.7.20).

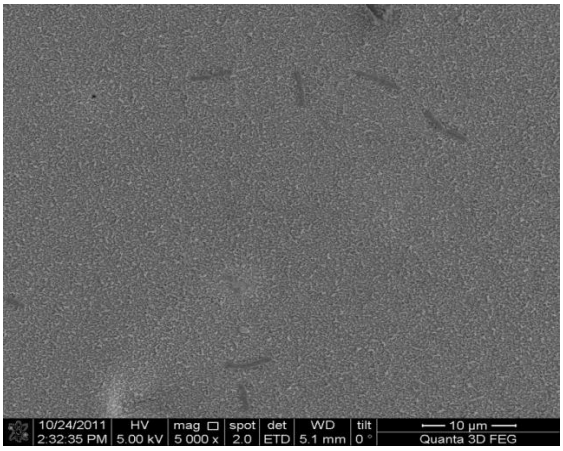

(a)

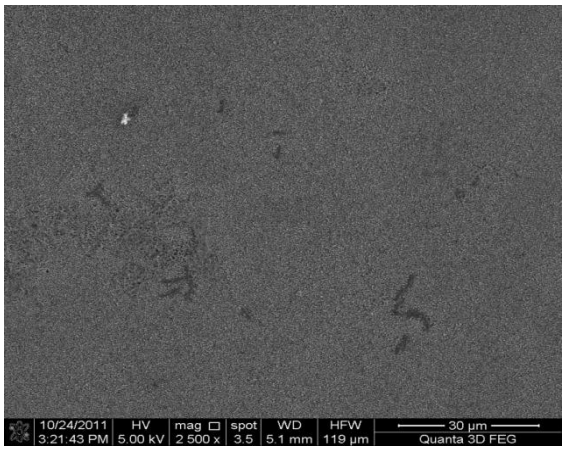

(b)

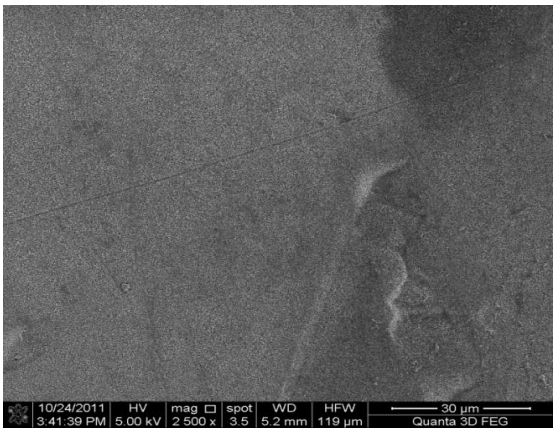

(c)

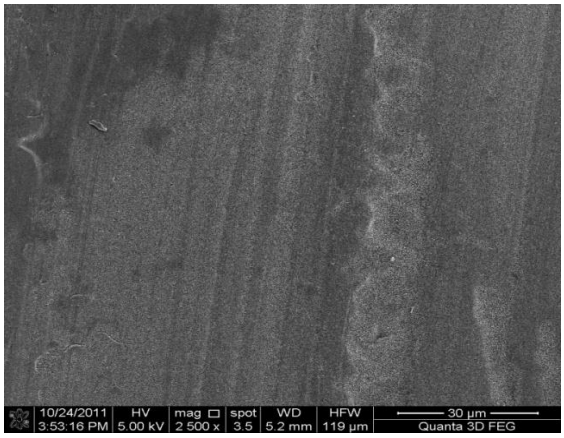

(d)

Figure 7.18 SEM images at lower magnification (2500x) showing bacterial adhesion on virgin (a,b) and membranes coated with a copolymer film of 40% PFA (c,d)

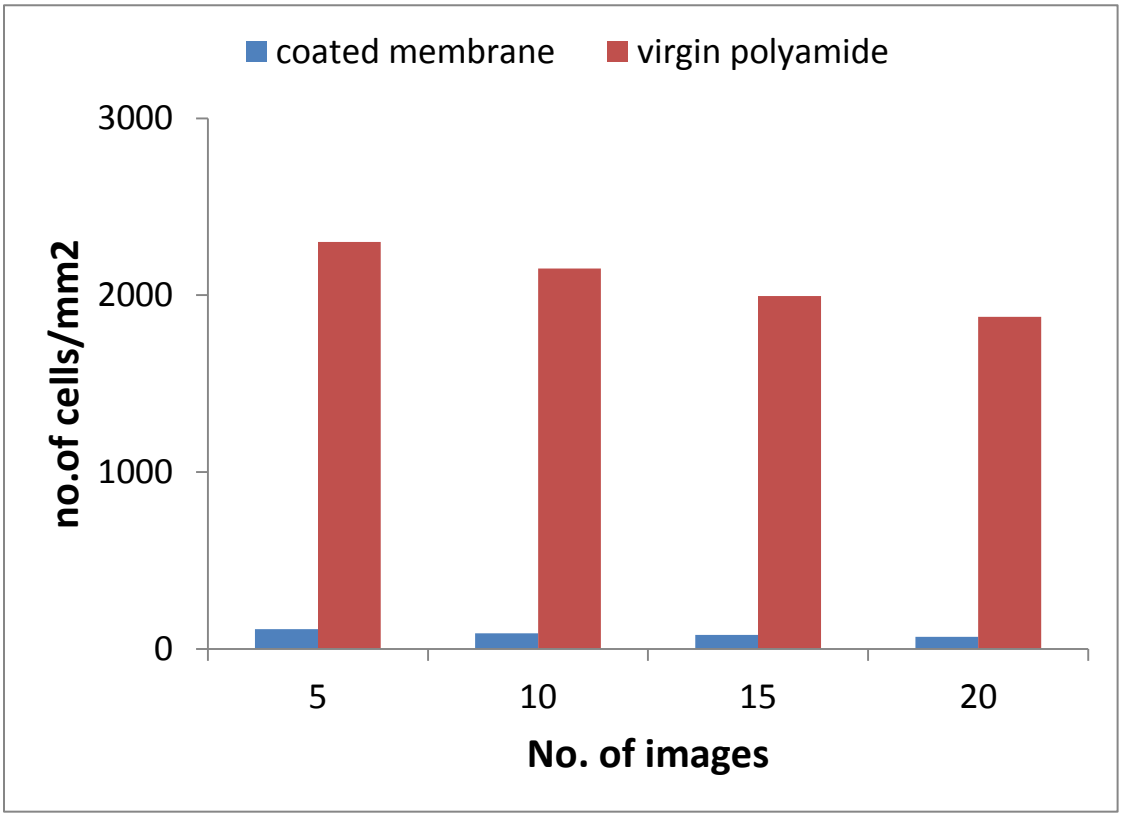

Figure 7.19 Average number of bacterial cells per unit area for both coated and uncoated membranes

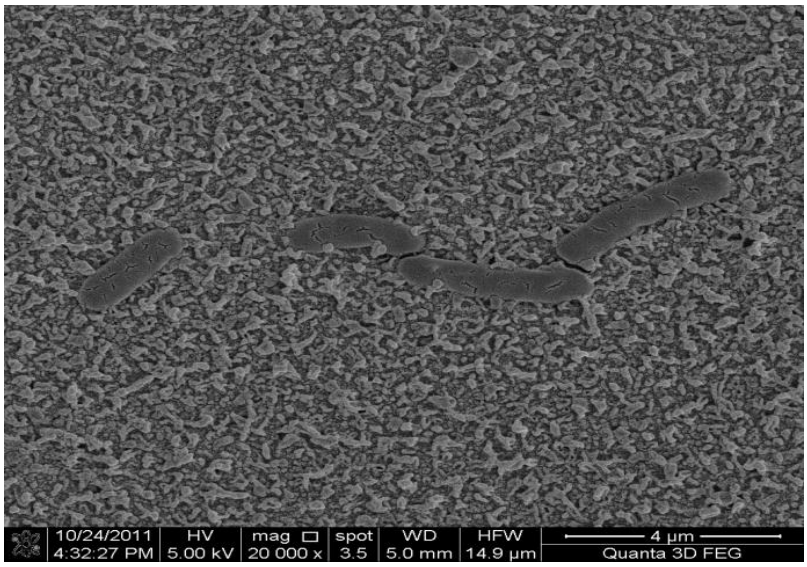

(a)

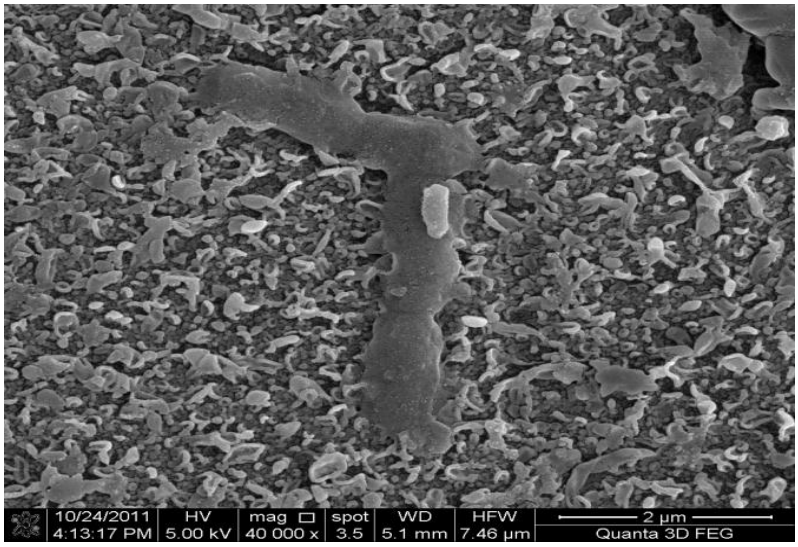

(b)

Figure 7.20 SEM images at high magnifications showing the bacteria on (a) virgin (b) coated membrane

In order to study the effect of the copolymer film chemistry on bacterial adhesion, membrane samples coated with different compositions were exposed to a bacterial suspension of *E.coli*. The films included the pure homopolymers, PHEMA and PPFA, as well as several intermediate chemistries. Following the earlier procedure, several SEM images were taken at different magnifications for all the samples.

The more hydrophobic chemistries i.e. 78 and 95% PFA undoubtedly show the highest tendency to attach bacteria (Fig.7.21). This is in accordance with a plethora of studies that show microbial liking for hydrophobic surfaces.

On the other hand, the no. of bacteria adhering to the hydrophilic surfaces is relatively less (Fig.7.21). The minimum seems to occur for an intermediate chemistry corresponding to an amphiphilic surface. Interestingly, increasing hydrophilicity also seems to enhance bacterial adhesion. So the pure PHEMA monomer has the highest no. of bacteria on its surface on the hydrophilic side of the film chemistries. This trend correlates well with the findings on protein adsorption by Gleason and coworkers [105].

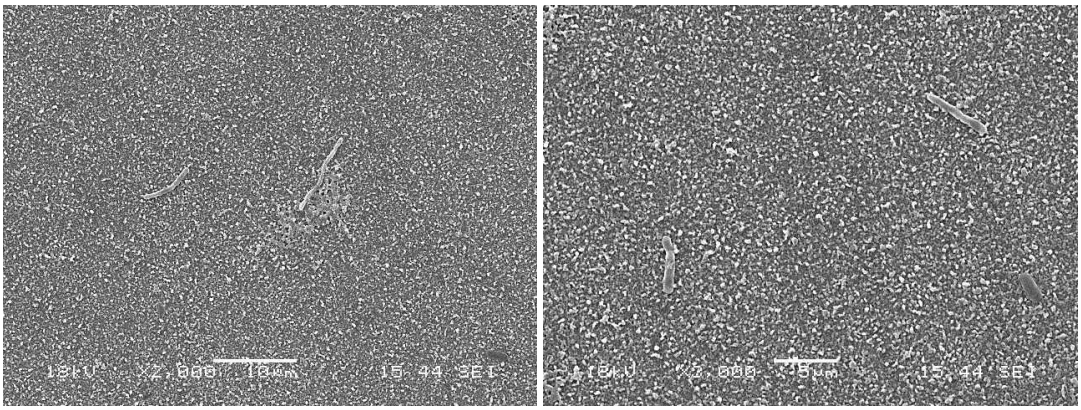

(a) (b)

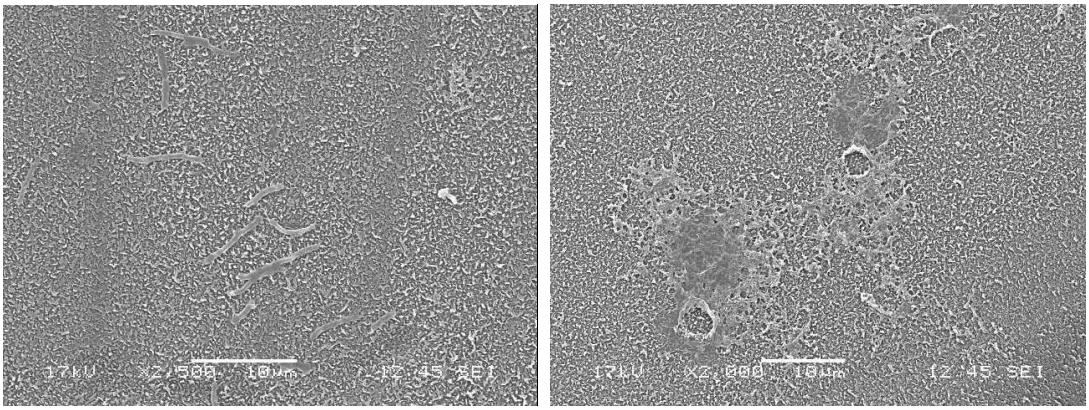

(c) (d)

Figure 7.21 SEM images of bacterial adhesion of membrane samples coated with different copolymer film chemistries (a) 17 (b) 40 (c) 78 (d) 95% PFA

Fluorescence Microscopy

In addition to SEM, fluorescence microscopy was also used to observe the membrane samples exposed to a known concentration of bacterial cells. The fluorescence images of the virgin and coated membrane samples are shown in Fig.7.22. The image of the commercial sample is very bright whereas that of the copolymer film specimen is quite dark. Since the bacterial suspension in which the samples were immersed was stained with a dye, the observed fluorescence comes only from the bacteria attached to the surface.

The above images, together with the SEM pictures, clearly show the effectiveness of the amphiphilic copolymer film in reducing the irreversible adhesion of bacteria and hence, membrane Biofouling. By interfering with the adsorption of proteins [105] and other relevant biopolymers (Figs.7.15 & 7.17), it is infact discouraging the attachment of microorganisms. On the other hand, the adhesion of a large no. of cells on the polyamide membrane can be explained by the presence of amine groups that are relatively hydrophobic.

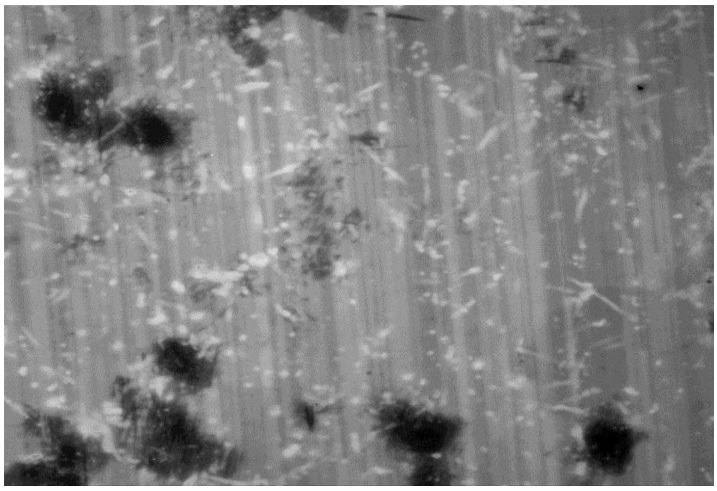

(a)

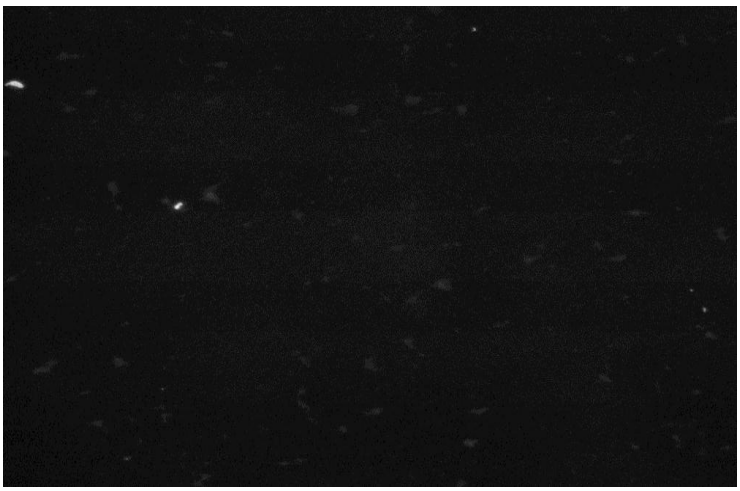

(b)

Figure 7.22 Fluorescence microscope images of (a) Virgin, and (b) membrane with 37%PFA film after 1 hour exposure to bacteria in LB medium at 22°C

In addition to the comparison of commercial membrane and the intermediate film chemistry, the effect of the coating composition on the bacterial adhesion was also studied. For this purpose, membrane samples coated with different chemistries were observed under the fluorescence microscope after exposure to a microbial suspension of *E.coli* cells. Several images were taken from different locations at two different magnifications (10, 20).

Fig.7.23 shows some representative images of the different samples at a magnification of 10 times. The bright spots at different locations of the samples emanates from the bacterial colonies present on the surface. Therefore, the number and brightness of these spots is a good indicator of the quantity of bacteria attaching to the surface.

As expected, the most hydrophobic surface (75% PFA) shows the highest number of the colonies. The amphiphilic chemistry i.e. 35% PFA shows the least no. of colonies on its surface. Interestingly, the moderately hydrophilic composition (20% PFA) shows higher microbial attachment as compared to the moderately hydrophobic one (60% PFA). This can be explained the enhanced adsorption of both sodium alginate and humic acid on the more hydrophilic surfaces (Figs.7.15 & 7.17).

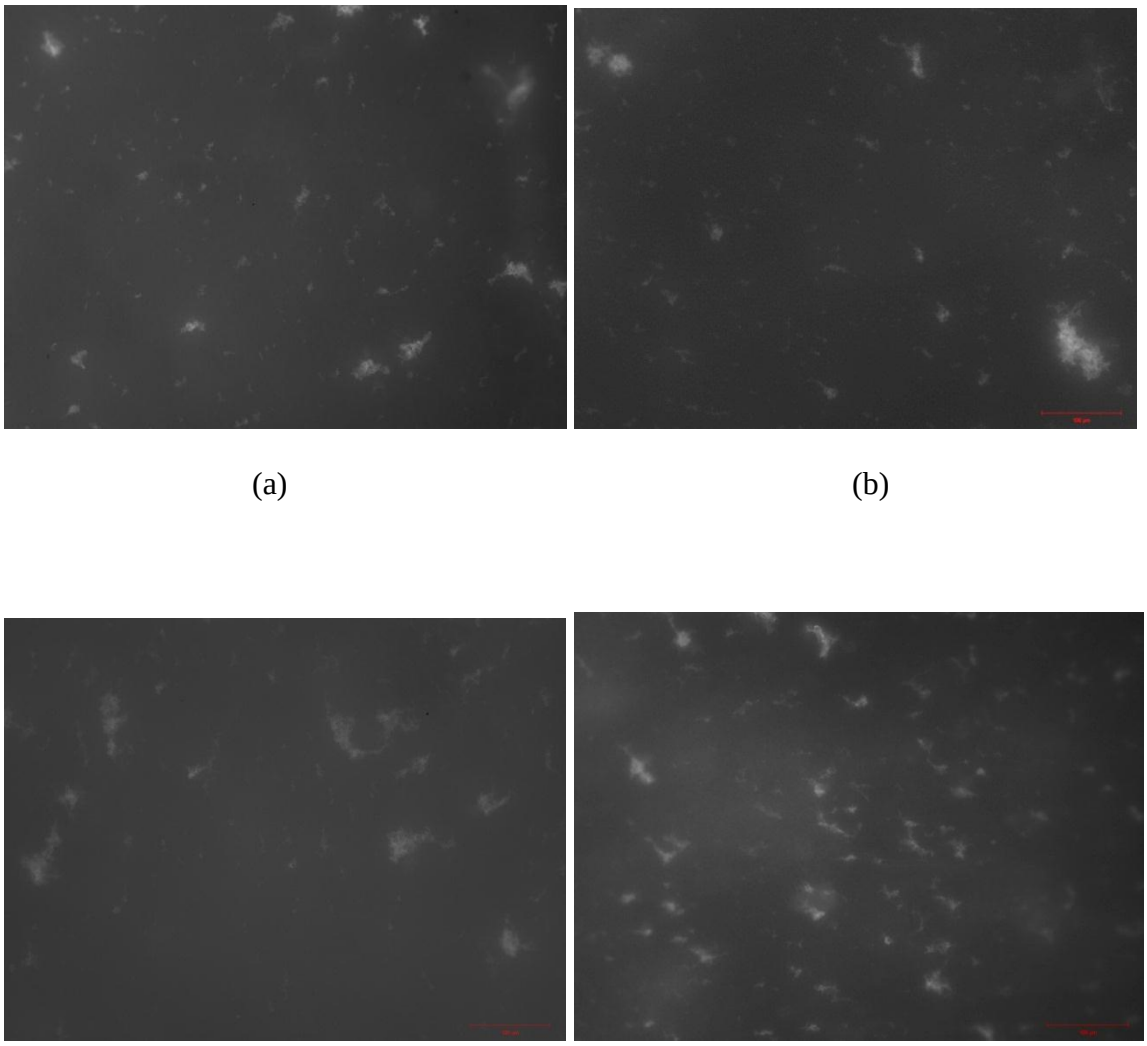

(a) (b)

(c) (d)

Figure 7.23 Fluorescence microscope images of samples with varying copolymer film chemistry exposed to bacteria for 2 hours at 37°C (a) 20 (b) 35 (c) 60 (d) 75% PFA

7.9 Coating Stability

A crucial parameter is to analyze the stability of the copolymer film deposited on the RO membrane during long-term permeation testing. In order to overcome the inherent osmotic pressure due to the high concentration of salts in seawater, very high pressures are applied externally to force the water molecules through the non-porous polyamide layer present on the membrane surface. Therefore, any coating deposited on the membrane should be able to withstand the high pressure.

Figure 7.24 shows the XPS survey scans of an UTC-80B membrane coated with a copolymer film of composition 37% PFA and thickness 20nm. The surface compositions were determined both before and after permeation tests of 48 hours. The results clearly show the presence of Fluorine peak with almost the same intensity even after permeation. This peak originates from the PFA present in the copolymer film and is a strong evidence of its presence.

The peaks for the remaining two elements, Carbon & Oxygen, are also pretty much similar for both samples. The results of the XPS scans confirm that the copolymer film is not affected by the application of high pressure. There is a possibility of some sort of bond formation between similar functional groups present in the polyamide as well as the copolymer e.g. carboxylic in the former and hydroxyl from the HEMA.

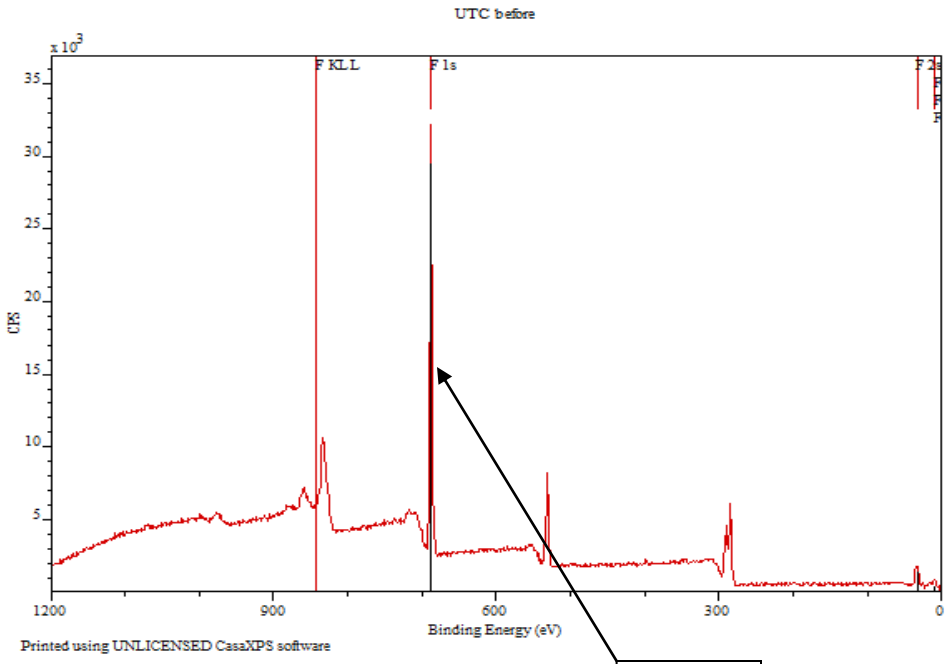

(a)

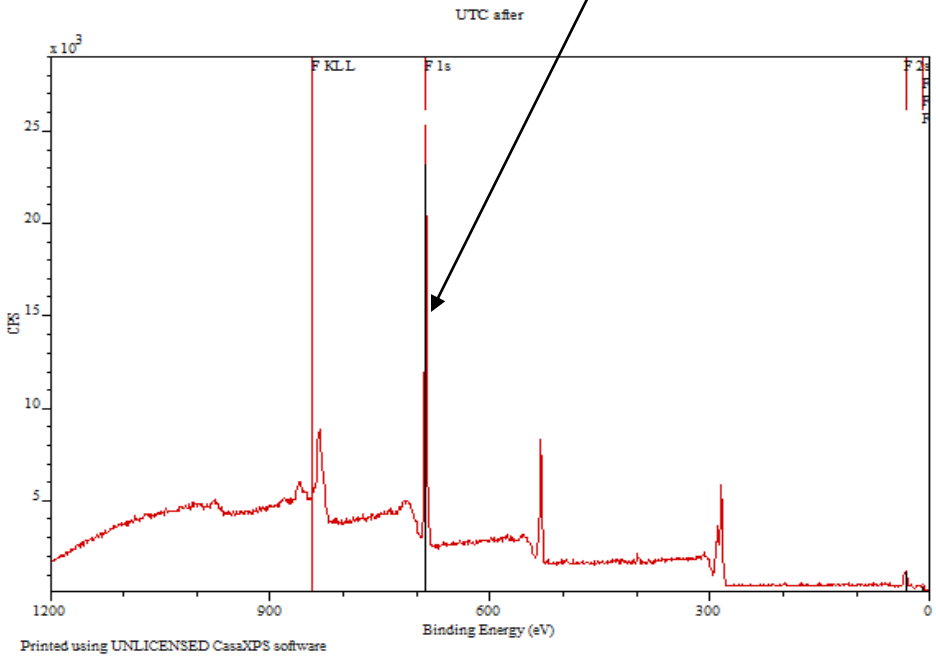

(b)

Figure 7.24 XPS results for UTC-80B membrane with copolymer film of 37% PFA (a) before, and (b) after permeation

7.10 Permeation

7.10.1 Water Flux

The foremost of concerns regarding any potential antifouling coating on water purification membranes is its transport properties i.e. water permeability and salt rejection. In order to assess the feasibility of the copolymer films for RO applications, permeation tests of several hours duration were performed on the different membranes. The testing conditions such as applied pressure, feed temperature and flow rate have been mentioned in Chapter 5 of this thesis.

Figure 7.25 shows the average flux values for the three different membranes in the absence of the copolymer film. The TFC-HR membrane from *Koch Membrane Systems* has the highest flux with an average of ~ 120 L/m^{2}h. The other two membranes have much lower flux with averages of around 45 and 25 L/m^{2}h respectively. The above results are in perfect agreement with the manufacturer's specifications.

Although of similar chemistry and structure, yet there is a significant difference between the membrane permeabilities. How can one explain this difference considering that the active layer (polyamide) is identical in the different membranes? This can be explained by the difference in the thickness of the polyamide layer: high flux membranes such as the TFC-HR have active layer thickness of around 100 nm (Figs.7.8) while typical seawater desalination membranes have much thicker polymide layers ~ 200 nm. One must keep in mind that the polyamide layer thickness is a variable and can be controlled by manipulation of the process parameters of the interfacial polymerization process.

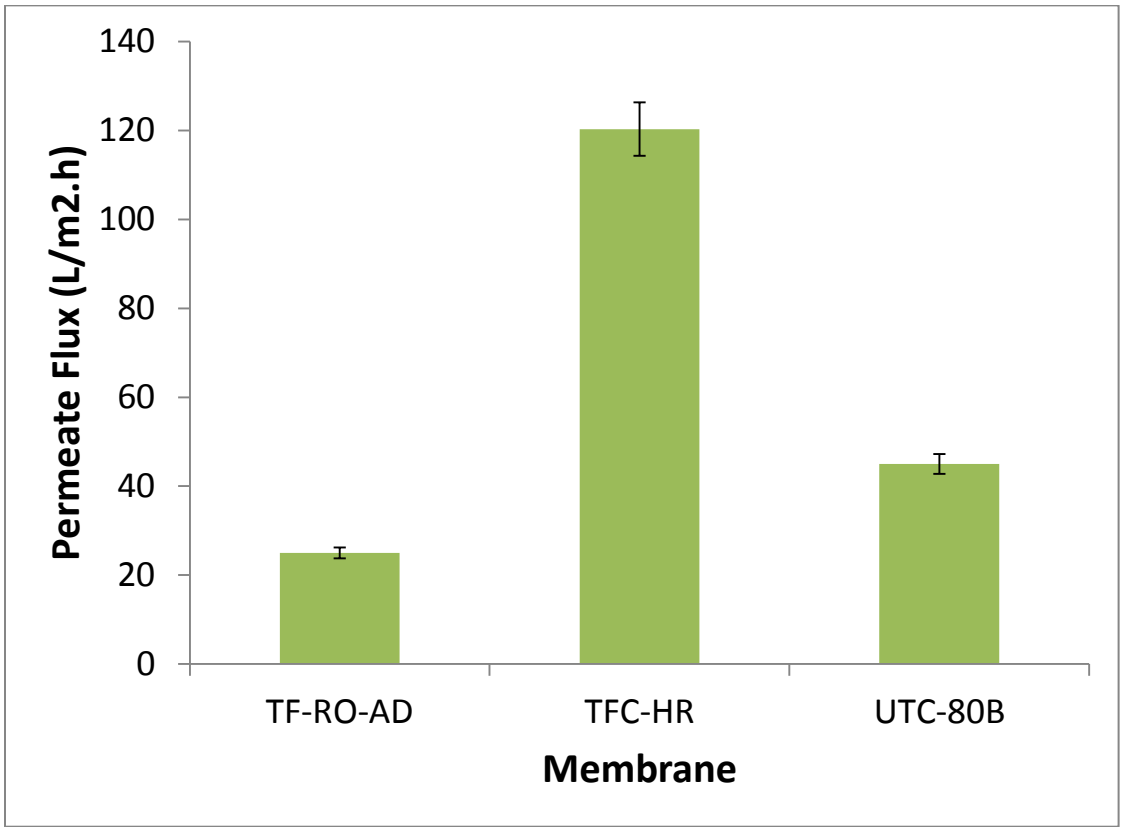

Figure 7.25 Average permeate values for the virgin commercial membranes with DI water

The membranes were then coated with copolymer films of optimum chemistry (40% PFA) and thickness (30nm). Permeation tests were then carried out under similar conditions of pressure and temperature. Figure 7.26 gives flux values both with and without the coating for all three membranes.

It is evident that the presence of the film does not cause a significant decline in the permeate flux. The decrease in flux was determined to be about 10-15% for all the membranes. For instance, the high flux TFC-HR registered a decline from 120 L/m^2h to an average value of 108 L/m^2h that corresponds to a mere 10%. Similarly, the seawater desalination membrane from Toray (UTC-80B) witnessed a decrease from 45 L/m^2h to a value of ~ 40 L/m^2h that is equivalent to a decline of 11%.

The permeation results are indicative of the copolymer film's higher permeability compared to the polyamide layer of the RO membrane. As measured from the high-resolution TEM images (Figs.7.8), the polyamide layer thickness in the TFC-HR is around 120nm. Deposition of a copolymer film 30 nm thick implies an increase in the barrier layer thickness by 25%. However, the resulting decline in permeate flux is only 10%, which is a clear proof of the copolymer film's superior permeability.

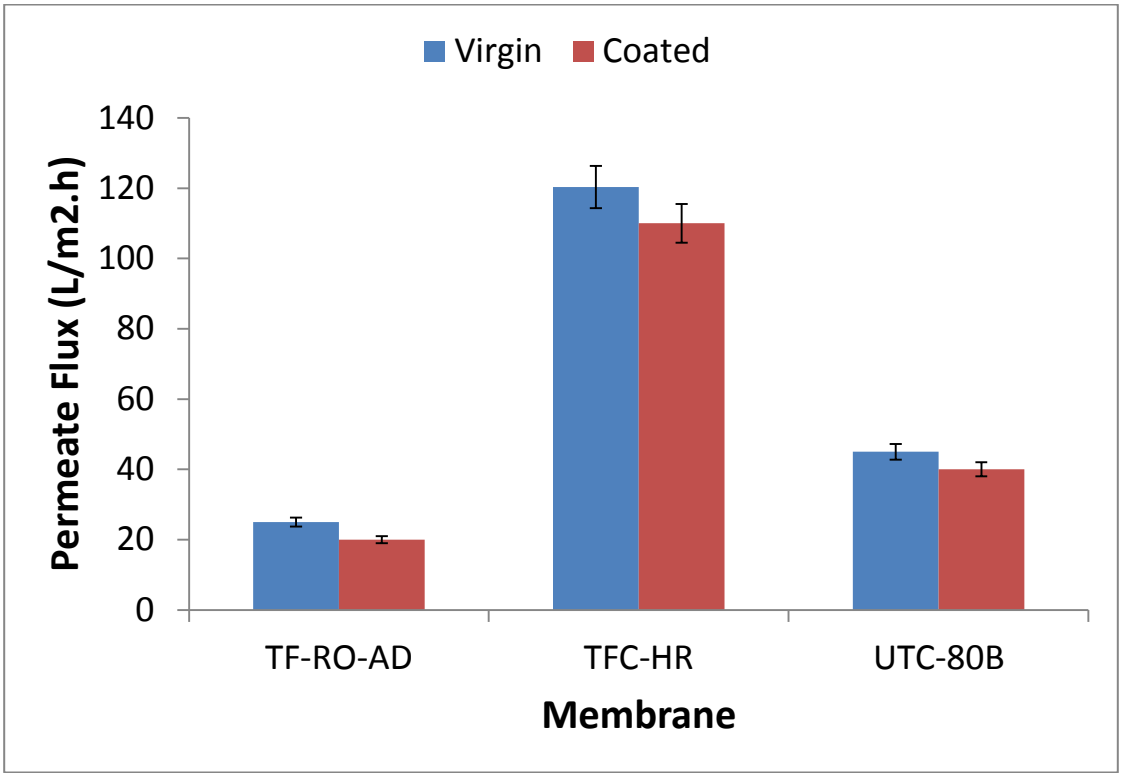

Figure 7.26 Permeation data for virgin and membranes coated with film of 40% PFA and 20nm thickness

7.10.2 Salt Rejection

The other important parameter investigated was the salt rejection of the commercial and surface-modified membranes. Measurement of this performance parameter is crucial as it determines the quality of permeate water that ascertains whether its fit for human consumption or not. For any membrane to qualify for a certain water purification technique, it's absolutely essential that it blocks the huge majority of salt ions present in the feed water and allows only a minimal fraction to pass through.

Figure 7.27 shows the salt rejection as a percentage for all the membranes used in this study both with and without the copolymer film. The concentration of sodium chloride in the feed solution was maintained at 2000 ppm. The results show that at this solute concentration, all the three membranes have near complete salt rejection. This is expected because of the virtually nonporous nature of the polyamide layer that has pore sizes less than the hydrated sodium ion radius.

The results also confirm that the presence of the copolymer film does not affect the salt rejection in an adverse manner. The earlier results for the permeate flux (Fig.7.26) has shown the coating to be more permeable and hence, most likely more porous than the polyamide layer of the RO membrane. In such a situation, one would expect higher salt passage through the copolymer film as compared to the polyamide layer. However, any salt passing through the HEMA-PFA coating is definitely blocked by the dense polyamide.

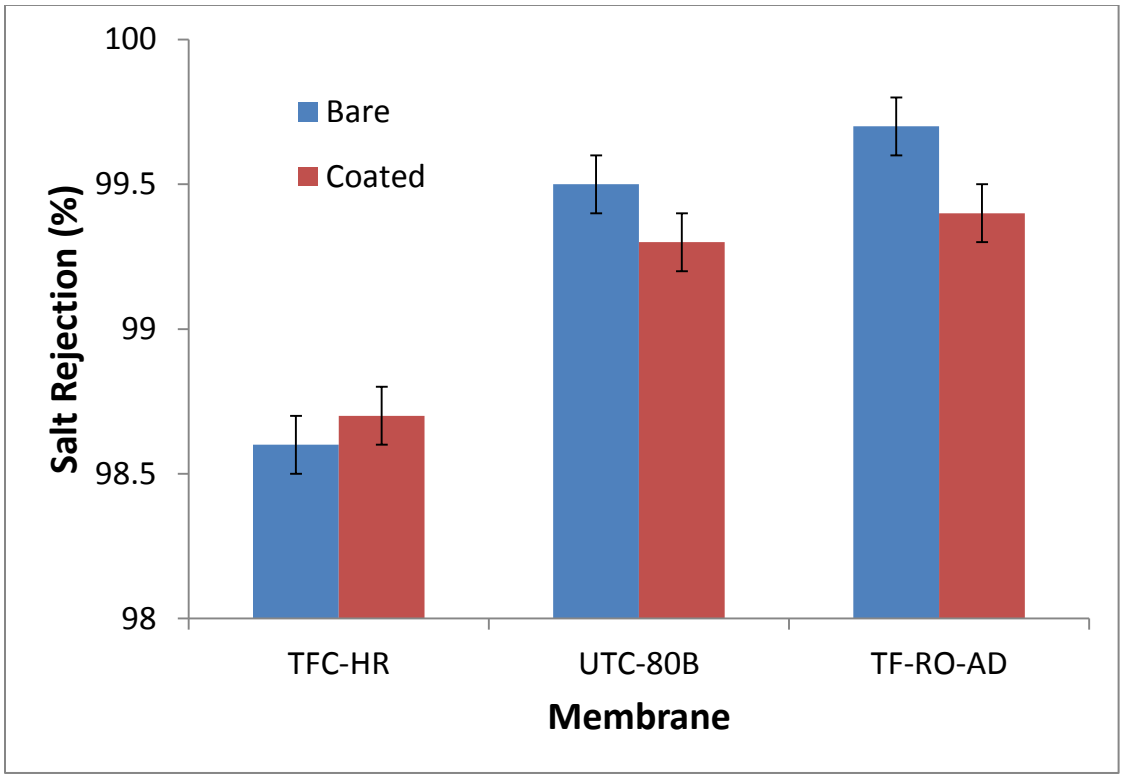

Figure 7.27 Salt rejection of the membranes with and without the copolymer film of chemistry 40% PFA and thickness of 30 nm

Chapter 8. Conclusions & Recommendations

8.1 Conclusions

The main objective of this work was to enhance the biofouling resistance of commercial RO membranes via modification of the active layer. This objective was achieved by successfully depositing a copolymer thin film on top of the polyamide layer. Copolymer films of hydroxyethyl methacrylate (HEMA) and the perfluorodecylacrylate (PFA) were synthesized and deposited on three different commercial RO membranes using an *initiated* CVD technique. The unique nature of the *i*CVD process allowed for solventless deposition at ambient temperatures without any damage to the substrate. The coating composition and thickness was controlled by adjusting the relative flow rates of the monomer gases and *in situ* laser interferometry. Later on, the use of variable angle ellipsometry (VAE) confirmed the accuracy of this technique.

Several characterization studies were carried out to determine the efficacy and compatibility of the deposited copolymer films. Surface topology measurements with AFM showed the coatings to be very smooth and rather improved the inherent surface roughness of the commercial membranes. TEM images of the cross-section confirmed the conformal and continuous nature of the coatings. Furthermore, they also corroborated the thickness determination by VAE.

To test the antifouling characteristics of the deposited copolymer film, model biopolymers, Sodium Alginate (SA) and Humic Acid (HA) were adsorbed using QCMD. Adsorption studies demonstrated that the intermediate chemistry corresponding to an amphiphilic (~40%PFA) surface shows the highest resistance to adsorption of SA and HA. The investigation was further extended to examine the resistance of the copolymer

film to the irreversible attachment of model bacterium *E. coli*. Bacterial attachment studies confirmed that copolymer coatings with amphiphilic chemistries also showed the highest resistance to irreversible attachment of *E. coli* bacterium. The bacterial adhesion on coated membranes was reduced by about 90% compared to the adhesion on virgin commercial membranes.

The coated membranes were then tested to compare their separation performance with the virgin membranes. Cross flow permeation test results proved that the presence of the films does not cause any significant flux decline in comparison to the virgin membranes. Furthermore, salt rejection also remained more or less unaffected by the presence of the coating. XPS analysis performed on the tested coated membranes confirmed that the deposited copolymer films remained stable and intact after long-term (100 hour) permeation testing under high (700 psi) pressure conditions.

As a final conclusion it can be safely said that the surface modification of the commercial RO membranes by the deposition of copolymer thin films show great promise to significantly enhance the biofouling resistance of commercial RO membranes. However, further studies are needed in order to unearth their real potentials of this copolymer tin film surface modification strategy for improving the biofouling resistance of SWRO membranes.

8.2 Recommendations

The results of this study have shown a great promise for these copolymer films as far as both the performance and stability is concerned. However, long-term tests of 200 – 250 hours duration are needed with feed water containing actual seawater biofoulants to assess the copolymer film's effectiveness in retarding the permanent flux decline

normally associated with Biofilm formation. Moreover, the performance of the surface-modified membrane needs to be judged in the presence of actual seawater/brackish water samples.

The effect of permeation variables on the performance of the coated membranes also needs to be considered. For example, the feed temperature is an important variable especially for the gulf region where temperatures around 50°C are not uncommon during the peak summer periods. This is also critical from the point of view of biofouling, as higher temperatures promote/accelerate the growth of microorganisms. Currently, tests were performed at a salt concentration of 2000 ppm which is a nominal value. Permeation runs need to be carried out at much higher concentrations that are more representative of actual seawater concentrations such as 25,000 ppm (less saline seawater e.g. Tampa Bay, USA), 35000 ppm (average value for seawater), and 45000-55,000 ppm (typical values for the Arabian Gulf).

Permeation tests show the copolymer film to be more permeable than the polyamide layer on the RO membrane: a 25% increase in the overall thickness of the active layer results in a flux decline of around 10-15%. An interesting study would be to explore replacing the polyamide active layer with the copolymer film as the active layer. This could be achieved by the deposition of thicker (150-200 nm) thick copolymer films on polysulfone ultrafiltration membranes and testing the performance of such a membrane to see if such a membrane can be used as a potential new RO seawater desalination membrane.

References

1. V. Gewin, Industry lured by the gains of going green, *Nature* 436 (2005) 173.

2. M.A. Shannon, P.W. Bohn, M. Elimelech, J.G. Georgiadis, B.J. Marinas, A.M. Mayes, Science and technology for water purification in the coming decades. *Nature* 452 (2008) 301-310

3. M. Elimelech, The global challenge for adequate and safe water, *J. Water Supply Res. Technol*. -Aqua 55 (2006) 3.

4. R. F. Service, Desalination freshens up, *Science*, 313 (2006) 1088-1090

5. T. Oki and S. Kanae, Global hydrological cycles and world water resources, *Science*, 313 (2006) 1068-1071.

6. A.G. Fane and G.L. Leslie, Membrane technology – the key to water reuse, Proceedings, IWA Conference on Water Environment-Membrane Technology, 875–883, Seoul, Korea (2004).

7. R.W. Baker, *Membrane Technology and Applications* , 2nd ed., John Wiley & Sons, Chichester, New York, 2004

8. A.P. Rao, N.V. Desai, R. Rangarajan, Interfacially synthesized thin film composite RO membrane for seawater desalination, *J. Membr. Sci*. 124 (1997) 263

9. Z. Amjad, *Reverse Osmosis: Membrane Technology, Water Chemistry, and Industrial Applications*, Van Nostrand Reinhold, New York, 1993.

10. J. E. Cadotte, Evolution of composite reverse osmosis membranes in Materials Science of Synthetic Membranes, D. R. Lloyd (Ed.), Vol. 269, American Chemical Society, Washington D.C., 1985, pp. 273-294.

11. P. W. Morgan, *Condensation Polymers: By Interfacial and Solution Methods*, Interscience Publishers, New York, 1965.

12. W. E. Mickols, Composite membrane and method for making the same, U.S. Patent 6,562,266 B2 (2003).

13. R. J. Petersen, Composite reverse osmosis and nanofiltration membranes, *J. Membr. Sci.* 83 (1993) 81-150.

14. GE Water and Process Technologies AG RO Product Specification, *http://www.gewater.com* (2008).

15. S. Hong, M. Elimelech, Chemical and physical aspects of natural organic matter (NOM) fouling of nanofiltration membranes, *J. Membr. Sci*. 132 (1997) 159

16. S. Belfer, Y. Purinson, R. Fainshtein, Y. Radchenko, O. Kedem, Surface modification of commercial composite polyamide reverse osmosis membranes, *J. Membr. Sci*. 139 (1998) 175

17. X. Zhu, M. Elimelech, Colloidal fouling of reverse osmosis membranes: measurements and fouling mechanisms, *Environ. Sci. Technol*. 31 (1997) 3654

18. K.L. Jones, C.R. O'Melia, Protein and humic acid adsorption onto hydrophilic membrane surfaces: effects of pH and ionic strength, *J. Membr. Sci*. 165 (2000) 31-46

19. H.F. Ridgway, Biological fouling of separation membranes used in water treatment applications, AWWA Research Foundation, 2003

20. J.S. Vrouwenvelder, J.A.M. Passen, L.P. Wessels, A.F. van Dam, S.M. Bakker, The Membrane Fouling Simulator: A practical tool for fouling prediction and control, *J. Membr. Sci*. 281 (2006) 316-324

21. H.-C. Flemming, Reverse Osmosis Membrane Biofouling, *Exp. Therm. Fluid Sci.* 1997, 14, 382-391

22. M.F.A. Goosen, S.S. Sablani, H. Al-Hinai, S. Al-Obeidani, R. Al-Belushi, D. Jackson, Fouling of reverse osmosis and ultrafiltration membranes: a critical review, *Sep. Sci. Technol*. 39 (2005) 2261

23. H.C. Flemming, G. Schaule, T. Griebe, J. Schmitt, A. Tamachkiarowa, Biofouling – the Achilles heel of membrane processes, *Desalination* 113 (1997) 215

24. J.S. Baker, L.Y. Dudley, Biofouling in membrane systems – A review, *Desalination* 118 (1998) 81-90

25. H.-C. Flemming, Biofouling in water systems – cases, causes and countermeasures, *Appl. Microbiol. Biotechnol.* 59 (2002) 629-640

26. D. Beer, P. Stoodley, Microbial Biofilms. In: *Prokaryotes* (2006) 1:904–937 DOI: 10.1007/0-387-30741-9_28

27. S.B. Sadr Ghayeni, P.J. Beatson, R.P. Schneider, A.G. Fane, Adhesion of wastewater bacteria to reverse osmosis membranes, *J. Membr. Sci*. 138 (1998) 29-42

28. M.M. Ramsey, M. Whiteley, *Pseudomonas aeruginosa* attachment and biofilm development in dynamic environments, *Mol. Microbiol.* 53 (2004) 1075-1087

29. H.-C. Flemming, Mechanistic aspects of RO membrane biofouling and prevention. In: *Reverse Osmosis: Membrane Technology, Water Chemistry, and Industrial Applications*, Z.Amjad, ed., Van Nostrand Reinhold, New York, 1993

30. J.S. Vrouwenvelder, S.A. Manolarakis, J.P. van der Hoek, J.A.M. van Paassen, W.G.J. van der Meer, J.M.C. van Agtmaal, H.D.M. Prummel, J.C. Kruithof, M.C.M. van Loosdrecht, Quantitative biofouling diagnosis in full scale nanofiltration and reverse osmosis installations. *Wat. Res*. 42 (2008) 4856-4868

31. C. Sommariva, A. Comite, G. Capannelli, A. Bottino, Relationship between biofouling and recovery ratio: the theoretical approach and one experimental case. *Desalination* 204, 175-180

32. R.P. Schneider, L.M. Ferreira, P. Binder, E.M. Bejarano, K.P. Goes, E. Slongo, C.R. Machado, G.M.Z. Rosa, Dynamics of organic carbon and of bacterial populations in a conventional pretreatment train of a reverse osmosis unit experiencing severe biofouling. *J. Membr. Sci*. 266 (2005) 18-29

33. M. Herzberg, M. Elimelech, "Biofouling of reverse osmosis membranes: Role of biofilm-enhanced osmotic pressure" *J. Membr. Sci.* 295 (2007) 11-20

34. J.S. Vrouwenvelder, D.A. Graf von der Schulenburg, J.C. Kruithof, M.L. Johns, M.C.M. van Loosdrecht, Biofouling of spiral-wound nanofiltration and reverse osmosis membranes: A feed spacer problem, *Wat. Res*. 43 (2009) 583-594

35. H.F. Ridgway, Microbial Adhesion and Biofouling of Reverse Osmosis Membranes. In *Reverse Osmosis Technology*, B.S. Parekh, Ed., pp. 429-481, Marcel Dekker, New York, Basel, 1988

36. H.F. Ridgway, J. Safarik, Biofouling on Reverse Osmosis Membranes. In *Biofouling and Biocorrosion in Industrial Water Systems*. H.C. Flemming and G.G. Geesey, Eds., pp. 81-111, Springer Verlag, Heidelberg, Berlin, 1991

37. H.-C. Flemming, G. Schaule, R. McDonogh, How do performance parameters respond to initial biofilm formation on separation membranes? *Vom Wasser* 80 (1993) 177-186

38. P.A. Cantor, B.J. Mechalas, Biological degradation of cellulose acetate reverse osmosis membranes, *J. Polym. Sci*. 28 (1969) 225-241

39. J. K. Beasley, The evaluation and selection of polymeric materials for reverse osmosis membranes, *Desalination* 212 (1977) 181-189

40. J.E. Cadotte, R.J. Petersen, R.E. Larson, E.E. Erickson, A new thin-film composite seawater reverse osmosis membrane, *Desalination* 32 (1980) 25-31

41. A.P. Murphy, C.D. Moody, R.L. Riley, S.W. Lin, B. Murugaverl, P. Rusin, Microbiological damage of cellulose acetate RO membranes, *J. Membr. Sci*. 193 (2001) 111–121

42. S. Beverly, S. Seal, S. Hong, Identification of surface chemical functional groups correlated to failure of reverse osmosis polymeric membranes, *J. Vac. Sci. Technol*. A 18.(2000) 1107-1113

43. M. Al-Ahmad, F.A.Abdel Aleem, A. Mutiri, A. Ubaisy, Biofouling in RO membrane systems Part I: Fundamentals and control, *Desalination* 132 (2000) 173-179

44. H.-C. Flemming, G. Schaule, R. McDonogh, H.F. Ridgway, Mechanism and Extent of Membrane Biofouling. In *Biofouling and Biocorrosion in Industrial Water Systems*, G.G. Geesey, Z. Lewandowski, and H.-C. Flemming, Eds., pp. 63-89, Lewis Publishers, Chelsea, MI, 1994

45. S.R. Ahmed, M.S. Alansari, T. Kannari, Biological Fouling and Control at Ras Abu Jarjur RO Plant: A New Approach, *Desalination* 74 (1989) 69-84

46. A.B. Mindler, S.T. Bateman, *Pilot Plant Study on Marine Microorganisms and Organic Matter in Seawater Desalination by Reverse Osmosis*, prepared for Office of Water Research and Technology, Washington DC, pp. 2, 126

47. D.H. Paul, Reverse Osmosis: scaling, fouling and chemical attack. *International Desalination & Water Reuse*, 1, 8-11

48. M.G. Khedr, Membrane fouling problems in reverse osmosis desalination plants, *Desalination & Water Reuse* 10 (3) 8-17

49. H.F. Ridgway, *Membrane biofouling: an international workshop*. National Water Research Institute occasional paper number NWRI-97-3. Sydney, Australia, 1997, pp.75-79

50. C.K. Teng, M.N.A. Hawlader, A. Malek, An experiment with different pretreatment methods, *Desalination* 156 (2003) 51-58

51. S. Ebrahim, M. Abdel-Jawad, S. Bou-Hamad, M. Safar, Fifteen years of R&D program in seawater desalination at KISR. Part I. Pretreatment technologies for RO system, *Desalination* 135 (2001) 141

52. Y. Taniguchi, An overview of pretreatment technology for reverse osmosis desalination plants in Japan, *Desalination* 110 (1997) 21

53. A. Brehant, V. Bonnelye, M. Perez, Comparison of MF/UF pretreatment with conventional filtration prior to RO membranes for surface seawater desalination, *Desalination* 144 (2002) 353

54. K.T. Chua, M.N.A. Hawlader, A. Malek, Pretreatment of seawater: results of pilot trials in Singapore, *Desalination* 159 (2003) 225

55. R.P. Schneider, L.M. Ferreira, P. Binder, E.M. Bejarano, K.P. Goes, E. Slongo, C.R. Machado, G.M.Z. Rosa, Dynamics of organic carbon and of bacterial populations in a conventional pretreatment train of a reverse osmosis unit experiencing severe biofouling. *J. Membr. Sci*. 266 (2005) 18-29

56. V. Lund, K. Ormerod, The influence of disinfection processes on biofilm formation in water distribution systems, *Water Res*. 29 (1995) 1013

57. C.R. Bartels, M. Wilf, K. Andes, J. Iong, Design considerations for wastewater treatment by reverse osmosis, *Water Sci. Technol*., 51 (2005) 473-482

58. G. Petrucci, M. Rosellini, Chlorine dioxide in seawater for fouling control and post-disinfection in potable networks, *Desalination*, 182 (2005) 283-291

59. G.D. Kang, C.J. Gao, W.D. Chen, X.M. Jie, Y.M. Cao, Q. Yuan, Study on hypochlorite degradation of aromatic polyamide reverse osmosis membrane, *J. Membr. Sci*., 300 (2007) 165-171

60. Y.N. Kwon, J.O. Leckie, Hypochlorite degradation of crosslinked polyamide membranes – II. Changes in hydrogen bonding behavior and performance, *J. Membr. Sci.* 282 (2006) 456-464

61. N.P. Soice, A.C. Maladono, D.Y. Takigawa, A.D. Norman, W.B. Krantz, A.R. Greenberg, Oxidative degradation of polyamide reverse osmosis membranes: Studies of molecular model compounds and selected membranes, *J. Appl. Polymer Sci*. 90 (2003) 1173-1184

62. L.E. Applegate, C.W. Erkenbrecher, H. Winters, New Chloramine Process to Control Aftergrowth and Biofouling in Perasep B-10 RO Surface Seawater Plants, *Desalination*, 74 (1989) 51-67

63. I.Jr. Moch, A. Ben Hamida, H. Pohland, (1995), *Proceedings of the IDA World Congress on Desalination*, Abu Dhabi, UAE, Nov. 18-24, Vol. **IV**, 59-72.

64. S. Sorlini, C. Collivignarelli, Trihalomethane formation during chemical oxidation with chlorine, chlorine dioxide and ozone of ten Italian natural waters, *Desalination*, 176 (2005) 103-111

65. T.R. Bott, Bio-fouling. In *Fouling of Heat Exchanger Surfaces,* M. Bohnet, Ed., Vol. 1, pp. 5.1-5.20

66. K. Kaur, T.R. Bott, B.S.C. Leadbeater, Effect of Ozone on *Pseudomonas fluorescens*. In *Biofilms: Science and Technology*, L.F. Melo, M.M. Fletcher, T.R. Bott, B. Capdeville, Eds., pp.589-594, Kluwer, Dordrecht, 1992.

67. I. Koyuncu, M.R. Wiesner, C. Bele, G. Coriton, M.-Djafer, J. Cavard, Bench-scale assessment of pretreatment to reduce fouling of salt-rejecting membranes, *Desalination*, 197 (2006) 94-105

68. J.C. Perrins, W.J. Cooper, J.H. van Leeuwen, R.P. Herwig, Ozonation of seawater from different locations: Formation and decay of total residual oxidant – implications for ballast water treatment, *Mar. Pollution Bull*., 52 (2006) 1023-1033

69 . K. Tyrovola, E. Diamadopoulos, Bromate formation during ozonation of groundwater in coastal areas in Greece, *Desalination*, 176 (2005) 201-209

70. B.S. Oh, H.Y. Jang, Y.J. Jung, J.W. Kang, Microfiltration of MS2 bacteriophage: Effect of ozone on membrane biofouling, *J. Membr. Sci*., 306 (2007) 244-252

71. G. Tragardh, Membrane cleaning, *Desalination*, 1989. 71: p. 325–334.

72. S.S. Madaeni, T. Mohammadi, M.K. Moghadam, Chemical cleaning of reverse osmosis membranes, *Desalination* 134 (2001) 77–82.

73. J.J. Sadhwani, J.M. Vesa, Cleaning tests for seawater reverse osmosis membranes, *Desalination* 139 (2001) 177–182.

74. A.S. Al-Amoudi, A.M. Farooque, Performance, restoration and autopsy of NF membranes used in seawater pretreatment, *Desalination* 178 (2005) 261–271.

75 . T.K. Osta, L.M. Bakheet, Pretreatment system in reverse osmosis plants, *Desalination* 63 (1987) 71–80.

76 . A.G. Fane, Proc., Symposium on Characterization of Polymers with Surface, Lappeenranta, Finland, (1997) 51.

77. H. Lee, G. Amy, J. Cho, Y. Yoon, S.H. Moon, I.S. Kim, Cleaning strategies for flux recovery of an ultrafiltration membrane fouled by natural organic matter, *Wat. Res.* 35 (2001) 3301–3308.

78. G. Morel, N. Ouazzani, A. Graciaa, J. Lachaise, Surfactant modified ultrafiltration of nitrate ions removal, *J. Membr. Sci*. 134 (1997) 47–57.

79. T. Mohammadi, S.S. Madaeni, M.K. Moghadam, Investigation of membrane fouling, *Desalination* 153 (2002) 155–160.

80. M. Ulbricht, G. Belfort, Surface modification of ultrafiltration membranes by low temperature plasma 0.2. Graft polymerization onto polyacrylonitrile and polysulfone. *J. Membr. Sci*. 1996, 111, 193-215

81. V.M. Kochkodan, N. Hilal, V.V. Goncharuk, L. Al-Khatib, T.I. Levadna, Effect of the surface modification of polymer membranes on their microbiological fouling, *J. Colloid* 2006, 68, 267-273

82. Q. Li, S. Mahendra, D.Y. Lyon, L. Brunet, M.V. Viga, D. Li, P.J.J. Alvarez, Antimicrobial nanomaterials for water disinfection and microbial control: Potential applications and implications, *Wat. Res*. 42 (2008) 4591-4602

83. E. Gazit, Self-assembled peptide nanostructures: the design of molecular building blocks and their technological utilization, *Chem. Soc. Rev*. 2007, 36, 1263-1269

84. Y. Zhou, S. Yu, C. Gao, X. Feng, Surface modification of thin film composite polyamide membranes by electrostatic self deposition of polycations for improved fouling resistance, *Sep. Purif. Technol*. 66 (2009) 287–294.

85. C. Sagle, E.M. van Wagner, H. Ju, B.D. McCloskey, B. D. Freeman, M.M. Sharma, PEG-coated reverse osmosis membranes: Desalination properties and fouling resistance, *J. Membr. Sci.* 340 (2009) 92–108.

86. G. Kang, M. Liu, B. Lin, Y. Cao, Q. Yuan, A novel method of surface modification on thin-film composite reverse osmosis membrane by grafting poly(ethylene glycol), *Polym*. 48 (2007) 1165–1170.

87. USEPA 2007 In: Science Policy Council (Ed.), US Environmental Protection Agency nanotechnology white paper. EPA 100/B-07/001 Washington D.C.

88. L. Qi, Z. Xu, X. Jiang, C. Hu, X. Zou, Preparation and antibacterial activity of chitosan nanoparticles, *Carbohydr. Res*., 339 (2004) 2693-2700

89. J.R. Morones, J.L. Elechiguerra, A. Camacho, K. Holt, J.B. Kouri, J.T. Ramirez, M.J. Yacaman, The bactericidal effect of silver nanoparticles, *Nanotechnology* 16 (2005) 2346-2353

90. M. Cho, H. Chung, W. Choi, J. Yoon, Different inactivation behavior of MS-2 phage and *Escherichia coli* in TiO_2 photocatalytic disinfection, *Appl. Environ. Microbiol*. 71 (2005) 270-275

91. D.Y. Lyon, L.K. Adams, J.C. Falkner, P.J.J. Alvarez, Antibacterial activity of fullerene water suspensions: effects of preparation method and particle size, *Environ. Sci. Technol*. 40 (2006) 4360-4366

92. S. Kang, M. Pinault, L.D. Pfefferle, M. Elimelech, Single-walled carbon nanotubes exhibit strong antimicrobial activity, *Langmuir* 23 (2007) 8670-8673

93. A. Mills, S.L. Hunte, An overview of semiconductor photocatalysis, *J. Photochem. Photobiol. A: Chem.* 108 (1997) 1-35

94. Y. Kikuchi, K. Sunada, T. Iyoda, K. Hashimoto, A. Fujishima, Photocatalytic bactericidal effects of TiO_2 thin films: dynamic view of the active oxygen species responsible for the effect, *J. Photochem. Photobiol. A. Chem.* 106 (1997) 51-56

95. S.-Y. Kwak, S.H. Kim, S.S. Kim, Hybrid Organic/Inorganic Reverse Osmosis (RO) Membrane for Bactericidal Anti-Fouling. Part 1. Preparation and characterization of TiO_2 nanoparticle self-assembled aromatic polyamide thin-film composite (TFC) membrane, *Environ. Sci. Technol*., 35 (2001) 2388-2394

96. S.H. Kim, S.-Y. Kwak, B.-H. Sohn, T.H. Park, Design of TiO_2 nanoparticle self-assembled aromatic polyamide thin-film composite (TFC) membrane as an approach to solve biofouling problem, *J. Membr. Sci*. 211 (2003) 157-165

97. K.H. Cho, J.E. Park, T. Osaka, S.G. Park, The study of antimicrobial activity and preservative effects of nanosilver ingredient, *Electrochimica Acta* 51 (2005) 956-960

98. X. Xu, Q. Yang, Y. Wang, H. Yu, X. Chen, X. Jing, Biodegradable electrospun poly(lactide) fibers containing antibacterial silver nanoparticles, *European Polymer Journa*l 42 (2006) 2081-2087

99. W. Zhang, X. Qiao, J. Chen, Synthesis of nanosilver colloidal particles in water/oil microemulsion, *Colloids and Surfaces A: Physicochemical and Engineering Aspects* 299 (2007) 22-28

100. Q.L. Feng, J. Wu, G.Q. Chen, F.Z. Cui, T.N. Kim, J.O. Kim, A mechanistic study of the antibacterial effect of silver ions on *Escherichia coli* and *Staphylococcus aureus*, *J. Biomed. Mat. Res*. 52 (2000) 662-668

101. H.-L. Yang, J.C. Lin, C. Huang, Application of nanosilver surface modification to RO membrane and spacer for mitigating biofouling in seawater desalination, *Wat. Res*. 43 (2009) 3777-3786

102. M.R. Wiesner, G.V. Lowry, P. Alvarez, D. Dionysiou, P. Biswas, Assessing the risks of manufactured nanomaterials, *Environ. Sci. Technol*. 40 (2006) 4336–4337.

103. T.M. Benn, P. Westerhoff, 2008. Nanoparticle silver released into water from commercially available sock fabrics. *Environ. Sci. Technol*., doi:10.1021/es7032718.

104 . D.Y. Lyon, D.A. Brown, E.R. Sundstrom, P.J.J. Alvarez, Assessing the antibiofouling potential of a fullerene-coated surface. *Int. Biodeterior. Biodegradation*, in press. doi:10.1016/j.ibiod.2007.11.007.

105 .S.H. Baxamusa, K.K. Gleason, Random copolymer films with molecular-scale compositional heterogeneities that interfere with protein adsorption, *Adv. Funct. Mater*. 2009, 19, 1-8

106. N. Setter, D. Damjanovic, L. Eng, G. Fox, S. Gevorgian, S. Hong, A. Kingon, H. Kohlstedt, N. Y. Park, G. B. Stephenson, I. Stolitchnov, A. K. Taganstev, D. V. Taylor, T. Yamada and S. Streiffer, Ferroelectric thin films: Review of materials, properties, and applications, *Journal of Applied Physics* 100 (2006) 051606.

107. Y. Fu, H. Du, W. Huang, S. Zhang and M. Hu, TiNi-based thin films in MEMS applications: a review, *Sensors and Actuators* A 112 (2004) 395-408.

108. C. D. Dimitrakopoulos and P. R. L. Malenfant, Organic Thin Film Transistors for Large Area Electronics, *Advanced Materials* 14 (2002) 99-117.

109. I. Tokarev and S. Minko, Stimuli-responsive hydrogel thin films, *Soft Matter* 5 (2009) 511-524.

110. M. A. C. Stuart, W. T. S. Huck, J. Genzer, M. Müller, C. Ober, M. Stamm, G. B. Sukhorukov, I. Szleifer, V. V. Tsukruk, M. Urban, F. Winnik, S. Zauscher, I. Luzinov and S. Minko, Emerging applications of stimuli-responsive polymer materials, *Nature Materials* 9 (2010) 101–113.

111. D. Braun, H. Cherdron, M. Rehahn, H. Ritter and B. Voit, *Polymer Synthesis: Theory and Practice: Fundamentals, Methods, Experiments*, (2005) 152-155.

112. R. D. Deegan, O. Bakajin, T. F. Dupont, G. Huber, S. R. Nagel and T. A. Witten, Capillary flow as the cause of ring stains from dried liquid drops, *Nature* 389 (1997) 827-829.

113. S. G. Im, K. K. Gleason, Solvent-free modification of surfaces with polymers: the case for initiated and oxidative chemical vapor deposition (CVD), *AIChE* 57 (2011) 276-285.

114. W. Kern and V. S. Ban, Chemical vapor deposition of inorganic thin films, *Thin Film Processes* (1978) 257-331.

115. M. E. Alf, A. Asatekin, M. C. Barr, S. H. Baxamusa, H. Chelawat, G. Ozaydin-Ince, C. D. Petruczok, R. Sreenivasan, W. E. Tenhaeff, N. J. Trujillo, S.Vaddiraju, J. Xu and K. K. Gleason, Chemical Vapor Deposition of Conformal, Functional, and Responsive Polymer Films, *Advanced Materials* 22 (2009) 1993-2027.

116. W.E. Tenhaeff, K.K. Gleason, Initiated and Oxidative Chemical Vapor Deposition of Polymeric Thin Films: iCVD and oCVD, *Adv. Funct. Mater*. 2008, 18, 979

117. K.K.S. Lau, K.K Gleason, Particle Surface Design using an All-Dry Encapsulation Method, *Adv. Mater*. 2006, 18, 1972

118. S.H. Baxamusa, L. Montero, J.M. Dubach, H.A. Clark, S. Borros, K.K. Gleason, Protection of Sensors for Biological Applications by Photoinitiated Chemical Vapor Deposition of Hydrogel Thin Films, *Biomacromolecules* 2008, 9, 2857

119. K.K.S. Lau, K.K Gleason, Initiated Chemical Vapor Deposition (iCVD) of Poly(alkyl acrylates): An Experimental Study, *Macromolecules* 2006, 39, 3695

120. K. Chan, K.K. Gleason, Initiated Chemical Vapor Deposition of Linear and Cross-linked Poly(2-hydroxyethyl methacrylate) for Use as Thin-Film Hydrogels, *Langmuir* 2005, 21, 8930

121. R. W. Baker and J. G. Wijmans, The solution-diffusion model: A Review, *J. Membr. Sci*. 107 (1995) 1-21.

122. D. R. Paul, Reformulation of the solution-diffusion theory of reverse osmosis, *J. Membr. Sci*., 241 (2004) 371-386.

123. R. B. Bird, W. E. Stewart, E. N. Lightfoot, Transport Phenomena, 2nd ed., John Wiley & Sons, Inc., New York, 2002.

124. J. M. S. Henis, M. K. Tripodi, Composite hollow fiber membranes for gas separation: the resistance model approach, *J. Membr. Sci*., 8 (1981) 233-246.

125. A. Subramani, E.M.V. Hoek, Direct observation of initial microbial deposition onto reverse osmosis and Nanofiltration membranes, *J. Membr. Sci*. 319 (2008) 111-125

126. W.G. Characklis, K.C. Marshall, Biofilms, John Wiley & Sons, 1990

127. F.I. Loeb, R.A. Neihof, Marine conditioning films. In: Baier RE (ed) Applied chemistry at protein interfaces. American Chemical Society, Washington DC pp 319-335

128. H.-C. Flemming, G. Schaule, Biofouling on membranes – a microbiological approach, *Desalination* 70 (1988), 95-119

129. K.A. Marx, Quartz Crystal Microbalance: A Useful Tool for Studying Thin Polymer Films and Complex Biomolecular Systems at the Solution-Surface Interface, *Biomacromolecules* (2003) 4 1099-1120

130. M. Rodahl, F. Hook, A. Krozer, P. Brzezinski, B. Kasemo, Quartz crystal microbalance setup for frequency and Q-factor rneasurements in gaseous and liquid environments, *Rev. Sci. Instrum*. 1995, 66, 3924-3930

131. T.A. Davis, M. Ramirez, A. Mucci, B. Larsen, Extraction, isolation and cadmium binding of alginate from *Sargassum* spp., *J. Appl. Phycol*. 2004, *16*, 275-284

132. V. Korstgens, H.C. Flemming, J. Wingender, W. Borchard, Influence of calcium ions on the mechanical properties of a model biofilm of mucoid Pseudomonas aeruginosa, *Water Sci. Technol*, 2001;43(6):49-57

133. M. Pasmore, P. Todd, S. Smith, D. Baker, J. Silverstein, D. Coons, C.N. Bowman, Effects of ultrafiltration membrane surface properties on *Pseudomonas aeruginosa* biofilm initiation for the purpose of reducing Biofouling, *J. Membr. Sci.* 2001, 194, 15-32

134. N. Schürks, J. Wingender, H. -C. Flemming, C. Mayer, Monomer composition and sequence of alginates from *Pseudomonas aeruginosa*, *Int. J. Biol. Macromol*. 2002, 30, 105-111

135. P.K. Cornel, R.S. Summers, P.V. Roberts, Diffusion of humic acid in dilute aqueous solution, *J. Colloid Interface Sci*. 110 (1) 1986, 149

136. M. Elimelech, X. Zhu, A.E. Childress, S. Hong, Role of membrane surface morphology in colloidal fouling of cellulose acetate and composite aromatic polyamide reverse osmosis membranes, *J. Membr. Sci*. 127 (1997) 101

137. C.R. Bouchard, J. Jolicoeur, P. Kouadio, M. Britten, Study of humic acid adsorption on nanofiltration membranes by contact angle measurements, *Can. J. Chem. Eng*. 75 (1997) 339

138. M. NystroÈm, K. RuohomaÈki, L. Kaipia, Humic acid as a fouling agent in filtration, *Desalination* 106 (1996) 79.

139. Y. Kaiya, Y. Itoh, K. Fujita, S. Takizawa, Study on fouling materials in the membrane treatment process for potable water, *Desalination* 106 (1996) 71.

140. K. Ghosh, M. Schnitzer, Macromolecular structures of humic substances, *Soil Sci*. 129(5) (1980) 266.

141. L.A. Bjergbaek, J.A. Haagensen, S. Molin, P. Roslev, Effect of oxygen limitation and starvation on the benzalkonium chloride susceptibility of Escherichia coli. *J. Appl. Microbiol.* 2008, 105, 1310-1317

142. S. H. Baxamusa, K. K. Gleason, Thin Polymer Films with High Step Coverage in Microtrenches by Initiated CVD, *Chem. Vap. Deposition*, 2008, 14, 313–318.

143. M. Karaman, S.E. Kooi, K.K. Gleason, Vapor deposition of hybrid organic-inorganic dielectric bragg mirrors having rapid and reversibly tunable optical reflectance. *Chem Mater*. 2008; 20: 2262–2267.

144. A. Matin, G. Ozaydin-Ince, Z.U. Khan, S.M.J. Zaidi, K.K. Gleason, D. Eggenspiler, Random copolymer films as potential antifouling coatings for reverse osmosis membranes, *Desalination and Water Treatment* 34 (2011) 100–105

145. M. Hirose, H. Ito and Y. Kamiyama, Effect of skin layer surface structures on the flux behaviour of RO membranes, *J. Membr. Sci.*, 121 (1996) 209-215.

146. S.-Y. Kwak and D. W. Ihm, Use of atomic force microscopy and solid-state NMR spectroscopy to characterize structure-property-performance correlation in high-flux reverse osmosis (RO) membranes, *J. Membr. Sci.*, 158 (1999) 143-153.

147. E. M. Vrijenhoak, S. Hong and M. Elimelech, Influence of membrane surface properties on initial rate of colloidal fouling of reverse osmosis and Nanofiltration membranes, *J. Membr. Sci*., 188 (2001) 115-128.

148. J. S. Louie, I. Pinnau, I. Ciobanu, K. P. Ishida, A. Ng and M. Reinhard, Effects of polyether-polyamide block copolymer coating on performance and fouling of reverse osmosis membranes, *J. Membr. Sci.*, 280 (2006) 762-770.

149. S. Kang, E.M.V. Hoek, H. Choi, H. Shin, Effect of Membrane Surface Properties During the Fast Evaluation of Cell Attachment, *Sep. Sci. Tech*. Volume 41, Issue 7, 2006

150. M. Elimelech, X. Zhu, A. Childress, S. Hong, Role of surface morphology in colloidal fouling of cellulose acetate and composite polyamide RO membranes. *J. Membr. Sci*. 127 (1997) 101–109.

151. Q. Li, Z. Xu, I. Pinnau, Fouling of reverse osmosis membranes by biopolymers in wastewater secondary effluent: Role of membrane surface properties and initial permeate flux, *J. Membr. Sci*. 290 (2007) 173–181

152. R.M. Donlan, Biofilms: microbial life on surfaces, *Emerging Infect. Dis*. 8 (2002) 881–890.

153. E. Bullitt, L. Makowski, Structural polymorphism of bacterial adhesion pili, *Nature* 373 (1995) 164–167.

154. Abu Tarboush, B. J., Rana, D., Matsuura, T., Arafat, H. A., and Narbaitz, R. M., "Preparation of Thin-Film-Composite Polyamide Membranes for Desalination Using Novel Hydrophilic Surface Modifying Macromolecules", *J. Membr. Sci.* 325 (2008) 166-175

155. Y. Mao, K. K. Gleason, Vapor-Deposited Fluorinated Glycidyl Copolymer Thin Films with Low Surface Energy and Improved Mechanical Properties, *Macromolecules* 2006, 39, 3895.

156. M.S. Lord, M.H. Stenzel, A. Simmons, B.K. Milthorpe, The effect of charged groups on protein interactions with poly(HEMA) hydrogels, *Biomaterials* 2006, 27, 567-575

157. S. Sharma, K.C. Popat, T.A. Desai, Controlling Nonspecific Protein Interactions in Silicon Biomicrosystems with Nanostructured Poly(ethylene glycol) Films, *Langmuir* 2002, 18, 8728

158. C. Werner, K.J. Eichhorn, K. Grundke, F. Simon, W. Grahlert, H.J. Jacobasch, Insights on structural variations of protein adsorption layers on hydrophobic fluorohydrocarbon polymers gained by spectroscopic ellipsometry (part I) *Colloids Surf. A* 1999, 156, 3

159. F. Hook, J. Voros, M. Rodahl, R. Kurrat, P. Boni, J.J. Ramsden, M. Textor, N.D. Spencer, P. Tengvall, J. Gold, B. Kasemo, A comparative study of protein adsorption on titanium oxide surfaces using in situ ellipsometry, optical waveguide lightmode spectroscopy, and quartz crystal microbalance/dissipation *Colloids Surf. B* 2002, 24, 155

160. A.E. Contreras, Z. Steiner, J. Miao, R. Kasher, Q. Li, Studying the role of common membrane surface functionalities on adsorption and cleaning of organic foulants using QCM-D, *Environ. Sci. Technol*. 2011, 45, 6309-6315

Vita

Department of Mechanical Engineering 056-5448593
King Fahd University of Petroleum & Minerals amatin@kfupm.edu.sa
Dhahran 31261, Saudi Arabia

EDUCATION

PhD, Mechanical Engineering January 2012
King Fahd University of Petroleum & Minerals, Saudi Arabia
Dissertation: Improving the Biofouling Resistance of Reverse Osmosis Membranes by a Novel Surface Modification Technique

MS, Materials Science & Engineering June 2002
University of Cincinnati, USA

BS, Metallurgical & Materials Engineering June 1998
Middle East Technical University, Turkey

RESEARCH EXPERIENCE

Research Assistant June 2009 – December 2011
King Fahd University of Petroleum & Minerals, Saudi Arabia

- Developed fouling-resistant RO membranes by the synthesis and deposition of Amphiphilic Copolymer films using an initiated CVD technique
- Optimized the chemistry and thickness of the anti-fouling coatings by carrying out adsorption studies with biopolymers using a QCM-D technique

Visiting Graduate Student October 2009 – June 2010
Massachusetts Institute of Technology, USA

- Achieved almost complete resistance to irreversible adhesion of bacteria by the surface modification of RO membranes
- Demonstrated the effectiveness of the copolymer film in retarding the long-term flux decline associated with membrane Biofouling

TEACHING EXPERIENCE

Lecturer-B, 2007 – 2012
King Fahd University of Petroleum & Minerals, Saudi Arabia
Taught the following laboratory courses to undergraduate students

- Materials Science
- Manufacturing Processes for Materials
- Thermofluids Laboratory

Assistant Professor 2004 – 2006
COMSATS Institute of Tehcnology, Pakistan
Taught the following courses to undergraduate students

- Solid State Physics
- Microfabrication of Semiconductor Devices

FELLOWSHIPS & AWARDS

Doctoral Fellowship, King Fahd University of Petroleum & Minerals 2007 – 2012
University Graduate Scholarship, University of Cincinnati 1999 – 2001
Honor Student, Middle East Technical University 1994 – 1998

PUBLICATIONS

A. Matin, G.O.-Ince, Z.U. Khan, S.M.J. Zaidi, K.K. Gleason, Damien Eggenspiler, "Random Copolymer Films as Potential Antifouling Coatings for Reverse Osmosis Membranes", *Desalination & Water Treatment*, 34 (2011) 100–105

- A. Matin, Z.U. Khan, S.M.J. Zaidi, M.C. Boyce, "Biofouling of RO membranes for Seawater Desalination: A Review", *Desalination* 281, (2011), 1-16
- G. O.-Ince, A. Matin, Z.U. Khan, K.K. Gleason, "Surface Modification of RO membranes by thin-film coatings deposited by initiated chemical vapor deposition", submitted to *Thin Solid Films*
- A. Matin, G.O.-Ince, Z.U. Khan, K.K. Gleason, S.M.J. Zaidi, Studying Biopolymer Adsorption on Copolymer Films Deposited using an initiated Chemical Vapor Deposition (iCVD) technique, submitted to *Colloids & Surfaces A*
- A. Matin, K.K. Gleason, M.M. Khaled, S.M.J. Zaidi, Z.U. Khan, A. Khalil, Reverse Osmosis Membranes Incorporating Random Copolymer Films Discourage Irreversible Adhesion of Bacteria, submitted to *Journal of Membrane Science*

PATENTS

Z.U. Khan, A. Matin, K.K. Gleason, R. Yang, M.M. Khaled, S.M.J. Zaidi, Antifouling Coatings on RO Membranes Prevent Microbial Attachment, *under preparation*

A. Matin, Z.U. Khan, G.O.-Ince, K.K. Gleason, S.M.J. Zaidi, Random Copolymer Films Interfere with Biopolymer Adsorption, *under preparation*

REFERENCES

Zafarullah Khan
King Fahd University of Petroleum & Minerals
Dhahran 31261, Saudi Arabia
zukhan@kfupm.edu.sa

Mary Cunningham Boyce
Massachusetts Institute of Technology,
Cambridge, MA 02139, USA
mcboyce@mit.edu

Karen K. Gleason
Massachusetts Institute of Technology,
Cambridge, MA 02139, USA
kkg@mit.edu